Developing Novel Biosensors for detection of L-Aspartate and N-Acetyl Aspartate

Aditi Kibe

A thesis submitted in partial fulfilment of the requirements for the degree of

Doctor of Philosophy in Life Sciences

University of Warwick, School of Life Sciences

May 2021

Table of Contents

List of Figures

List of Tables

Acknowledgement

It was in the late nineties when my father gave me Jurassic Park to read. A book that remains a firm favourite and sparked my interest in molecular biology, a term unheard of at that time in India. Two decades later, I am submitting my thesis and it's been an incredible journey.

I would like to thank my supervisor Prof. Nicholas Dale for his unconditional support, guidance and insight that always steered the project in the right direction and kept me going even when things didn't work. Prof. David Evans and Dr Emma Anderson for their encouragement when I started at Warwick as a technician. Faming Tian for teaching me how to make sensors and the team at Sarissa Biomedical who were always so helpful.

Dr Deborah Brotherton for her help and with protein purification. Members of C10 laboratory for their help with protein preps and assays.

My advisory panel, Prof. Bruno Frenguelli and Prof. Alex Cameron for their valuable comments on the reports.

Dr Mark Wall, Emily and Monica for their help with electrophysiology and Dr Amol Bhandare for the immunology experiments.

I would also like to thank Prof. Keith Leppard, Nicola Glover and Kerry Davies for helping whenever I reached out to them for advice.

My colleagues Martina, Pippa, Jess, Sarb, and everyone in the group who were there to boost morale and provided much needed cheer and bonhomie.

My amazing circle of friends who were always there and my beautiful family: mum and pa, aai-baba, Kapil and Aditya for their love, support and encouragement, for believing in me and pulling me through some difficult times and has been my support system without whom this thesis was not possible.

Declarations

This thesis is submitted to the University of Warwick in support of my application for the degree of Doctor of Philosophy. The work in this thesis is original and has not been submitted in any previous application for any degree.

The work presented (including data generated and data analysis) was carried out by the author except in the cases outlined below:

Dr Deborah Brotherton (University of Warwick, Coventry, UK)

Bacmid DNA preparation, transfection of Sf9 insect cells and cell extraction protocol (Figures 4-4, 4-5 and 4-7)

Dr Amol Bhandare (University of Warwick, Coventry, UK)

Induction of epilepsy, mouse brain slice preparation and imaging (Figure 5-18, Figure 5-19)

Dr Tobias Engel and Dr Aida Menendez Mendez (Royal College of Surgeons, Dublin, Ireland)

Western blot on mice and human tissue (Figure 5-20, Figure 5-21)

Abstract

Microelectrode biosensors have proven to be an invaluable tool in direct measurement of extracellular concentration of analytes. Real-time measurement of released neuroactive compounds with simultaneous recording of electrophysiological activity has been made possible because of enzyme based sensors specific for their analytes. By using the sol-gel coating method of sensor fabrication, enzyme-based sensors for L-aspartate (L-Asp) and N-acetyl aspartate (NAA) were fabricated on a Platinum (Pt) microelectrode. The L-Asp sensor was made using the enzyme L-aspartate oxidase (LAO) and was fully characterised. The sensor achieved a steady state response to L-Asp within 15 s, had a lower detection limit of 3 µM with a sensitivity of 0.0016 µA/µM/cm^2 (R=0.99). The L-Asp sensor also detected real-time release of L-Asp in area CA1 of hippocampal brain slices. L-Asp release was enhanced by independent application of excitatory amino acid transporter blocker DL-threo-β-Benzyloxyasparticacid (TBOA) and L-albizziine (L-Alb) an inhibitor for L-Asp metabolising enzyme. L-Alb also induced seizure-like activity with accompanying L-Asp release. These results bolster the idea of L-Asp as a possible co-transmitter or neuromodulator.

NAA is a derivative of L-Asp and is the second most abundant compound in the brain after L-glutamate. NAA is also a marker for stroke and traumatic brain injury. NAA sensor was fabricated using the enzymes aspartoacylase (ASPA) and LAO. A novel method for detection of ASPA activity and proof of concept data for the NAA sensor is presented. The principle and methodology for NAA sensor fabrication can be extended to develop integrated electrochemical sensor array such as SMARTChip.

Both the L-Asp and NAA sensor can provide valuable insight into the role of these compounds in functional aspects of brain physiology.

Abbreviations

4-AP	4-aminopyridine
5HT	5-hydroxytryptamine
8-CPT	8-cyclopentyltheophylline
aCSF	Artificial cerebrospinal fluid
AEBSF	4-benzenesulfonyl fluoride hydrochloride
Amp	Ampicillin
AMPA	α-amino-3-hydroxy-5-methyl-4-isozazole-propionic acid
APTMOS	3-Aminopropyltrimethoxy silane
ARed	Amplex red
Arg	Arginine
ASD	Asparagine synthetase deficiency
ASNS	Asparagine synthetase
ASPA	Aspartotoacylase
BSA	Bovine serum albumin
Chlor	Chloramphenicol
CNS	Central nervous system
CV	Column volume
DAAO	D-amino acid oxidase
D-AP5	D-(-)-2-amino-5-phosphonopentanoic acid
D-Asp	D-aspartate
D-Asp	D-aspartate

	Dentate gyrus
DMB	1,2-diamino-4,5-methylenedioxybenzene dihydrochloride
DMSO	Dimethyl sulfoxide
DTT	Dithiothreitol
DTT	Dithiothreitol
EAAT	Excitatory amino acid transporter
EcLAO	Escherichia coli L-aspartate oxidase
EGTA	Ethylene glycol-bis(β-aminoethylether)-N,N,N',N'-tetraacetic acid
EPSP	Excitatory postsynaptic potential
FAD	Flavin adenine dinucleotide
fEPSP	Field excitatory postsynaptic potential
FT	Flow through
GABA	Gamma amino butyric acid
GLAST	Glutamate/ aspartate transporter
GOPTMOS	3-glycidyloxypropyl(trimethoxy)-silane
GST	Glutathione S transferase
hASPA	Human aspartoacylase
HFS	High frequency simulation
HPLC	High-performance liquid chromatography
HRP	Horseradish peroxidase
IB	Inclusion body
IF	Insoluble fraction
IPTG	Isopropyl-β-D-thiogalactopyranoside

Kan	Kanamycin
KO	Knock out
LAAO	L-amino acid oxidase
L-Alb	L-albizziine
L-Asn	L-asparagine
L-Asp	L-aspartate
LAO	L-aspartate oxidase
L-Gln	L-glutamine
L-Glu	L-glutamate
LGO	L-glutamate oxidase
mASPA	Mouse aspartoacylase
mGluR3	Metabotropic glutamate receptor 3
MMS	Methyl-tris(trymethylsiloxy) silane
MPD	4,5-methylenedioxy 1-2 phenylenediamine dihydrochloride
MRS	Proton magnetic resonance
NAA	N-acetyl aspartate
NAAG	N-acetylaspartylglutamate
NMDA	N-methyl-D-aspartate
NT	Neuro transmitter
OAA	Oxaloacetate
PEG	Polyethylene gycol
PEI	Polyethylenimine
PIPES	Piperazine-N,N'-bis(2-ethanesulphonic acid)
PpLAO	Pseudomonas putida L-aspartate oxidase

Pt	Platinum
RT	Room temperature
SD	Standard deviation
SE	Status epilepticus
SF	Soluble fraction
StLAO	Sufolobus tokodaii L-aspartate oxidase
TBI	Traumatic brain injury
TBOA	DL-threo-β-Benzyloxyasparticacid
TLE	Temporal lobe epilepsy
TMOS	Tetramethyl orthosilicate
TP	Total protein
VGLUT	Vesicular glutamate transporter
WB	Western blot
WT	Wild type

Chapter 1

Introduction

The human brain is a complex structure with astonishing capabilities. The brain and the spinal cord make the central nervous system (CNS), and together are involved in processing, integrating and co-ordinating the information they receive from the sense organs. Our learning, behaviour, movement, cognition, regulation of internal organs, everything is under the control of the central nervous system. There are about 10^{11} neurons and the amazing ability of the brain to process information comes from the ability of these neurons to connect with each other to form a synapse and to relay information across complex neural networks.

Chemical signalling is at the heart of neural communication. Neurons and glial cells communicate by releasing diverse chemical substances or neurotransmitters (NT). In simple terms, the presynaptic neuron releases the neurotransmitter, that is received by the post synaptic neuron via specialised proteins on the cell membrane called receptors.

The first NT was discovered by Otto Loewi in 1926, when he demonstrated that the release of acetylcholine from the vagus nerve slowed the cardiac rhythm. Since then several small molecule neurotransmitters and over 100 neuroactive compounds have been identified (González-Espinosa and Guzmán-Mejía 2014), (Hyman 2005).

The original criteria for a substance to be a NT was first reviewed by Werman in 1966 (Werman 1966).

According to his review, for a compound to be NT, it should fulfil certain criteria such as (adapted from Werman 1966):

1. Presence of the transmitter in the presynaptic neuron.
2. Synthesis of the transmitter, presence of precursors and a synthesizing enzyme in the presynaptic neuron.
3. The criterion for a specific release mechanism.
4. The criterion of collectability of the transmitter.
5. The criterion of the inactivating enzyme.
6. The criterion of identical actions.

The criterion of collectability meant that the agent suspected to be a NT should be detectable in the extracellular fluid collected from the synaptic cleft. However, given the complex nature of the brain extracellular space, this criterion is an oversimplification.

The other criteria are still accepted, albeit with certain extensions. In light of advancements made in the field it is now generally accepted that for a chemical to be a NT it should be (Sudhof 2004; Dalangin, Kim, and Campbell 2020):

1. Present in the presynaptic neuron, which has the synthesizing enzymes and precursors.
2. Stored in vesicles and must be released from the neuron by the mechanism of exocytosis in a Ca^{2+} dependent manner upon depolarization.
3. Cleared from the synaptic cleft by inactivating enzymes or specific transporters that can remove the NT to prevent its accumulation.
4. Received by the post-synaptic neuron via specific receptors.

These are all in line with the original criteria, in addition to these there was also a criterion of identical actions, which is the fundamental criteria. The application of the NT to the postsynaptic neuron should produce or mimic its stimulation of the presynaptic neuron.

There is activity dependent release of NTs, which is the ability of the nerve cells to change the amount of NT being released in response to activity. Synaptic plasticity specifically refers to the activity- dependent modification of the strength of synaptic transmission and plays an important role in learning and memory. It also contributes to the early development of neural circuitry (Citri and Malenka 2008).

The main small molecule NTs, which play an important role in synaptic plasticity are acetylcholine, L-glutamate (L-Glu), dopamine, gamma amino butyric acid (GABA), serotonin, adrenaline and noradrenaline, and histamine (González-Espinosa and Guzmán-Mejía 2014). In addition to these there are many other molecules (e.g. D-serine) and small neuropeptides that are more recognised as neuromodulators and are important in regulation of synaptic plasticity (Bazzari and Parri 2019).

L-Glu is the main excitatory NT and GABA has been recognized as the inhibitory NT in the brain (Zhou and Danbolt 2014; Petroff 2002). While the role of L-Glu and GABA as NTs is well established and undisputed, the role of L-Asp is still a matter of debate.

1.1 Evidence for and against L-Asp as a NT

1.1.1 Presence and mechanisms of regulated release

In the 1960s, experiments by Curtis and Watkins identified L-Glu and L-Asp as excitants on mammalian neurons (Curtis and Watkins 1963). Several years later Nadler et al. showed K^+ evoked Ca^{2+} -dependent release of L-Glu, GABA and L-Asp. They studied the reduction in L-Asp release by destruction of the commissural innervation of the dentate gyrus (DG) and in area CA1 of hippocampus (Nadler et al. 1976; Nadler et al. 1978).

Immunohistolocalization studies by Gundersen *et al.* have demonstrated aspartate-like and glutamate-like immunoreactivities colocalized in the nerve terminals in stratum radiatum of area CA1. Upon K^+ induced depolarization, there was loss of both L-Asp and L-Glu from the nerve

terminals with simultaneous increase in immunoreactivities in glial cells. Their quantitative immunogold analysis showed that L-Asp localized in synaptic vesicles (Gundersen, Ottersen, and Storm-Mathisen 1991; Gundersen et al. 1998). By using a different approach, vesicular accumulation of [^{3}H]-labelled L-Asp, L-Glu and D-Asp into intact synaptosomes was studied by Fleck *et al.* They showed that L-Asp and L-Glu indeed accumulate into a common vesicular pool, and there are differences in their affinities suggesting that they are accumulated by different transporters (Fleck, Barrionuevo, and Palmer 2001). In comparison to these reports, a recent study involving metabolic profiling of synaptic vesicles showed no enrichment of L-Asp (Chantranupong et al. 2020).

Depolarization induced Ca^{2+}- dependent release of L-Asp from rat purified cerebrocortical synaptosomes (Cavallero, Marte, and Fedele 2009) and from hippocampal synaptosomes was independently studied (Zhou et al. 1995; Bradford and Nadler 2004). In these reports, L-Asp release was largely Ca^{2+} dependent. However, in a separate study on purified cerebrocortical synaptosomes, Ca^{2+} dependent release of L-Asp was not detected (Wilkinson and Nicholls 1989). There are several findings that have noted that there might be different mechanisms of release for L-Asp and L-Glu, with the suggestion that L-Asp might be released at a distance from the synaptic cleft (Nadler 2011).

Evidence for exocytotic release of L-Asp has also been demonstrated. By utilizing botulinum neurotoxin A, B or C, Ca^{2+} -dependent release of L-Asp was found to be reduced, almost as much as L-Glu (Wang and Nadler 2007; Cavallero, Marte, and Fedele 2009). Immunogold electron microscopy studies by Gundersen *et al.* have also provided further support for exocytosis of L-Asp from synaptic vesicles in the hippocampus (Aleksander Talgøy Holten 2008; Gundersen, Holten, and Storm-Mathisen 2004; Gundersen et al. 1998).

The exocytotic release mechanism of L-Asp would require a vesicular transporter for L-Asp, such as the vesicular glutamate transporters (VGLUTs), Miyaji *et al.* proposed the role of sialin as a possible vesicular transporter for

L-Asp (Miyaji, Omote, and Moriyama 2011). However, this was contradicted by Morland *et al*. (Morland et al. 2013), and so far, no other study has confirmed the role of sialin as a possible transporter for L-Asp. Indeed, there is a possibility of another transporter as noted in other reports (Fleck, Barrionuevo, and Palmer 2001; Aleksander Talgøy Holten 2008). VGLUT-1 and VGLUT-2 are considered as specific for glutamatergic neurons, while VGLUT-3 has been associated with non-glutamatergic neurons (El Mestikawy et al. 2011). VGLUT-3 has been shown to co-localise with GABAergic neurons, which co-release L-Glu and L-Asp (Fasano et al. 2017; Docherty, Bradford, and Wu 1987), suggesting that it might be involved in vesicular transport of L-Asp.

1.1.2 Inactivating Mechanisms

Na^+ -dependent active transport of L-Asp into plasma membrane vesicles was first studied in rat brain synaptosomes (Marvizón et al. 1981). Few years later Storck *et al.* identified a Na^+- dependent glutamate/aspartate transporter (GLAST) as a plasma membrane transporter for L-Asp, which could remove L-Asp from the extracellular space after its release. The protein was purified from rat brain and its specificity for transport of L-Glu and L-Asp in a Na^+ dependent manner was also demonstrated (Storck et al. 1992).

Excitatory amino acids are cleared from the extracellular space by highly efficient transporters present on the plasma membrane. Transport of L-Glu is mediated by glutamate transporter proteins derived from five genes, that are generally referred as excitatory amino acid transporters (EAATs) marked EAAT 1-5. The human EAAT-1 is homologous to rodent GLAST (Šerý et al. 2015) and is the only known plasma membrane transporter for L-Asp.

1.1.3 Identity of postsynaptic action

For the final criterion which is presence of specific receptors on post synaptic neuron, there is evidence that L-Asp selectively activates the N-methyl-D-aspartate (NMDA) receptors. Patneau and Mayer studied the activation of excitatory amino acid receptors in rat hippocampal neurons and

showed that while L-Glu could activate both NMDA and α-amino-3-hydroxy-5-methyl-4-isozazole-propionic acid (AMPA) receptors, L-Asp did not activate AMPA (Patneau and Mayer 1990). This result was supported independently by Curras and Dingledine in 1992. By injecting NMDA and AMPA receptor mRNA into xenopus oocytes, they found that L-Asp failed to activate AMPA receptors with concentrations as high as 10 mM (Curras and Dingledine 1992). In 1993, Fleck et al. also demonstrated that both L-Glu and L-Asp have high affinities for NMDA receptors, while only L-Glu had affinity for AMPA receptors (Fleck et al. 1993). This observation demonstrates that L-Asp cannot be the unique excitatory transmitter in the brain, as AMPA receptors are well known to mediate in excitatory postsynaptic potentials in every brain area.

The primacy of L-glutamate as the principal excitatory amino acid neurotransmitter was demonstrated by Herring *et al.* These authors utilized a VGLUT-1 knock out mouse to demonstrate that excitatory neurotransmission in the hippocampus was completely absent (Herring et al. 2015). As VGLUT-1 transports L-Glu but not L-Asp, this comprehensively ruled out a role for L-Asp in generating EPSPs in the hippocampus. Despite this very compelling evidence, a neurotransmitter role for L-Asp remains possible for example in other brain areas or in other synaptic signalling contexts not explored by these authors within the hippocampus.

Thus, with respect to receptor activation, activity of L-Asp overlaps with L-Glu and therefore it is difficult to completely distinguish the role of L-Asp from that of L-Glu. Development of a microelectrode biosensor, specific for L-Asp would not only allow for measurements of L-Asp release, but it would also help in differentiating the electrophysiological action of L-Asp from other NTs.

1.2 N-acetyl aspartate (NAA) and Aspartoacylase (ASPA)

NAA a derivative of L-Asp, is the second most abundant metabolite in the brain and is present in high concentration (up to 10 mM) in the neurons. NAA produces the largest peak in the proton magnetic resonance (MRS) of healthy individuals and is routinely employed as a marker for neuronal health.

NAA levels are markedly reduced in major neuropathologies such as stroke and traumatic brain injury (TBI). Reduced NAA levels have also been reported for other brain disorders including epilepsy and schizophrenia (Bhakoo 2012). Using immunohistochemistry, Moffet *et al* (1991) (Moffett et al. 1991) showed that NAA was mostly localized to hippocampal and cortical neurons.

NAA has a unique tricellular metabolism which was documented in 2000 (Baslow 2018). The synthesis of NAA occurs in the neurons from L-Asp and acetyl coenzyme A by enzyme L-aspartate N-acetyltransferase. NAA is then utilized to synthesize the dipeptide N-acetylaspartylglutamate (NAAG) via enzyme NAAG synthase. NAAG released by the neurons gets transported to the astrocytes by metabotropic Glu receptor 3 (mGluR3), where it is again cleaved to release NAA. Interestingly, there is no enzyme for catalysis of NAA in the neurons or the astrocytes. Astrocytes again release NAA, to be taken up by oligodendrocytes where it is metabolised by aspartoacylase (ASPA) to release acetate (Figure 1-1– from (Baslow 2018)). In the oligodendrocytes, the released acetate is utilized for fatty acid synthesis, cytoplasmic protein and nuclear histone acetylation ((Moffett et al. 2013)

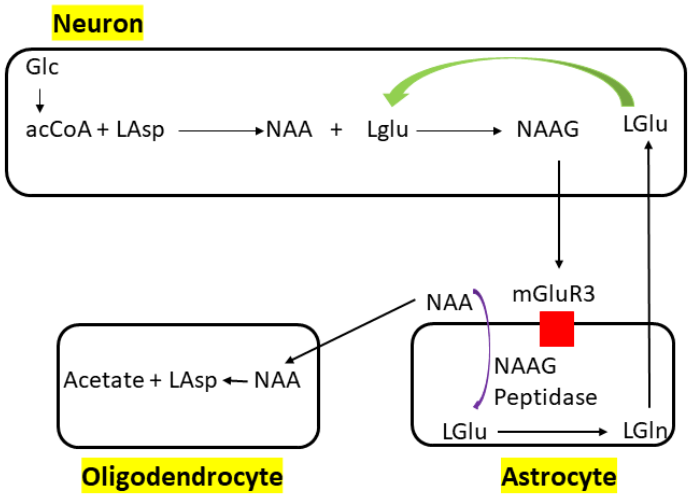

Figure 1-1. Schematic diagram for the tricellular metabolism of NAA (Morris and David 2016; Baslow 2018).

NAA synthesis occurs in the neurons, where it gets converted to NAAG. NAAG is transported to astrocytes where it is cleaved to release NAA. Finally, astrocytes release NAA, to be taken up by oligodendrocytes where NAA is metabolised by ASPA.

NAA is considered as the main source of acetate, which is required for lipid synthesis and myelination. The enzyme ASPA, is the only enzyme for metabolism of NAA and facilitates the release of acetate. Mutations in the gene for ASPA are associated with Canavan disease, a fatal neurological disorder (Reuben Matalon 2015; Appu et al. 2017). Absence of ASPA leads to high accumulation of NAA, low levels of acetate and spongy degeneration of the brain.

Because NAA is present at such high concentrations, it has been developed as one of the key indicators of brain health. In addition to MRS, levels of NAA along with certain candidate markers such as neuron specific enolase (Stevens et al. 1999) are measured in serum/cerebrospinal fluid for diagnosis of stroke and TBI. Methods for measuring NAA include microdialysis, high-performance liquid chromatography (HPLC) (Shannon et al. 2016), tandem mass spectroscopy (Sangaraju et al. 2017). Recently, an optofluidic device based on the principle of surface enhanced Raman-scattering has been developed for rapid label-free detection of NAA (Rickard et al. 2020). This device can detect NAA levels at picomolar range and is being developed as a point of care testing device to aid faster diagnosis of TBI.

1.3 Biosensors and enzymatic biosensors

Biosensors are a self-contained analytical device that can measure analytes in the body fluids, cell cultures and also in tissue slices. Biosensors utilize a biologically sensitive recognition element, coupled with a physical transducer to selectively and quantitatively convert a biological event into a physical signal that can be measured. A number of different recognition elements can be used such as enzymes, antibodies, receptors, nucleic acids; that can bind to the target analyte which can be a substrate, antigen, ligand or complementary nucleic acid. The physical transducer converts the reaction into a physical signal which can be electrical, thermal or optical (Mehrotra 2016; Bhalla et al. 2016).

Enzymatic biosensors gained importance because the integrated enzymes can convert an analyte into an active product that can be measured and because of advances in enzyme purification techniques. Enzyme based sensors measure changes in current when a fixed potential is applied between two electrodes. These sensors are robust, can be miniaturized and can work with very small sample volume. First generation enzyme sensors utilise enzymes which convert the analyte into an electroactive product that transduces to the electrode surface to elicit a response; these enzymes are generally oxidases or dehydrogenases. Second generation sensors use a mediator to act as electron carrier, while in third generation sensors there is direct electron transfer between the enzyme and electrode (Rocchitta et al. 2016).

The development of an enzyme electrode/first enzyme-based biosensor for detection of glucose by Clark and Lyons in 1962 sparked significant interest in the field. In the 1970s Adams and co-workers showed the utility of electrochemical measurements for measuring catecholamines in CNS. Indeed, the glucose biosensor incorporating the enzyme glucose oxidase remains the most thoroughly investigated.

Electrochemical sensors have proven useful in study of various biological processes, with majority of work focused on neuroscience. Real-time monitoring of changes in concentrations of neurochemicals has furthered the understanding of the role of different neuroactive compounds (Wilson and Gifford 2005). The enzymatic biosensors used in brain research mostly utilize an oxidase enzyme. These biosensors have been developed on the principle of amperometric detection, which involves use of oxygen to oxidase the substrate, resulting in the generation of H_2O_2 which is measured at the surface of a Pt electrode, polarized to 500 – 700 mV relative to an Ag/AgCl reference. However, as not all substrates have a direct oxidase available for metabolism, a cascade of two to three enzymes in the sensor matrix, can be used, where the first enzyme is specific for the analyte of interest (Dale et al. 2005).

Based on the principle of amperometric detection, an enzyme electrode called the ‘dialysis electrode’ for real time continuous measurement of NT glutamate was prepared using the enzyme glutamate oxidase. This electrode combined the techniques of microdialysis with voltammetry. The electrode could be implanted in striatum of freely moving rats and allowed monitoring of changes in L-Glu concentration (Albery, Boutelle, and Galley 1992). By using the technique of enzyme immobilization, glucose oxidase enzyme was immobilized on Pt microelectrodes to prepare an amperometric glucose biosensor which was used for studying changes in glucose concentration in the right radiatum of freely moving rats (Lowry, Miele, et al. 1998; Lowry, O'Neill, et al. 1998). Additionally, these sensors also addressed the issue of interference from ascorbate and demonstrated the concept of differential measurement by performing simultaneous measurements for glucose and ascorbate. These sensors were the first in vivo monitoring devices, that demonstrated the importance of real-time measurements in brain extra cellular fluid and paved the way for microelectrode biosensors.

1.4 Microelectrode biosensors and their role in study of brain electrophysiology

The production of much smaller microelectrodes provides great utility in studying chemical signalling in the brain and allows for better temporal and spatial resolution. The performance criteria of the sensor depend on the nature of the analyte and also the intended application. For the sensor to perform efficiently, the sensor performance is evaluated on several parameters as noted in several reports (Wilson and Gifford 2005; Wilson and Johnson 2008; Georganopoulou et al. 2000). Amperomteric biosensors used in brain electrophysiology need to be sensitive with a faster response time as the extracellular concentration of NTs varies with very fast kinetics. The sensor should be selective as the presence of non-specific electroactive compounds such as urate, ascorbate interferes with the sensor response. Selectivity can be improved by using permselective polymer (such as Nafion, poly (phenylene diamine)) modified electrode which can screen for the interferents (Dale et al.

2005). The sensitivity and stability of the sensor depends on the method of enzyme immobilization as it determines how well the enzyme activity is preserved. There are several coating methods available for immobilization of enzymes and have been used to fabricate sensors for NTs. Some examples are: modified electropolymers such as pyrrole used for making sensors for L-Glu and dopamine (Cosnier et al. 1997); carbon fibre electrodes coated with redox hydrogels were used to make sensors for L-Glu and choline (Garguilo and Michael 1994; Kulagina, Shankar, and Michael 1999). Anodic electrodeposition paint has been reported for preparation of ATP sensor (Kueng, Kranz, and Mizaikoff 2004). Encapsulation of proteins in highly active form in silicate sol-gel (Dave et al. 1994) has led to the use of this method for biosensor fabrication (Sampath et al. 1996).

The Dale lab has been involved in the development of first-generation biosensors for detection of important signalling compounds in the brain. The lab has developed proprietary methods for coating microelectrodes with sol-gel layers containing active enzymes. The principle of this rapid and reproducible method is induction of a localized pH change to initiate crosslinking of silanes, which generates a porous layer and entraps the enzymes in a highly active state. A permselective layer is also added to screen for potential interferents and to retain the sensitivity of the sensors (Dale et al. 2005) (Dale and Frenguelli 2012). The design of the microelectrode biosensor and a view of the sensing layer is shown in Figure 1-2(a), along with the enzyme cascade for the ATP sensor in Figure 1-2(b) [adapted from (Dale et al. 2005)].

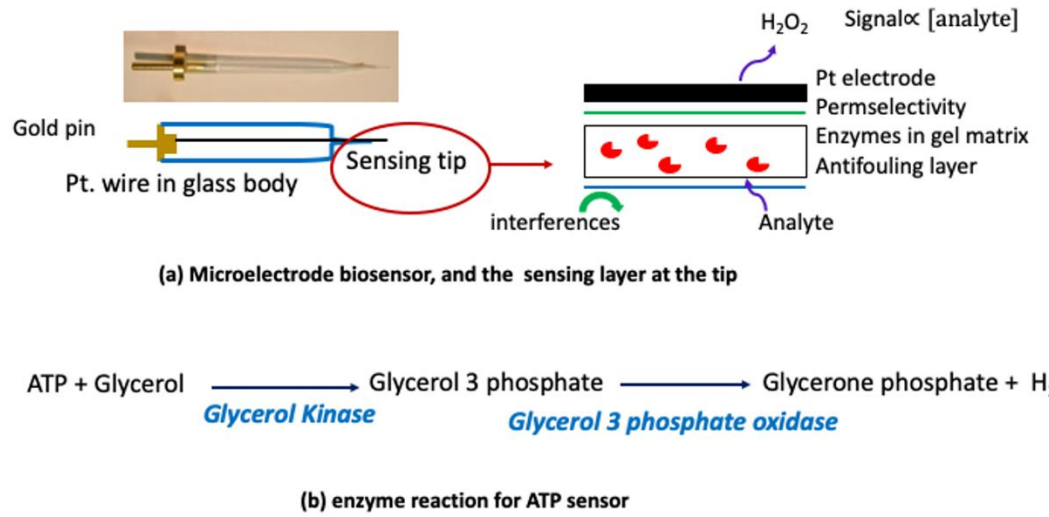

Figure 1-2. Schematic of an enzyme biosensor.

(a) Microelectrode biosensor and the sensing tip. The sol-gel layer with entrapped enzyme is shown. (b) Reaction cascade for ATP sensor.

Several biosensors have been developed using the sol-gel method and have been successfully used for measuring direct real-time release of neuroactive compounds in different areas of the brain. These include glutamate sensor (Tian et al. 2009), sensors for ATP and D-serine (Pankratov and Lalo 2015), and mainly purine sensors for detection of adenosine and ATP.

One of the main areas of focus in the lab has been the use of purine sensors in cortical brain slices and elucidating the role of ATP and adenosine as signalling molecules. The earliest measurement of adenosine release was done from the xenopus spinal cord during fictive locomotion. The technique involved the use of microdialysis tubing that contained adenosine metabolising enzymes (Dale 1998). Subsequent developments in biosensor coating technology, allowed for miniaturization of sensors with improved sensitivity and led to the fabrication of first microelectrode biosensor for adenosine (Llaudet et al. 2003), followed by a second sensor for ATP (Llaudet et al. 2005). The first use of biosensor for studying adenosine release by inserting into hippocampus was demonstrated in 2003 (Frenguelli, Llaudet, and Dale

2003). The lab has pioneered the use of purine sensors for measurement of purine release during metabolic stress and hypoxia which has revealed novel aspects of purinergic signalling. The purine sensors have also been used to investigate the release and effect of these molecules during seizure activity (Lopatář, Dale, and Frenguelli 2015).

These studies have highlighted the importance of the use of microelectrode biosensors for studying release of neurotransmitters and neuromodulators. The findings have also given valuable insight into the role of these compounds in brain physiology under different physiological conditions. As compared to other methods for/of detection of L-Glu, the development of amperometric sensor has been the most favoured method in vivo and in vitro as it provided fast and sensitive measurement of L-Glu (Albery, Boutelle, and Galley 1992; Tian et al. 2009).

Based on the principle of amperometric detection, microelectrode biosensors for L-Asp and NAA would be a novel addition to the repertoire of existing biosensors for neuroactive compounds and would help further the understanding of the role of these compounds in chemical signalling in the brain. The sol-gel method of coating would be used to develop these sensors. The enzyme L-aspartate oxidase (LAO) which oxidises L-Asp to release H_2O_2, (Leese et al. 2013) would be used for L-Asp sensor fabrication. The NAA sensor would require two enzymes: ASPA which metabolises NAA to L-Asp (Kaul et al. 1991), and LAO which can then act on L-Asp to release H_2O_2.

Aims of the project:

1. Develop and characterise microelectrode biosensor for L-Asp.

2. Use L-Asp sensor for real-time measurement of L-Asp release in brain slices

3. Develop microelectrode biosensor for NAA

Chapter 2

L-aspartate oxidase: Enzyme Purification and Properties

2.1 Introduction

The enzyme L-aspartate oxidase (LAO, EC 1.4.3.16) is an L-aspartate specific enzyme and belongs to the class of enzymes that catalyse oxidative deamination of L-amino acids. L amino acid oxidases (LAAO, EC 1.4.3.2) are flavin adenine dinucleotide (FAD) containing flavoenzymes, catalysing the stereoselective oxidative deamination of L-amino acids to an α-keto acid, and producing H_2O_2 in the process by reoxidising $FADH_2$. Several microbial and eukaryotic LAAOs have been identified, which have a catalytic specificity for hydrophobic and aromatic amino acids (Izidoro et al. 2014; Pollegioni, Motta, and Molla 2013; Andreo-Vidal, Sanchez-Amat, and Campillo-Brocal 2018). Because they have broad substrate specificity, these LAAOs are not suitable for biotechnological applications that require the enzyme to be specific for a particular analyte, and therefore not suitable for selective detection of L-Asp.

Similar to the LAAOs, the D-amino acid oxidases (DAAO, EC 1.4.3.3) are also widely distributed and catalyse the same reaction as LAAO. The main feature of these enzymes is their stereo-selectivity, hence amino acid oxidases with specificity for D or L isomers have evolved in nature (Takahashi 2020; Pollegioni et al. 2007). Several microbial LAAOs with strict preference for a specific amino acid have been identified, such as L-glutamate oxidase (LGO) (Arima et al. 2003), L-lysine oxidase, L-phenylalanine oxidase etc. These enzymes have been successfully overexpressed and studied (Pollegioni, Motta, and Molla 2013). The prokaryotic enzyme LAO encoded by the nadB gene is involved in the pathway for de novo biosynthesis of nicotinamide adenine dinucleotide (NAD^+). LAO was first identified in *E. coli* (EcLAO) and has been extensively characterised (Nasu, Wicks, and Gholson 1982; Mortarino et al. 1996). LAO from other prokaryotes including soil bacteria

Pseudomonas putida (PpLAO) (Leese et al. 2013) and thermophilic archea *Sulfolobus tokodaii* (StlLAO) (Bifulco et al. 2013) have also been purified and show very similar characteristics with EcLAO. The enzyme is a monomer of about 52-60 kDa and catalyses the same class of reaction as other LAAOs (Figure 2-1).

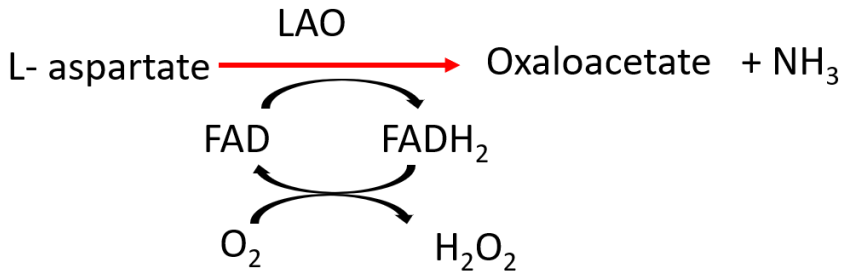

Figure 2-1. Reaction catalysed by LAO.
Oxidative deamination of L-Asp by LAO, with the simultaneous release of H_2O_2.

2.1.1 PpLAO as a suitable enzyme for sensor fabrication

To make efficient and stable enzyme-based sensors enzymes with a lower K_m that is appropriate to the desired analytical range and a high turnover number are preferred. To make the L-Asp biosensor, EcLAO was not considered as it had a high K_m of 4.9 mM and was a slow enzyme with a k_{cat} of 0.67 sec^{-1}. StLAO was the first LAO that had been immobilised and studied for biocatalysis (Armenia et al. 2017). It had a low K_m of 1.3 mM and since it was from thermophilic bacteria, it had a higher thermostability. Although these properties made StLAO an attractive candidate for making L-Asp sensor, it had some limitations. Firstly, the enzyme reached only 50% activity at temperature range of 25-37 °C. Secondly the preferred pH range was 8.0-11.0, with a pH optimum of 10.0 (Bifulco et al. 2013).These factors made StLAO unsuitable for the sensor as it would not function to its full potential at the required physiological pH (7.4) and temperature (37 °C). PpLAO had a K_m of 2.26 mM, higher reported k_{cat} of 10.6 sec^{-1}, showed optimum activity in the pH range 7.0-8.0, and was stable and active at temperatures from 20 °C - 40

°C. A comparison of the kinetic parameters of three LAO enzymes is shown in .

Table 2-1. (Tedeschi et al. 2010; Leese et al. 2013; Bifulco et al. 2013).

Table 2-1. *kcat* and *Km* values for EcLAO, StLAO and PpLAO

	k_{cat}	K_m (mM)
EcLAO	0.67 sec^{-1}	4.9mM
StLAO	1.05 sec^{-1}	1.3mM (with 0.21mM O_2 concentration)
PpLAO	10.6 sec^{-1}	2.26mM

PpLAO, with a higher k_{cat} than other two enzymes and lower K_m than EcLAO showed the highest kinetic efficiency at the required physiological conditions, making it an ideal choice for the sensor. Previously, a glutamate biosensor had been successfully made using the enzyme LGO. LGO had a K_m of 5.0 mM but a higher k_{cat} of 33 sec^{-1}, making it suitable for the sensor, as it showed a high sensitivity and response time. In addition, it also displayed high selectivity and specificity for L-Glu (Arima et al. 2003) (Tian et al. 2009). Thus, in order to make the L-Asp biosensor, it was important to check for these properties before sensor fabrication. Hence, the main aims for this chapter were to:

1. Express and purify PpLAO.
2. Test the activity and substrate specificity of PpLAO
3. Test the thermostability of PpLAO.

2.2 Material and Methods

2.2.1 Materials

Dithiothreitol (DTT), FAD, Horseradish peroxidase (HRP) and all amino acids were obtained from Sigma-Aldrich. Isopropyl-β-D-thiogalactopyranoside (IPTG) and 4-benzenesulfonyl fluoride hydrochloride (AEBSF) were obtained from VWR International. Amplex red (ARed) from Invitrogen and DNAseI was obtained from Roche. Sypro orange dye was obtained from Thermofisher. BL21(DE3), BL21(DE3)pLysS cells were obtained from NEB, while Bl21(DE3)GroES from Invitrogen. NEB pre stained protein marker (#P7712) was used for SDS PAGE.

2.2.2 Test expression of PpLAO

Codon optimised, (5' hexa-histidine tagged) nadB gene for LAO, from *Pseudomonas putida*, cloned into pET-28a(Kanamycin) was ordered from Genscript USA (pET28a:PpLAO). The plasmid was sequenced using T7 promoter (5'-TAATACGACTCACTATAGGG-3') and T7 terminator (5'-GCTAGTTATTGCTCAGCGG- 3') primers. For expression trials of PpLAO, the plasmid was transformed into *E.coli* BL21 (DE3), BL21(DE3) pLysS and BL21(DE3) GroES cells using heat-shock, 42 °C for 45s. Cells were plated on selective LB-Agar plates

Table 2-2: *E.coli* cell strains used in expression trials of pET-28a:PpLAO

Cell Strain	Antibiotic Resistance
BL21 (DE3)	Kanamycin (30 µg/mL)
Bl21(DE3) pLysS	Kanamycin (30 µg/mL), Chloramphenicol (35 µg/mL)
Bl21(DE3) GroES	Kanamycin (30 µg/mL), Ampicillin (100 µg/mL)

25ml of LB media with respective antibiotics was inoculated with a single transformed colony. Cells were grown at 37 °C or 25 °C with shaking at

180 rpm till they reached OD 600 of 0.6, upon which they were induced with IPTG to a final concentration of 1mM. For Bl21(DE3) cultures, samples were collected after 1, 2 and 3 hrs of induction; for both Bl21(DE3) plysS and Bl21(DE3) GroES cultures samples were collected after 3 hrs of induction. Cells were then harvested by centrifugation in bench top centrifuge (Eppendorf centrifuge 5424) at 11000g for 10 minutes. For analysing expression, samples were prepared as follows:

Total protein (TP) expression: 1ml of pelleted cells was resuspended in 2xSDS loading buffer (0.12M Tris-HCl, pH 6.8, 20% (v/v) glycerol, 4% (w/v) SDS, 10mM DTT, 0.01% (w/v) bromophenol blue). 200 µl/OD of loading buffer was added. Samples were then sonicated on ice for 5s (Bandelin sonoplus, UW2070).

Separation of soluble and insoluble fractions: 1ml of pelleted cells was resuspended in water: 100µl/OD. Resuspended samples were sonicated on ice for 5s, followed by centrifugation at 11000g for 10 minutes. The supernatant was collected and mixed with 2xSDS loading buffer in 1:1 ratio – soluble fraction (SF). The pellet was again resuspended in water (same volume as before) and then mixed with 2XSDS loading buffer in 1:1 ratio- insoluble fraction (IF).

All samples were boiled and cooled for 10 minutes, before loading on 12% SDS-PAGE gels for analysis.

2.2.3 Purification of PpLAO

pET-28a:PpLAO was transformed into chemically competent *E.coli* BL21 (DE3) cells using heat-shock, 42 °C for 45s. Cells were plated on Kanamycin (Kan), 30 µg/ml, selective LB-Agar plates. Two 50ml LB media, starter cultures were inoculated with a single transformed colony. Cells were grown at 25 °C overnight with shaking at 180 rpm. Two 500 ml cultures with 30 µg/ml Kan were inoculated with the 50 ml starter cultures. Cells were then grown at 25 °C with shaking at 180 rpm, till they reached OD 600 of 0.6, upon which they were induced with IPTG to a final concentration of 1mM. After 3

hours of induction cells were harvested by centrifugation at 8000g for 20 minutes using JA-10 rotor (Beckman Coulter centrifuge). Harvested cells were snap frozen in liquid N_2 and stored in -80 °C.

Cell pellet was thawed on ice, weighed and re-suspended (4 ml/gm of pellet) in resuspension buffer (50 mM Tris/HCl, 300 mM NaCl, 0.2 mg/ml protease inhibitor AEBSF, 10 µg/ml DNAseI, 60 µM FAD, pH 7.5). After placing on ice for 15 minutes, cells were sonicated on ice (6 times for 30 seconds at 60% power, with 1-minute cooling in between). Sonicated cell suspension was then spun in JA 25.5 rotor (Beckman Coulter), at 24000g for 45 minutes. Collected supernatant was filtered through a 0.45 µm and 0.2 µm syringe filter (Acrodisc) and adjusted to 0.5 M NaCl (final concentration). A 5 ml HisTrap^{tm} HP Ni column (GE Healthcare) was pre-equilibrated with equilibration buffer (50 mM Tris/HCl, 300 mM NaCl, 30 mM Imidazole, pH 7.5) in AKTA system (GE Healthcare) maintained at 4 °C. Column was then loaded with the supernatant. After washing the unbound protein with equilibration buffer, bound protein was eluted by running a gradient of 0- 350 mM imidazole within the elution buffer (50 mM Tris/HCl, 300 mM NaCl, 350 mM Imidazole, pH 7.5). 2 ml fractions were collected in deep well 96-well plate (ThermoFisher) and analysed on SDS-PAGE. Fractions showing the protein (correct molecular weight of ~60 kDa) were pooled together and dialysed against the dialysis buffer (50 mM Tris/HCl, 300 mM NaCl, 50% glycerol, pH 7.5). Dialysed protein was further concentrated using the Vivaspin 500 MWCO 10000 (GE Life sciences) column, by centrifugation at 3000g (Eppendorf centrifuge 5804R). Final protein concentration was measured on Implen NanoPhotometer N60/N50. Purified protein was then flash cooled in liquid N_2 and stored in -80°C. Protein gel bands were quantified using ImageJ (Schneider, Rasband, and Eliceiri 2012).

2.2.4 Activity assay

PpLAO enzyme activity was measured by measuring the initial rate of hydrogen peroxide (H_2O_2) production in Amplex Red/horseradish peroxidase (ARed/HRP) dye coupled assay. H_2O_2 formation was measured

spectrophotometrically with ARed at 555 nm (ε=54000 M−1cm−1) (Karamitros, Lim, and Konrad 2014). All solutions were freshly prepared. The assay mixture contained 0.05 mg/ml of HRP, 0.05 mM ARed, in phosphate buffered saline (PBS), pH 7.4, in a total volume of 0.2 ml. 1µl of purified PpLAO (50-60 mg/ml) was added and activity of PpLAO was measured against the following concentrations of L-Asp: 1 µM, 3 µM, 10 µM, 30 µM, 100 µM and 300µM. Substrate specificity of PpLAO was measured against: N-acetyl aspartate (NAA), L-asparagine (L-Asn), L-glutamate (L-Glu), L-glutamine(L-Gln) and D-aspartate (D-Asp) at 100µM concentration. Data was analysed using Origin (Pro) 2019b. All data presented as mean and SD from three independent assays, performed in triplicate.

2.2.5 Thermal shift assay

The thermal shift assay for PpLAO was done using the SYPRO orange dye (Sigma Aldrich). Increasing concentrations of the enzyme (0.84 μM, 1.6 μM, 4.2 μM and 8.4 μM) were mixed with 30x dilution of SYPRO orange dye, in 50 mM Tris/HCl, 300 mM NaCl, pH 7.5, to a final concentration of 20 μl. For each concentration, reactions were set in triplicate, including a blank, in a 96-well plate. The assay was conducted in an Agilent Mx3000p qPCR machine. The plate was heated from 25 °C to 95 °C at a rate of 1 °C/minute. Fluorescence was measured at excitation and emission wavelengths of 470 nm and 570 nm respectively. Data was analysed and Tm was calculated by performing a non-linear fit of truncated data to a Boltzmann sigmoidal curve, in GraphPad Prism (V 8.3). Data presented as mean and SD.

2.3 Results

2.3.1 Expression and purification of PpLAO

The 5’ hexa-histidine tagged nadB gene for PpLAO, cloned into pET-28a (Figure 2-2) was sequenced using the T7 promoter and T7 terminator primers. Sequencing of the plasmid showed that the gene was inserted correctly, and the translated sequence aligned with the amino acid sequence

of PpLAO available on the UniProt Consortium (UniProt: a worldwide hub of protein knowledge) (Figure 2-3).

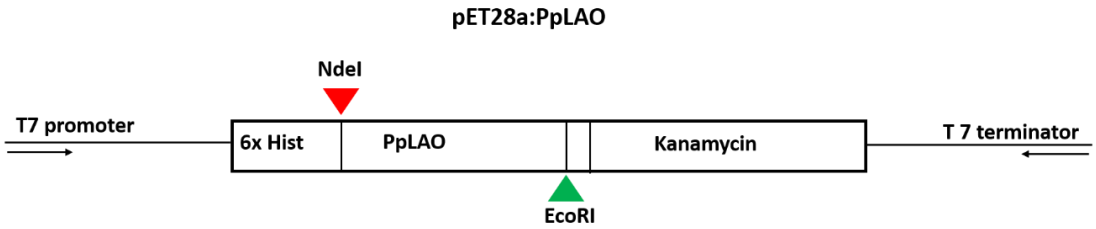

Figure 2-2: Vector pET28a with His-tagged PpLAO cloned between NdeI and EcoRI. T7 promoter and T7 terminator primers were used for full sequencing of the gene.

```
Translatedseq      HHHHHHSSGLVPRGSHMSQQFQHDVLVIGSGAAGLSLALNLPSHLRVAVLSKGDLSNGST
         60
Uniprotseq         ----------------MSQQFQHDVLVIGSGAAGLSLALNLPSHLRVAVLSKGDLSNGST
         44
                                   ******************************************

Translatedseq      FWAQGGVAAVLDNTDTVQSHVEDTLNAGGGLCHEDAVRFTVEHSREAIQWLIEQGVPFTR
         120
Uniprotseq         FWAQGGVAAVLDNTDTVQSHVEDTLNAGGGLCHEDAVRFTVEHSREAIQWLIEQGVPFTR
         104
                   ************************************************************

Translatedseq      DEHYSVDDGGFEFHLTREGGHSHRRIIHAADATGAAIFTTLLEQARQRPNIQLLEQRVAV
         180
Uniprotseq         DEHYSVDDGGFEFHLTREGGHSHRRIIHAADATGAAIFTTLLEQARQRPNIQLLEQRVAV
         164
                   ************************************************************

Translatedseq      DLITERRLGLPGERCLGAYVLDRNTGEVDTFGARFTVLATGGAAKVYLYTSNPDGACGDG
         240
Uniprotseq         DLITERRLGLPGERCLGAYVLDRNTGEVDTFGARFTVLATGGAAKVYLYTSNPDGACGDG
         224
                   ************************************************************

Translatedseq      IAMAWRAGCRVANLEFNQFHPTCLYHPQAKSFLITEALRGEGALLRLPNGERFMPRFDPR
         300
Uniprotseq         IAMAWRAGCRVANLEFNQFHPTCLYHPQAKSFLITEALRGEGALLRLPNGERFMPRFDPR
         284
                   ************************************************************

Translatedseq      EELAPRDIVARAIDHEMKRLGVDCVYLDITHKPADFIKSHFPTVYERCLAFGIDITRQPI
         360
Uniprotseq         EELAPRDIVARAIDHEMKRLGVDCVYLDITHKPADFIKSHFPTVYERCLAFGIDITRQPI
         344
                   ************************************************************

Translatedseq      PVVPAAHYTCGGVMVDDCGHTDVPGLYAIGETSFTGLHGANRMASNSLLECFVYGRAAAA
         420
Uniprotseq         PVVPAAHYTCGGVMVDDCGHTDVPGLYAIGETSFTGLHGANRMASNSLLECFVYGRAAAA
         404
                   ************************************************************

Translatedseq      DIQAHLEQVAMPKALPGWDASQVTDSDEDVIIAHNWDELRRFMWDYVGIVRTSKRLQRAQ
         480
Uniprotseq         DIQAHLEQVAMPKALPGWDASQVTDSDEDVIIAHNWDELRRFMWDYVGIVRTSKRLQRAQ
         464
                   ************************************************************

Translatedseq      HRIRLLLDEIDEFYSNYKVSRDLIELRNLAQVAELMILSAMQRKESRGLHYTLDYPGMLD
         540
Uniprotseq         HRIRLLLDEIDEFYSNYKVSRDLIELRNLAQVAELMILSAMQRKESRGLHYTLDYPGMLD
         524
                   ************************************************************

Translatedseq      EAKDTILNPL       550
Uniprotseq         EAKDTILNPL       534
                   **********
```

Figure 2-3: Amino acid sequence alignment for PpLAO.

nadB_LAO: sequence of PpLAO available on The UniProt consortium. PpLAO: translated sequence obtained after sequencing with T7 primers. Both sequences show perfect alignment. Hexa-histidine sequence and linker are highlighted at the beginning of the translated sequence.

Different cell strains and temperature conditions were tested to attain the best expression of PpLAO. SDS PAGE analysis of the protein fractions

from expression in BL21(DE3) cells indicated that the protein was present in both soluble and insoluble fractions, and the percentage of expressed protein in the soluble fraction was higher when it was expressed at 25 °C, compared to 37 °C (Figure 2-4).

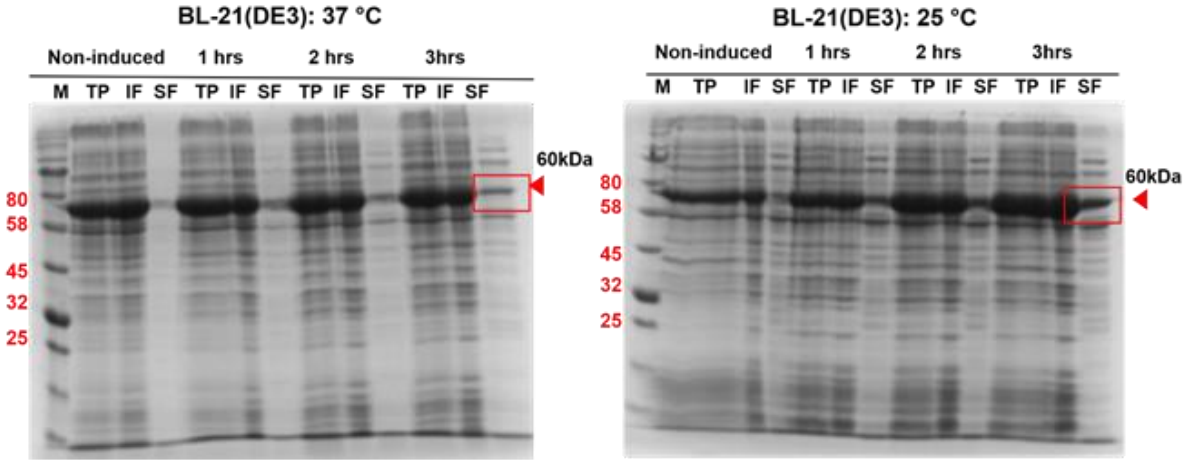

Figure 2-4: Expression of PpLAO in Bl21(DE3) at 37 °C and 25 °C after 1, 2 and 3 hrs of induction.

M: NEB pre-stained marker, TP: Total protein, IF: Insoluble fraction, SF: soluble fraction. Higher expression of PpLAO is observed after 3 hrs of induction at 25 °C.

BL21(DE3)pLysS and BL21(DE3)GroES cells were also tested at 25 °C and 37 °C, to see if changing the cell strain had any effect on overall protein expression and solubility (Figure 2-5). Expression in pLysS cells was reduced, while majority of the protein was present in insoluble compartment in GroES. A comparison of soluble fractions from the three cell strains (at 25 °C) showed that the best protein expression was seen in Bl21(DE3) cells (Figure 2-6). Hence, these cells were used for large-scale protein purification.

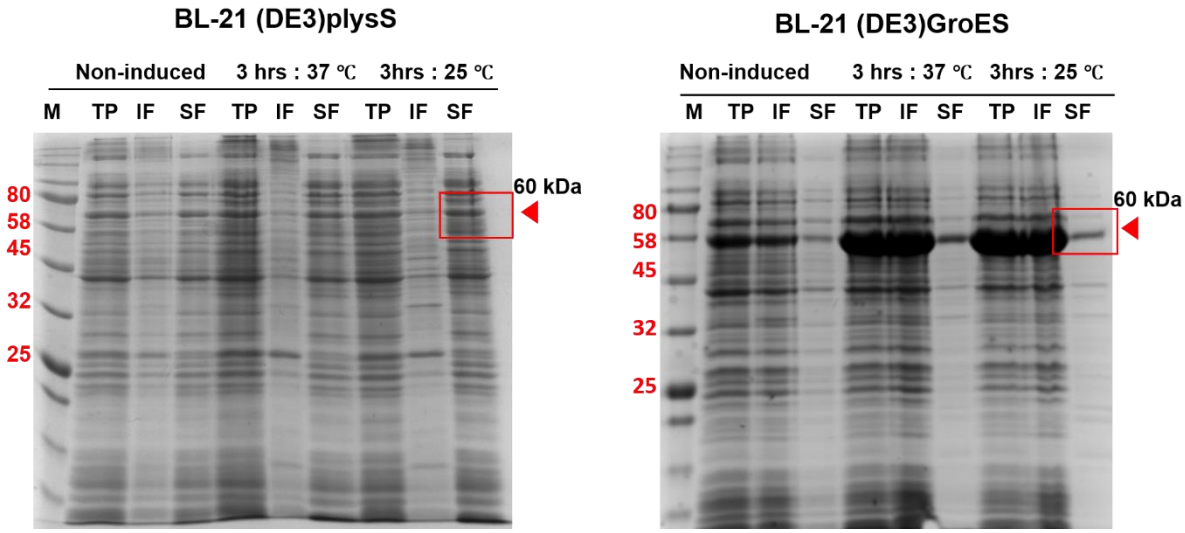

Figure 2-5: Expression of PpLAO in (Left) Bl21(DE3)pLysS and (Right) Bl21(DE3)GroES at 37 °C and 25 °C after 3 hrs of induction.

M: NEB pre-stained marker, TP: Total protein, IF: Insoluble fraction, SF: Soluble fraction. Very little expression was seen in pLyS cells. Good expression in GroES cells, but majority of protein in IF.

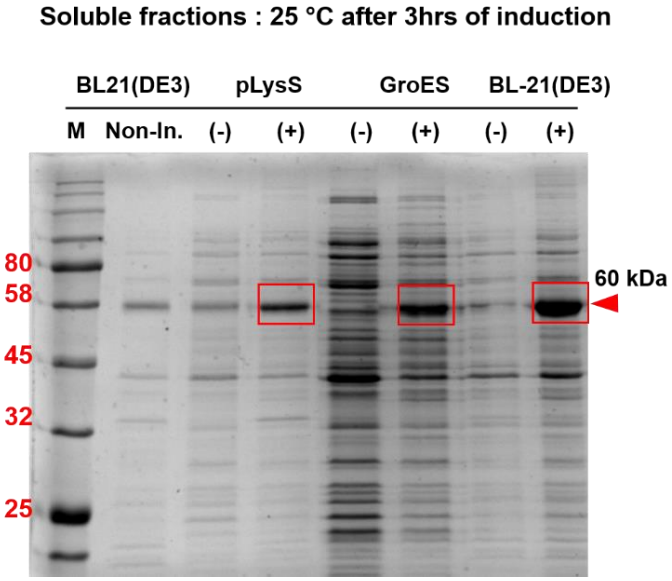

Figure 2-6: Comparison of soluble fractions from the three cell strains at 25 °C after 3 hrs of induction.

M: NEB pre-stained protein marker, Non-in: SF from non-induced BL-21(DE3) cells, (-): SF from non-induced cell, (+): SF from induced cells. Maximum protein expression with high percentage of protein in soluble fraction was observed in BL21(DE3) cells.

PpLAO was purified from the soluble fraction. The presence of the hexa-His tag at the N-terminus, allowed for the protein to be purified on a Nickel column. A gradient of 0-350mM imidazole was applied to elute the protein; PpLAO eluted in a tight peak (Figure 2-7), with practically all of the protein present in the fractions corresponding to the area under the peak (fractions D1-D9) (Figure 2-8 (a)). These fractions were pooled together and dialysed to remove imidazole. The protein was of the expected size of 60 kDa (Figure 2-8 (b)) and imageJ analysis of the gels showed that it was >90% pure. Pure protein was yellow in colour, indicating presence of bound oxidised FAD. On average, protein yield after dialysis was 12-15 mg/ml from 2L culture, and it was further concentrated to 50-60 mg/ml (final volume 2 mls). 100µl aliquots of the protein were flash cooled in liquid N2 and stored in -80° C until use.

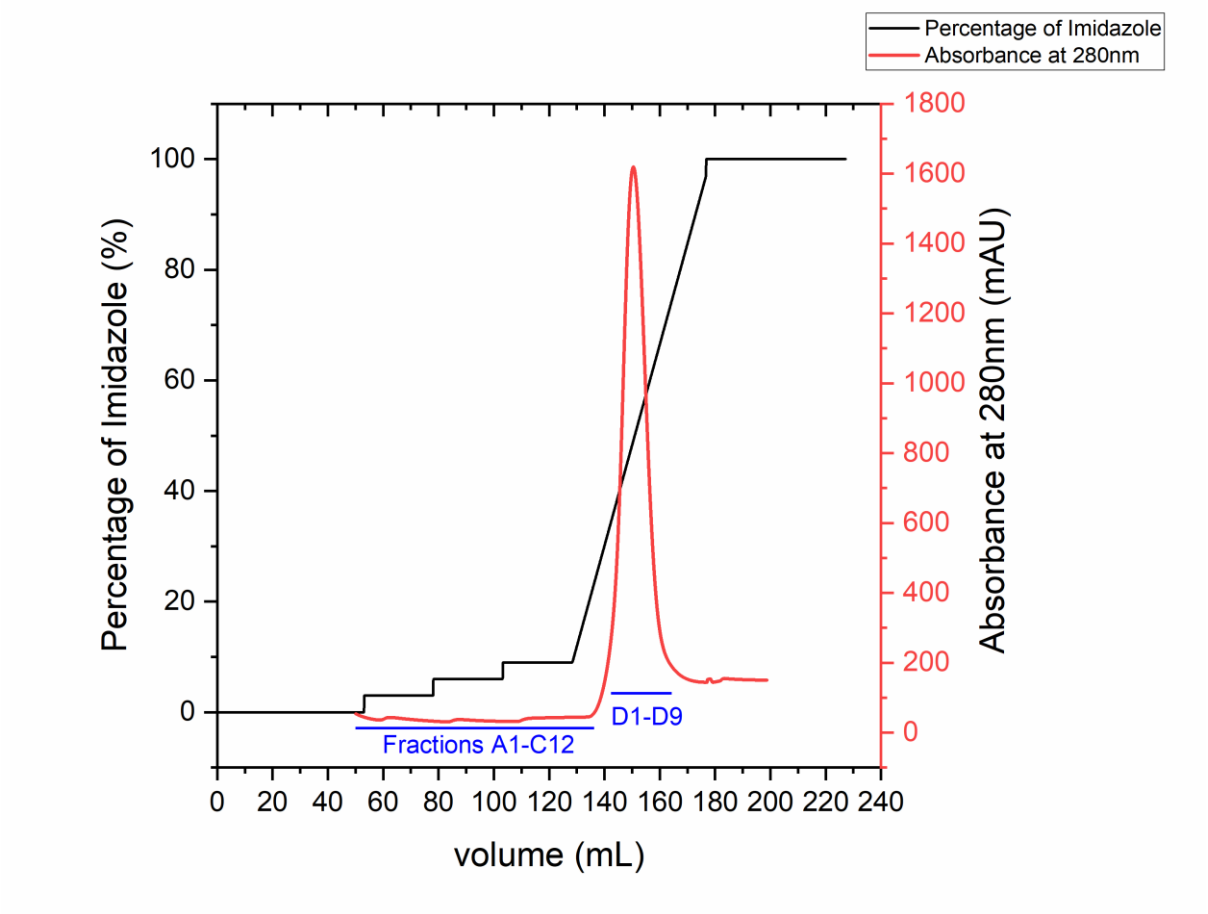

Figure 2-7: Purification of PpLAO on HisTrap™ column.

PpLAO eluted in a tight peak with increasing gradient of imidazole

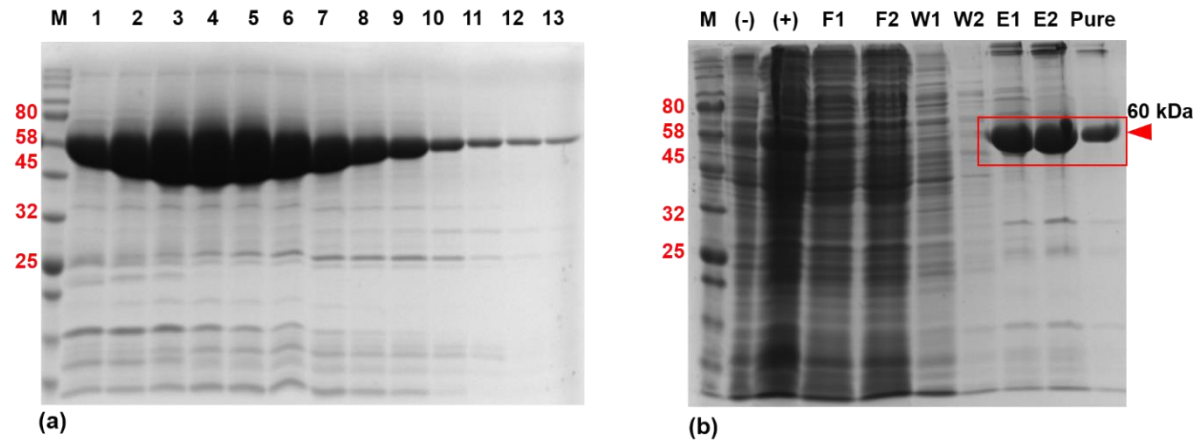

Figure 2-8: PpLAO purification gels.

(a) Lanes 1-9: fractions D1-D9, maximum protein present in these fractions, Lanes 10-13: fractions D10-D12 and E1. (b)(-):Total protein non-induced cells, (+) Total protein from induced cells, F1-F2: load flow through, W1-W2: column washes before applying elution buffer. E1-E2: eluted protein before dialysis. Pure: pure protein after dialysis and concentrating.

2.3.2 Activity and specificity of PpLAO

The activity of PpLAO towards L-Asp was measured using the ARed/HRP coupled assay system. LAO oxidises L-Asp to OAA, simultaneously producing H_2O_2. ARed reagent in the presence of HRP, reacts with H_2O_2 and is converted to a fluorescent compound, resorufin (Figure 2-9)(Karamitros, Lim, and Konrad 2014). Rate of formation of resorufin was measured at 555 nm and depends on the rate of formation of H_2O_2 by LAO

The specific activity of the enzyme was measured against increasing substrate concentrations, at a fixed enzyme concentration. By performing a non-linear fitting of Lineweaver-Burk plot, K_m and V_{max} of PpLAO was. determined to be 222.2 µM and 6.67 µmol/min/mg (R^2 = 0.97) respectively. Using these parameters, k_{cat} was calculated to be 6.7 s^{-1}. No activity was seen for L-Asp concentration of 1 µM, hence this data point was eliminated from analysis (Figure 2-10).

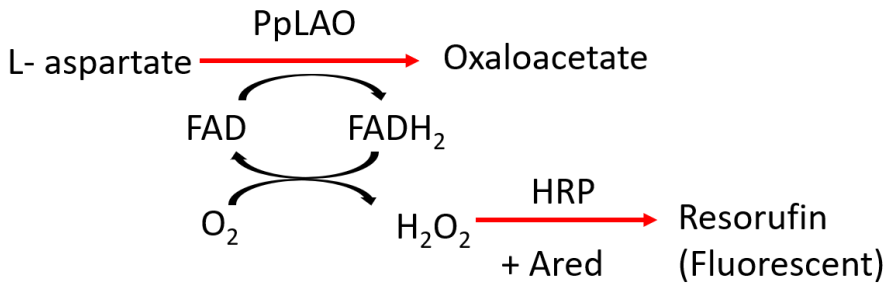

Figure 2-9: Amplex red coupled assay system for detection of PpLAO activity.

H_2O_2, in the presence of HRP, reacts with Ared reagent to form the fluorescent compound Resorufin. Appearance of Resorufin is measured at 555 nm.

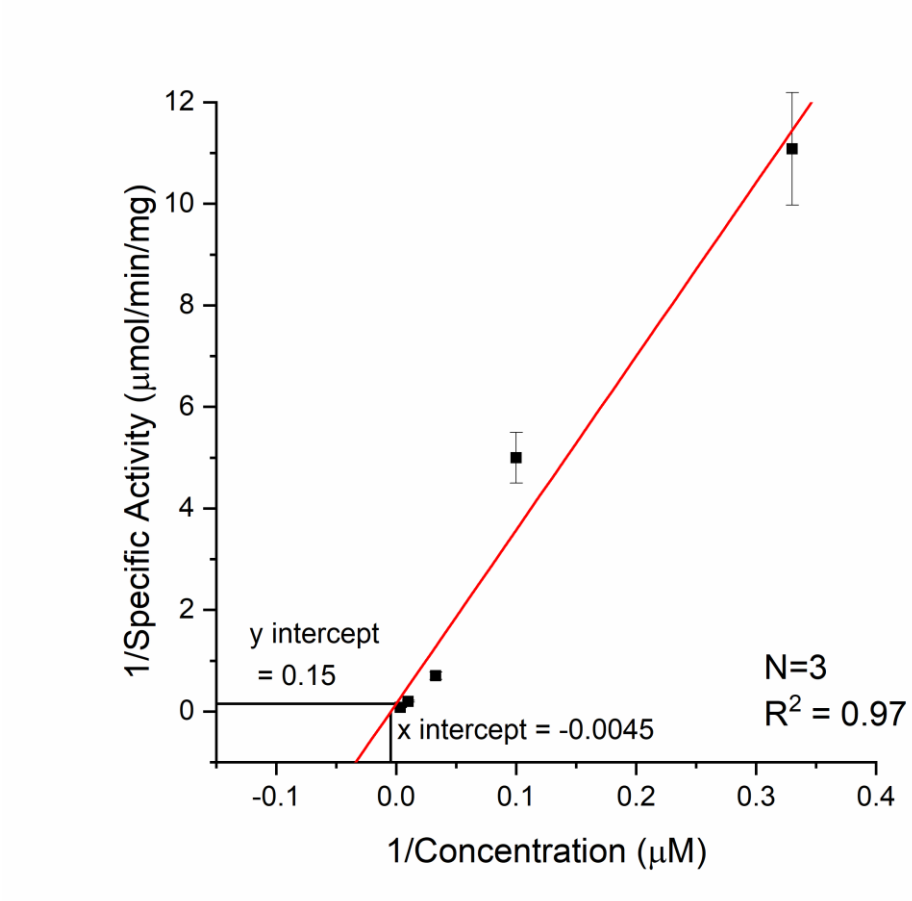

Figure 2-10: Lineweaver-Burk plot of initial velocity of PpLAO.

For each assay, activity was measured at fixed enzyme concentraion and increasing L-Asp concentration (1 µM, 3 µM, 10 µM, 30 µM, 100 µM, 300 µM). V_{max} is 1/y intercept = 6.67 µmol/min/mg, while *Km* = 1/ x intercept = 222.2 µM.

The PpLAO enzymatic activity (Figure 2-10) was analysed using double-reciprocal Lineweaver-Burk plot which can bring a significant instrumental error in K_m value at small concentration of substrate. This data was also analysed using the Eadie-Hofstee plot (V vs V/S).

The Lineweaver-Burk plot is the classical method used for determination of enzyme kinetics but is also prone to errors. As it is a reciprocal plot, it gives undue weight to measurements made at lower concentrations. In addition, some points are found on far too right of the y-axis, which requires large extrapolation to obtain the intercepts. Hence another method, the Eadie-Hofstee method was also used to determine K_m and specific activity (Figure 2-11). By performing a non-linear fitting of Lineweaver-Burk plot, K_m and V_{max} of PpLAO was determined to be 222.2 µM and 6.67 µmol/min/mg (R^2 = 0.97) respectively. K_m from Eadie-Hofstee method was found to be 214.6 µM while V_{max} was 14.5 µmol/min/mg (R^2 = 0.93). Both the methods gave very similar K_m values for LAO, but still lower than the reported value of 2.26 mM. The specific activity determined from Eadie-Hofstee method was higher than the reported value, while it was lower than the reported value of 10 µmol/min/mg. As observed from the R^2 value, a good fit was observed for both methods

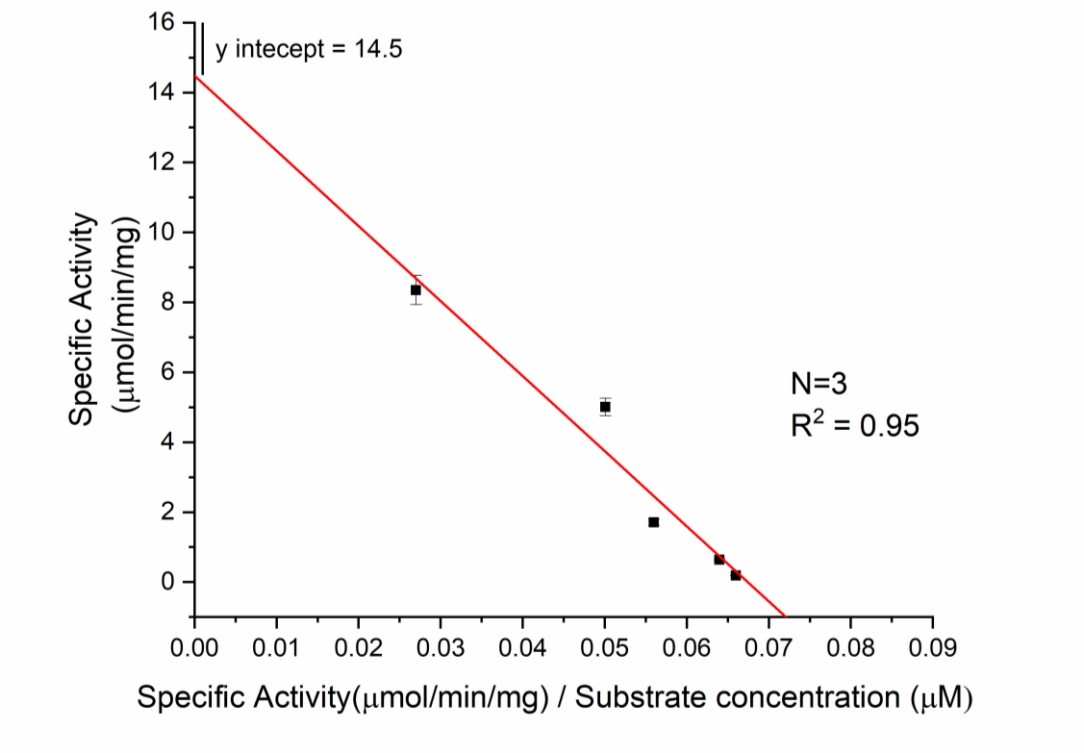

Figure 2-11: Eadie-Hofstee plot of initial velocity of PpLAO.

For each assay, activity was measured at fixed enzyme concentration and increasing L-Asp concentration (1 µM, 3 µM, 10 µM, 30 µM, 100 µM, 300 µM). V_{max} is y intercept = 14.5 µmol/min/mg, while *Km* is the slope = 214.6 µM.

Figure 2-12 shows the substrate specificity of PpLAO towards L-Asp. Reactions with no substrate and no enzyme were used as negative controls. The enzyme had no activity towards NAA, L-Glu and D-Asp (like the controls), while very little activity was observed towards L-Asn and L-Gln indicating that PpLAO was highly specific towards L-Asp

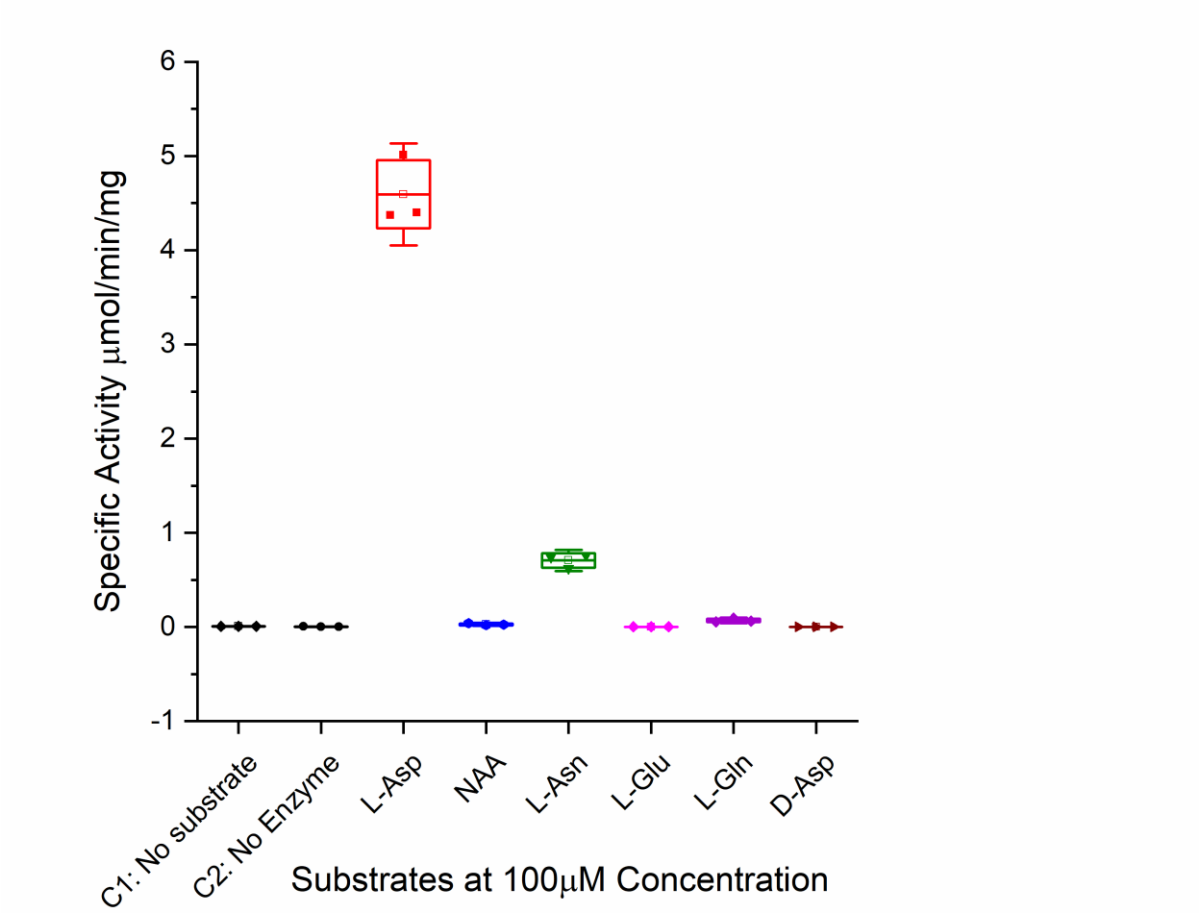

Figure 2-12. Substrate specificity of PpLAO.

Activity of PpLAO was measured against different substrates at fixed concentration of 100µM. Two reactions, one with no L-Asp and one with no enzyme were used as controls C1 and C2 respectively. PpLAO showed highest activity towards L-Asp indicating high substrate specificity

2.3.3 Thermal stability of PpLAO

Thermal stability assay of PpLAO was performed in order to determine its melting temperature (Tm). Tm of a protein is the temperature at which both the folded and unfolded state of the protein are equally present and gives an idea of the overall stability of the protein, higher the Tm, more stable the protein. Thermal stability curve and Tm can be obtained by incubating the protein with a temperature sensitive dye (SYPRO Orange), and by gradually increasing the temperature (Figure 2-13). As the temperature increases, the protein begins to unfold, allowing the dye to bind to the exposed hydrophobic regions of the denatured protein and causing an increase in fluorescence

which is monitored. Protein melting curves obtained are sigmoidal in nature, representing the cooperative unfolding of the protein. As the protein unfolds completely, there is protein aggregation and fluorescence quenching beyond the peak. Data is processed to truncate the dataset and remove post- peak quenching. The resulting sigmoidal curves can be fitted to a Boltzmann equation to determine the Tm.(Nettleship et al. 2008; Huynh and Partch 2015). The equation is useful as it describes fluorescence emission as a function of temperature.

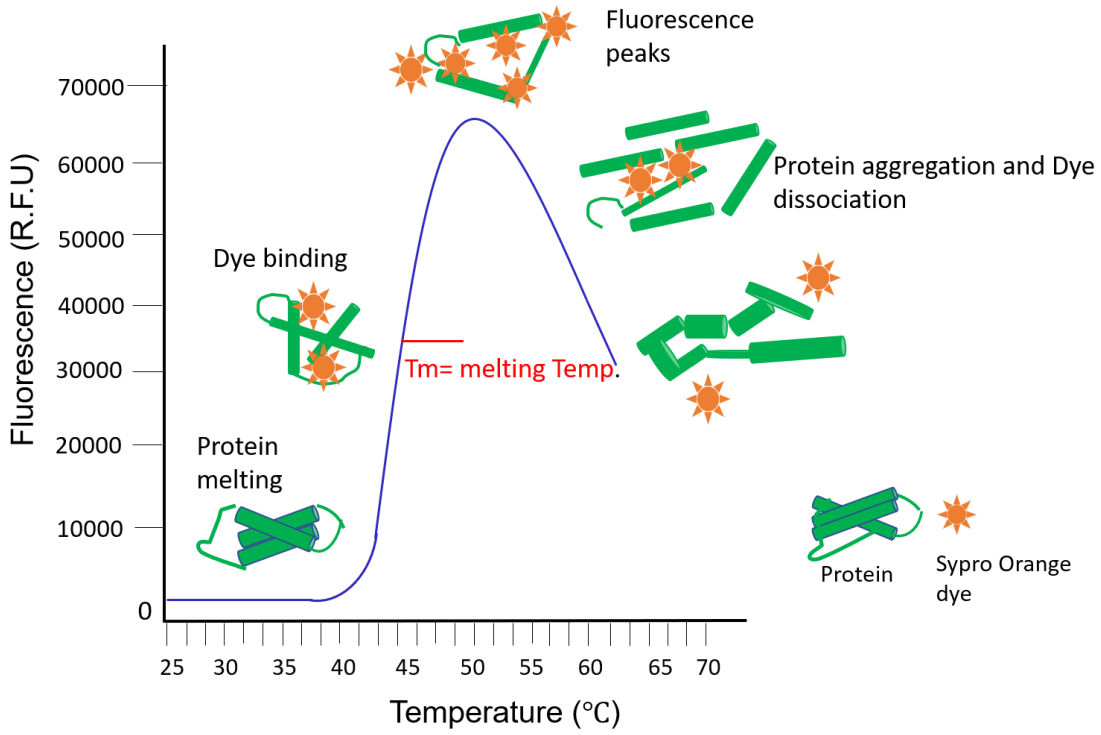

Figure 2-13: Thermal stability assay using SYPRO Orange dye.

Protein unfolding with increase in temperature is quantified by increase in fluorescence emission of the dye (R.F.U: relative fluorescence units). This increase reaches a peak where the protein is completely denatured, thereafter there is post-peak quenching as the protein aggregates and the dye dissociates

Thermal denaturation curves of PpLAO are shown in Figure 2-14. Average Tm of PpLAO was determined to be 47.6 °C in Tris/HCl storage buffer, indicating the protein to be fairly stable in this buffer.

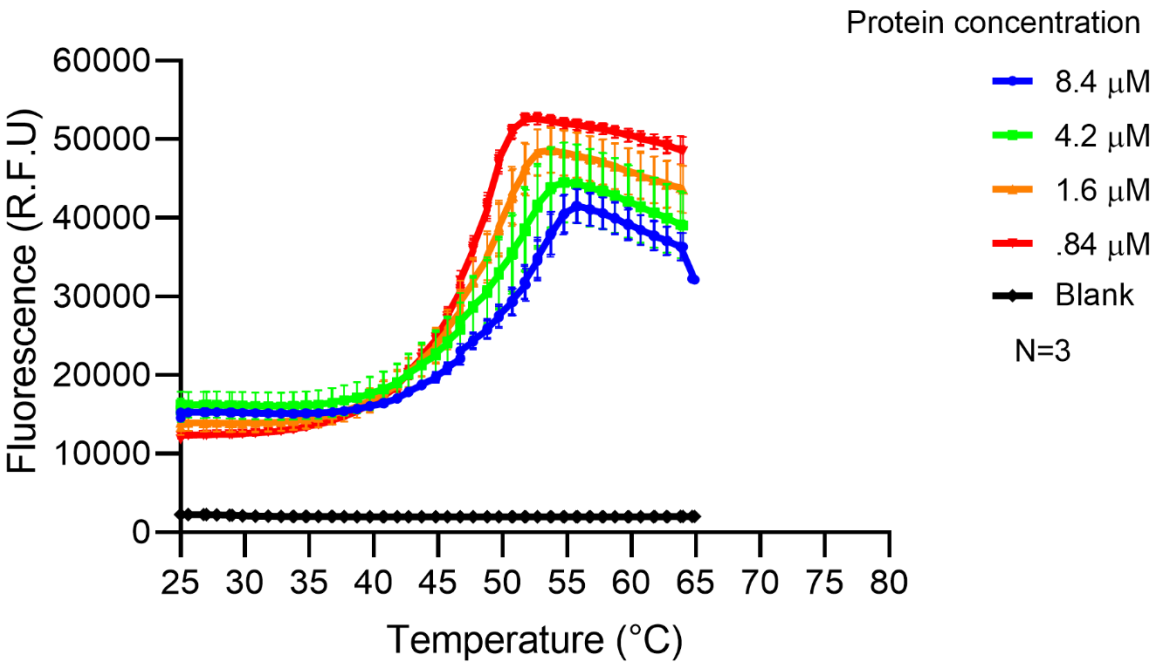

Figure 2-14: PpLAO thermal denaturation curves.

PpLAO denaturation curve at each concentration. Dataset is truncated to remove post-peak quenching and the curves undergo non-linear fitting to a Boltzmann equation to identify the average T_m for PpLAO as 47.6 °C.

2.4 Discussion

Recombinant protein expression of PpLAO showed that the protein is highly expressed, with a sufficient proportion in the soluble compartment. Because of the high expression, part of it is also present in the insoluble fraction. Overexpression of proteins often results in formation of inclusion bodies (IB) and recovery of correctly folded protein from IBs is an extensive and time-consuming process (Singh et al. 2015). Hence, different cells were tested to check if changing cell type improves solubility. However best expression was observed in BL21(DE3) cells and hence these cells were used for further purification.

The purification method I developed for PpLAO differed from previous reports(Leese et al. 2013; Bifulco et al. 2013), mainly in two aspects: firstly, the protein expression was at 25 °C, which resulted in better expression in soluble compartment. Secondly I used a lower concentration of imidazole (350

mM), than reported previously (500mM) (Leese et al. 2013). This lower temperature and elution concentration resulted in a better yield of the protein (~6 mg/l).

The ARed/HRP coupled assay was used for determination of PpLAO activity as it has low toxicity, and is a rapid and sensitive assay, for detection of H_2O_2. The ARed/HRP assay has been implemented for determination of several different oxidases at very low enzyme and substrate concentrations in a variety of different buffer systems (Karamitros, Lim, and Konrad 2014; Mishin et al. 2010; Rodriguez et al. 2010).

The assay allowed for the determination of PpLAO activity towards L-Asp concentration in micromolar range. K_m and V_{max} were found to be 222.2 µM and 6.67 µmol/min/mg respectively which are lower than the reported values of PpLAO (K_m of 2.26 mM and V_{max} of about 10 µmol/min/mg (Leese et al. 2013)) with L-Asp as substrate. This difference in kinetic parameters could be because previous assays of LAO were performed at a higher concentration range (1-50 mM) of the substrate, with different coupling reagents such as 4-aminoantipyrine (in the presence of phenol) or 2,4,6-tribromo3-hydroxybenzoic acid. Ideally, to measure the initial rates, the substrate concentration is set between 0.2-5 times the K_m (Brooks et al. 2004), suggesting a range of 0.4 -12 mM for L-Asp based on literature values. However, since my aim was to use the enzyme to make an L-Asp biosensor, detectable activity at a lower, physiologically relevant concentration range was desirable.

The enzyme showed a very high substrate specificity towards L-Asp, as in the spectrophotometric assay no activity was observed for NAA, L-Glu and D-Asp. Very low activity was observed for L-Asn, as well as L-Gln. Activity of PpLAO has been observed against L-Asn and L-Glu, but at very high concentrations,10-20 mM for L-Asn and >50mM for L-Glu (Leese et al. 2013). As reported for LAOs from other organisms (Nasu, Wicks, and Gholson 1982; Washio and Oikawa 2018), PpLAO was also stereoselective and did not show any activity against D-Asp.

Since the goal was to use this enzyme in enzyme-based L-Asp sensor, it was important to check its stability along with activity. Sensor fabrication protocol is carried out at room temperature (~ 25 °C), while experiments involving the use of the sensor are conducted either at room temperature or physiological temperature of 37 °C, hence the enzyme must remain stable at these temperatures for the sensor to perform reliably. SYPRO Orange thermal stability assay is a simple and useful tool to assess the stability of proteins at different temperatures and in the desired buffers. Melting curves of PpLAO, along with the average T_m of 47.6 °C, indicate that the enzyme is stable at these temperatures (in TRIS/HCl buffer) and begins to unfold only beyond 40 °C.

In conclusion, the purification method developed for PpLAO generated an enzyme with good yield and more than >90% purity. It had a promising K_m and activity in the micromolar range. The enzyme also had excellent substrate specificity towards L-Asp and good thermal stability and therefore a suitable enzyme to make the L-Asp biosensor.

Chapter 3

L-asp sensor: Optimisation, characterisation and detection

3.1 Introduction

Successful amperometric detection of L-Asp requires a biosensor that is fast, sensitive and selective in making L-Asp measurements, especially in *in vivo* samples. A previous approach for development of L-Asp biosensor involved use of a redox mediator- hexacyanoferrate, had an elaborate sensor design with five platinum (Pt) working electrodes and required several steps for sensor preparation and enzyme immobilisation. This sensor was low on sensitivity, with a lower detection limit of 1 mM (Röhlen et al. 2017). Hussain *et al.* have reported an enzyme-free sensor, that was fabricated by depositing iron oxide doped zinc oxide nanoparticles on dried glass carbon electrode. This sensor was not specific for L-Asp as it was designed for simultaneously detection of L-Asp and glycine (Hussain, Asiri, and Rahman 2020).

In order to make the L-Asp biosensor, I used an established silicate sol-gel method of enzyme immobilisation on Pt microelectrodes. Highly selective and sensitive microelectrode biosensors for detection of L-Glu and purines (ATP and Adenosine) have been constructed in the Dale lab using this method (Tian et al. 2009; Dale and Frenguelli 2012; Llaudet et al. 2005). These biosensors respond rapidly and exhibit a linear response to analyte concentrations. The L-Asp biosensor fabrication would involve immobilisation of purified PpLAO and the enzymatic scheme for L-Asp sensor is shown in Figure 3-1. The changes in current caused by oxidation of H_2O_2 would be detected at the surface of electrode and amount of H_2O_2 released would be proportional to the concentration of L-Asp.

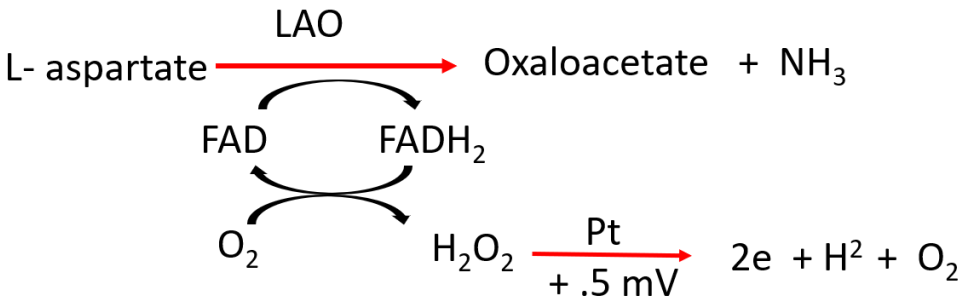

Figure 3-1. Enzymatic scheme for L-Asp sensor.

The H_2O_2 released during the reaction is detected by its oxidation on the electrode surface which is polarised to +0.5 mV relative to Ag/AgCl.

3.1.1 Sensor fabrication

Pt is an advantageous preferred material for the microelectrodes as Pt wires could reach the deep structures of the brain and oxidise H_2O_2 at currents +0.3 mV - +0.7 mV (Marinesco S. 2013). In addition to the electrode, the method of enzyme immobilisation on the sensor tip is an important step that could impact the overall performance of the sensor. The immobilised enzyme should be stable over time and retain significant catalytic activity. These requirements are met by the silicate sol-gel immobilisation method. In this method, the enzyme to be immobilised on the surface is added to a solution of gel precursors, which are a mix of hydrolysed alkoxy silanes. A localised change in pH around the surface of the microelectrode can then be induced electrochemically, which initiates the crosslinking of silanes into a porous gel layer that entraps the enzyme molecules. The gelation process in this method is a nucleophilic reaction which is chemically very mild. The method does not involve any free radical triggered polymerization or any cross-linking reagents. A simple pH change initiates the gel formation and helps preserve the enzyme activity. There is no direct interaction between the enzyme and the gel precursors. Before coating the electrode with the sol-gel, a permselective layer (poly (phenylene diamine)) can be added to the electrode to screen for potential interferents and improve biosensor selectivity (Dale et al. 2005).

The electrodeposition of enzyme-containing sol-gel layers involves the following steps. Firstly, (Figure 3-2) alkoxy silanes Si $(OR)_4$) such as:

Tetramethyl orthosilicate (TMOS), 3-aminopropyltrimethoxy silane (APTMOS) and 3-glycidyloxypropyl(trimethoxy)-silane GOPTMOS are hydrolysed in water and hydrochloric acid (HCl) to form silanol (Si (OH)) groups. In the next step, hydrolysed silanes are mixed with a buffer and other additives resulting in an increase of pH from that of the hydrolysed silanes (~pH 3) to pH 5-6 to prevent denaturing the enzymes, which are also added at this point.

Hydrolysis of precursors: alkoxy silanes $R\text{-}Si(OMe)_3$ in H_2O and HCl

$$R\text{-}Si(OMe)_3 + 4H_2O \longrightarrow R\text{-}Si(OMe)_{3-n}(OH)_n + {}_nMeOH$$

Figure 3-2. Sol-Gel method reactions.

The rate of gelation is very slow at pH 5-6 and the sol mixes are stable for many minutes. To achieve condensation and formation of a gel layer just at the electrode surface, a negative potential can be applied to generate OH^- ions and thus a basic pH shift confined to the electrode surface (Figure 3-3). This will result in the generation of a smooth transparent gel layer about 20 µm thick, containing the entrapped enzymes (Vasylieva N. 2013; Dale et al. 2005; Campas M. 2006). Transfer and storage to an “aging” buffer allows further maturation of the gel layer prior to drying and long- term storage.

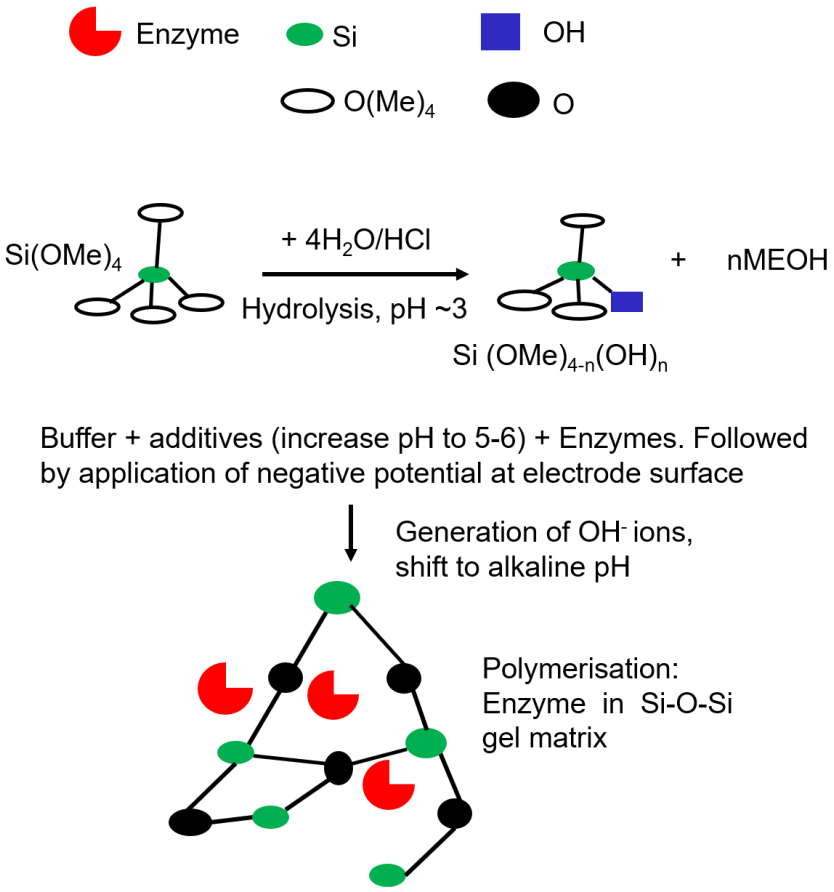

Figure 3-3. Sol-gel method of enzyme immobilisation.

Silane precursors are hydrolysed with water and HCl, pH of silanes is ~3. Buffer, additives (increase in pH to 5-6) and enzymes are added to prepare the sol-gel mix. Application of negative potential causes a local increase in pH, accelerating the polymerisation of silanol moieties and trapping the enzyme in the process**.**

As there are well established techniques for fabricating enzymatic biosensors I adapted these for the development of L-Asp biosensor, followed by characterisation of its analytical performance.

The main aims of this chapter were:

1. Fabrication and optimisation of the L-Asp biosensor using silicate sol-gel methods
2. Characterisation of the L-Asp sensor by studying
    a) its performance over a range of substrate concentrations
    b) its sensitivity to pH.
    c) its substrate specificity and selectivity.

3.2 Materials and Methods

3.2.1 Materials and instrumentation

All silanes, 4,5- methylenedioxy 1-2 phenylenediamine dihydrochloride (MPD), piperazine-N, N′-bis (2-ethanesulfonic acid) (PIPES), Polyethylene glycol (PEG), Polyethylenimine (PEI), amino acids and interferents – 5-hydroxytryptamine (5HT), ascorbate and urate were obtained from Sigma. Glycerol, KCl and NaCl were obtained from Fisher. All solutions were freshly prepared.

Sol-gel electrodeposition, cyclic voltammetry and amperometric experiments were performed using a CHI 660B workstation (CH instruments) or PG580 potentiostat-galvanostat (Uniscan instruments).

3.2.2 Sol-gel electrodeposition on Pt microelectrodes

Sensor optimisation: Pt microelectrodes with diameter of 50 μm, and length 0.5 mm (surface area 7.85×10^{-4} cm^2) were used for all experiments. All the Silanes were pre-hydrolysed with diluted HCl to desired concentration, pH of APTMOS was adjusted to 3.0 for full solubilisation. The silanes were mixed with an additive mix of 50 mM Tris/HCl, pH 7.0 or 50 mM PIPES pH 7.0, along with glycerol, PEG, PEI and NaCl. This sol-mix has a pH of about 5-6, it stabilises the enzymes and allows for generation of enough OH^- ions around the microelectrode which are required for gel formation. 10 μl of this mix was mixed with 1-2U of PpLAO and filled into a small glass capillary. Next, the Pt microelectrode along with the Ag/AgCl reference and counter electrode were inserted into a capillary from either side. A reduction potential between -0.9 to -1.2V was applied for 25-35 seconds during which time a layer was deposited on the electrode (Figure 3-4). By changing the voltage and time for deposition, gel thickness could be controlled, generally a larger voltage, applied for longer time resulted in a thicker gel. The electrode with the gel layer was then withdrawn and stored in the buffer (10 mM Sodium phosphate buffer, pH 7.4 or 50mM Tris/HCl buffer, pH 7.4). The sensors were then placed in 4 °C until use.

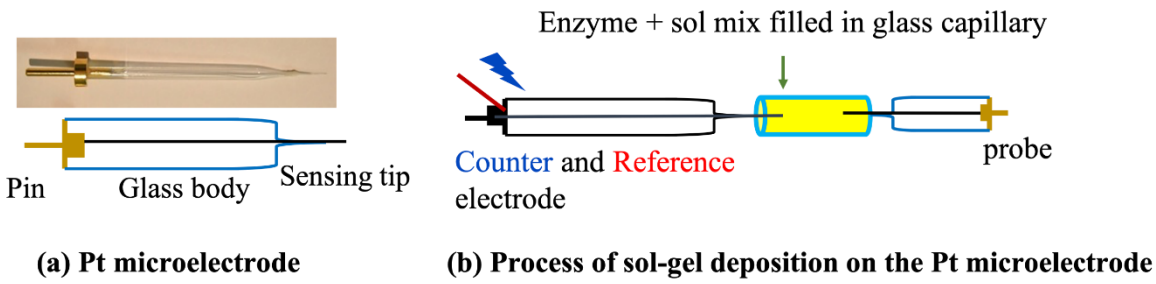

(a) Pt microelectrode **(b) Process of sol-gel deposition on the Pt microelectrode**

Figure 3-4. Sol gel electrodeposition on Pt microelectrode.

Sol mix with the enzyme is filled in the glass capillary. Pt microelectrode, reference and counter electrodes are inserted from either side. A reduction potential of -0.9 to -1.2V is applied for 25-35 secs, during which the gel is formed on the electrode.

Sensor characterisation: After the mix for L-Asp sensor was finalised, and to make biosensors that had good selectivity against electrochemical interferences, a screening layer was coated on the Pt microelectrode. 0.01M solution of MPD was prepared in 0.1M KCl and degassed with N_2 for 15 minutes. MPD was electrodeposited by scanning cyclic voltammetry from 0.2V to 0.8V at 10 mVs^{-1} for 4 cycles (prior to sol-gel deposition) and for 3 cycles after the sol-gel deposition. A three- electrode cell with Pt foil counter electrode (Goodfellow Cambridge), Ag/AgCl (saturated KCl) reference electrode was used. Sol-gel mix (in 50 mM PIPES buffer pH 7.0), was electrodeposited as per method described above. Electrode with the gel layer were stored in 10 mM sodium phosphate buffer pH 7.4 with 50µM FAD at 4 °C. Null sensors with no enzyme were also prepared by the same method.

3.2.3 Amperometric experiments

L-Asp and null sensors were tested in a flow system, with a Pt foil counter electrode and Ag/AgCl reference electrode. The sensor was operated at +500 mV relative to Ag/AgCl reference electrode for detection of H_2O_2 (amperometric detection) at the surface of the microelectrode, at room temperature. PBS was used as the running buffer in all experiments. Fresh solutions at the required working concentrations were made for each experiment. Response was recorded by applying L-Asp for 1-2 minutes, followed by 2-4 minutes of buffer. For sensor optimisation, three sensors were

tested for each mix against 100 μM of L-Asp. For sensor characterisation, five sensors were tested for each experiment. The average current was normalised against the surface area of the electrode (e.g., x μA/ 7.85 x 10^{-4} cm^2) and is reported in μA/cm^2. Origin Pro 2019, Origin 9.6 was used for data analysis. All data presented as mean and standard deviation.

3.3 Results

3.3.1 L-Asp sensor fabrication: performance in gel mix 1 and gel mix 2

In order to make the L-Asp sensors, the enzyme PpLAO was added to the sol-gel mix in different ratios. The sol-gel mix comprised of silanes: TMOS, APTMOS, GOPTMOS and methyl-tris (trimethylsiloxy) silane (MMS) in addition to other additives, mixed in certain volumes (Table 3.3.1). The silane TMOS, provides four cross-linking points, forming the bulk of the matrix and is negatively charged. APTMOS with the aminopropyl group adds the positive charge. MMS acts as a monovalent capping silane and prevents too much cross linking. GOPTMOS, along with additive PEG and glycerol helps in controlling the pore size of the gel.

The desired characteristics for the sol-gel mix with the enzyme were that it should generate a thick layer which produces a stable signal and the method for sensor fabrication should be reproducible. Therefore, different compositions of silanes, buffer and additives were tested to obtain conditions that would give a sensor that works on these levels.

Table 3-1: Silanes plus additive mixes: mix 1 and mix 2, along with their respective ageing buffers

Mix 1	Mix 2
Silanes	**Silanes**
TMOS - 60 μl	TMOS - 60 μl
APTMOS - 20 μl	APTMOS - 20 μl
GOPTMOS - 20 μl	GOPTMOS - 20 μl
	MMS - 20 μl
Additives	**Additives**
50 mM Tris/HCl pH 7.0 - 100 μl	50 mM Tris/HCl pH 7.0 - 100 μl
5 M Glycerol - 50 μl	5 M Glycerol - 100 μl
5% PEI - 100 μl	5% PEI - 100 μl
100% PEG 400 - 100 μl	30% PEG 400 - 100 μl
2 M NaCl - 60 μl	2 M NaCl - 60 μl
5 M Thioglycerol - 50 μl	
Ageing/ Storage buffer	**Ageing/Storage buffer**
10 mM Sodium phosphate buffer pH 7.4	50mM Tris/HCl pH 7.4
1mM $MgCl_2$	1mM $MgCl_2$
0.1M NaCl	0.1 M NaCl
2.5 mM Glycerol	1mM $CaCl_2$
	7.5 mM Glycerol

Although the signal for mix 1 was slightly higher, the response decreased with time as indicated in the amperometric current-time curve (Figure 3-5 (a)). The average response for 100 μM of L-Asp in mix 2 was found to be 0.39 μA/cm^2, while this response was 0.42 μA/cm^2 in mix 1 (Figure 3-5(b)).

(a)

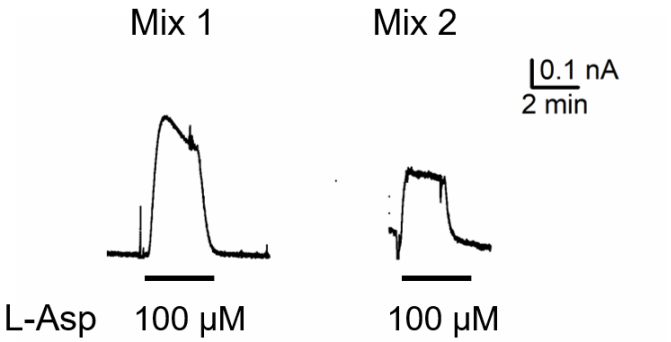

(b)

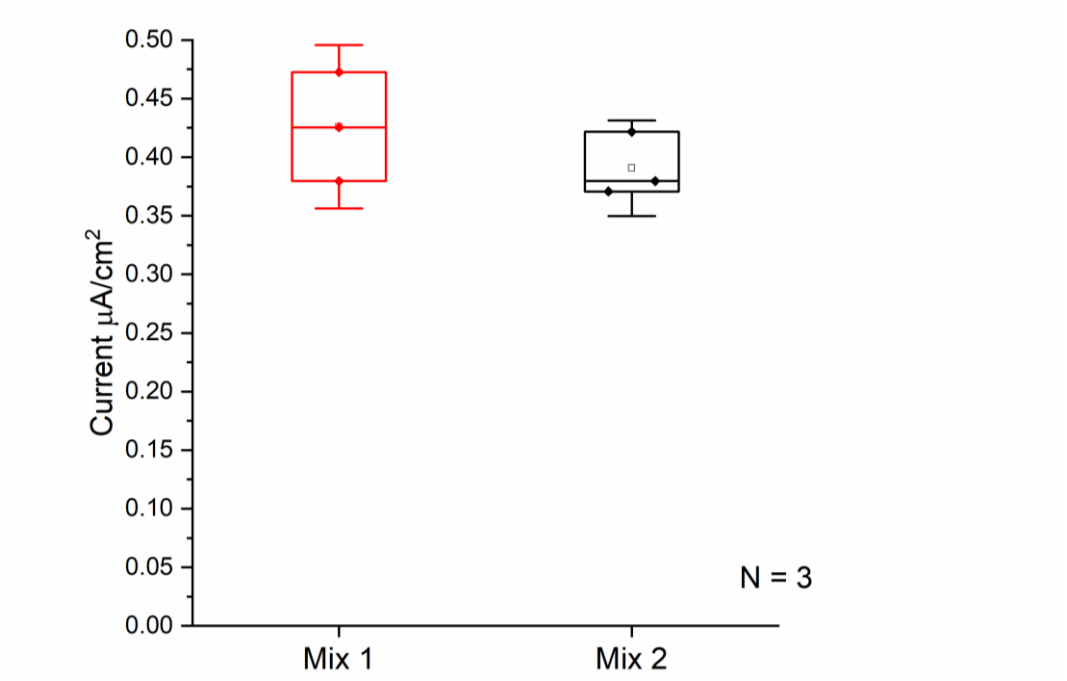

Figure 3-5. Response of L-Asp sensor in mix 1 and mix 2.

(a) Amperometric current-time curve for the two mixes, mix 1 gives a higher response, but it is uneven and falls over time. Response in mix 2 is more stable. (b) Sensor response in mix 1 is 0.42 μA/cm^2, while in mix 2 it is 0.39 μA/cm^2.

The unstable response in mix 1 could result from the presence of thioglycerol in mix 1, which might adversely affect the PpLAO activity. Thioglycerol is a reducing agent, and since PpLAO has cystine residues, presence of a reducing agent might be affecting the structure and hence the activity of the enzyme. It was also observed that there was some precipitation of the enzyme in mix 1 over time, making it difficult to coat multiple probes at the same time. The gel thickness for both mixes was similar, however a slight shrinkage was observed for mix 2 ageing buffer after some time.

Thus, for the next batch of sensors, silanes from mix 1 were used along with additives from mix 2 and sensors were kept in mix 1 ageing buffer. This new mix was now considered as L-Asp mix.

3.3.2 Gel layer of L-Asp sensor is better in PIPES buffer

While making the sensors in the previous mixes, slight precipitation of the enzyme was observed over time in the gel mix before deposition. To alleviate this problem, 50mM Tris/HCl buffer (pH 7.0) in the additives was replaced with 50 mM PIPES buffer (pH 7.0). As the silanes were at an acidic pH, the buffer in the additives was needed to balance the pH and create a favourable environment for the enzyme. Sol-gel mix with 50 mM PIPES and 50mM Tris/HCl was tested using pH strips in order to check for a mix with the better pH. It was observed that change in pH for mix in Tris/HCl buffer was from pH 7.0 to pH 5.3 upon addition of silanes, while for PIPES buffer it was from pH 7.0 to pH 6.1. Thus, sensors were prepared using Tris/HCl and PIPES buffer in additives. Response with Tris/HCl in additives was 0.41 $\mu A/cm^2$ while for PIPES, it was 0.43 $\mu A/cm^2$ (Figure 3-6). Although there was not a huge improvement in sensitivity, replacing PIPES buffer helped in stabilising the gel mix as no precipitation of the enzyme was observed. Hence L-Asp mix was adjusted accordingly (Table 3-2).

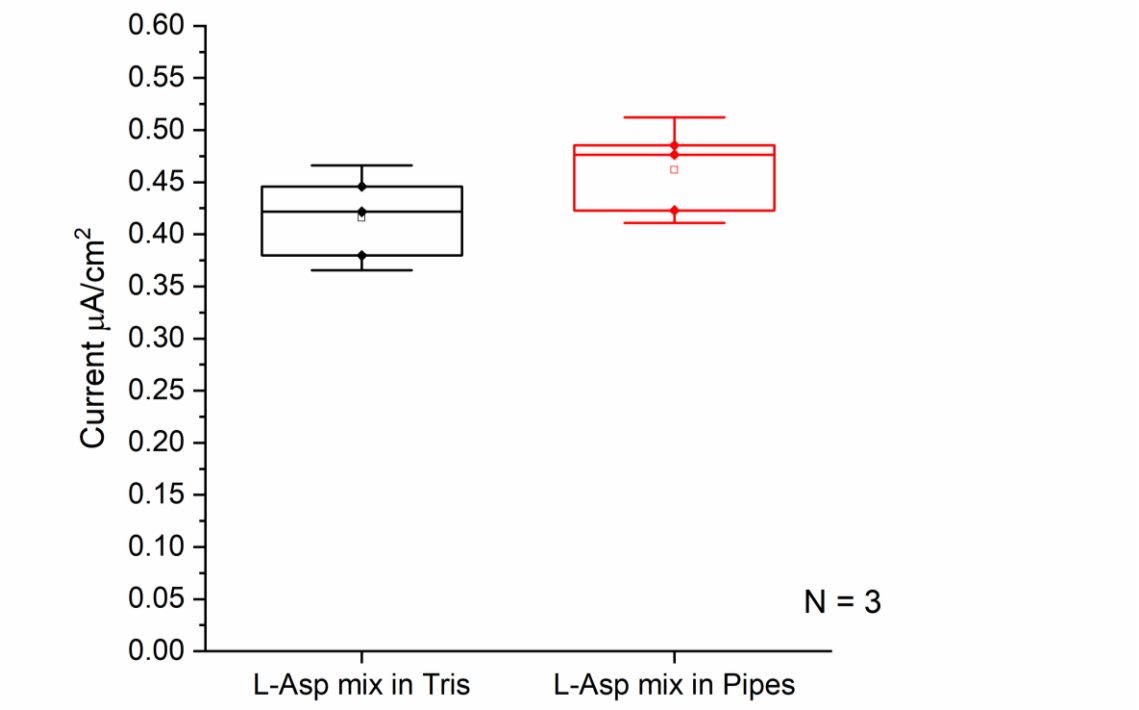

Figure 3-6. L-Asp sensor with PIPES buffer in additives.

Table 3-2: L-Asp sensor mix with 50mM PIPES buffer in additives

Silanes	**Ageing/ Storage buffer**
TMOS - 60 µl	10 mM Sodium phosphate buffer pH 7.4
APTMOS - 20 µl	1mM $MgCl_2$
GOPTMOS - 20 µl	0.1M NaCl
	2.5 mM Glycerol
Additives	
50 mM PIPES pH 7.0 - 100 µl	
5 M Glycerol - 50 µl	
5% PEI - 100 µl	
30% PEG 400 - 100 µl	
2 M NaCl - 60 µl	

3.3.3 PEI and PEG are necessary for sensor fabrication

In order to further explore, if the sensor response could be improved beyond the 0.41 - 0.43 $\mu A/cm^2$, several different conditions were tested. Principally if PEI and PEG 400 were removed from the mix, would it make any difference. The idea was as the enzyme is already present in 50% glycerol, if it was left in glycerol only without any additional components, would it improve the sensor performance? In other words, were silanes and glycerol enough to stabilise the immobilised enzyme or does enzyme stability require the presence of either PEI or PEG? Following conditions were tested and compared to the original mix:

1. L-Asp mix, sensor aged in 10mM Glycerol (high glycerol in ageing buffer)
2. L-Asp mix with 5% PEI only, (30% PEG 400 removed)
3. L-Asp mix with PEG only (5% PEI removed)
4. L-Asp mix with buffer and glycerol only (no PEI or PEG)
5. L-Asp mix with buffer and glycerol only (no PEI or PEG), aged in 10mM glycerol
6. L-Asp mix with reduced PEI - 0.3%.

Based on the results (Figure 3-7), it was concluded that both PEI and PEG were required for the stability of the immobilised enzyme. A shrinkage of gel layer was also observed for all the sensors without PEI/PEG.

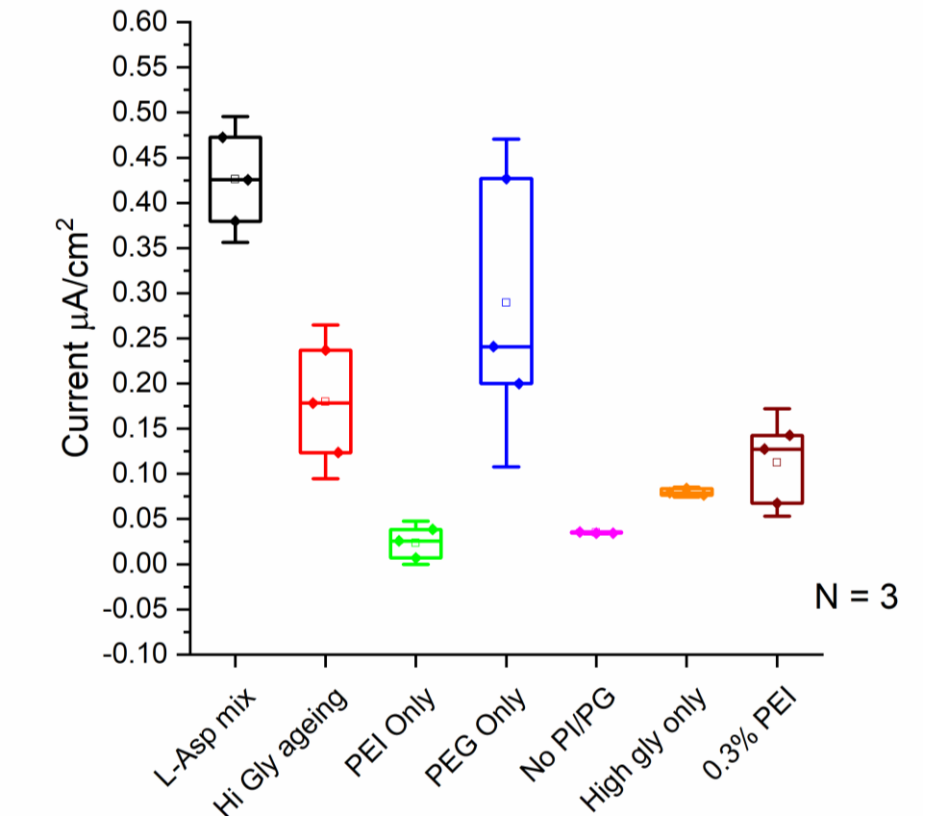

Figure 3-7. PEI and PEG are necessary for sensor response.

Removing PEI or PEG 400 from the mix caused the response to go down. The high value for PEG 400 (PEG only), was observed in only one sensor and could not be replicated. High glycerol in the ageing buffer (with or without PEG and PEI) also did not help in improving sensor response.

PEI was necessary for enzyme encapsulation as the cationic nature of the polymer formed electrostatic interactions with the enzyme and helped in retaining its structure and functional properties. PEI 'wrapped' around the enzyme and protected it during the process of immobilisation (Escobar et al. 2018) and was therefore required in the mix. Similarly, PEG was also required to retain good enzymatic activity in the gel matrix (Chae, Kim, and In 2000).

3.3.4 Addition of FAD and reducing volume of PEG 400 in ageing buffer helped improve the sensor response

FAD is a co-factor of PpLAO necessary for enzyme activity (Leese et al. 2013). As FAD is regenerated in each reaction cycle, additional FAD might improve enzyme activity as more co-factor is available in the matrix.

PEG is an important component in the gel matrix, required for enzyme stabilisation. PEG along with the silicates and glycerol influences the pore size during gel formation. Control of pore size is important to enable diffusion of small molecules (such as enzyme substrates), but also be small enough to prevent loss of large molecules from the gel. (Shalev and Miriam 2011).

PEG of different molecular weights was tested in the L-Asp mix, all at 30% concentration and 50 μl volume in the gel mix, (compared to 100μl in the original gel mix) and with 50 μM FAD in the ageing mix. Figure 3-8(a) and (b) show the effect of adding different PEGs to the L-Asp mix. It was observed that 30% PEG 400 at 50 μl gave the most stable response of 0.52 $\mu A/cm^2$.

This was the best response observed, which also gave a thick uniform gel. The PEG 400 volume in L-Asp mix was therefore adjusted to 50 μl (Table 3-3). This mix, along with FAD addition in the ageing buffer were found to be the best conditions for getting a good signal and were used in all the characterisation experiments of the L-Asp biosensor.

(a)

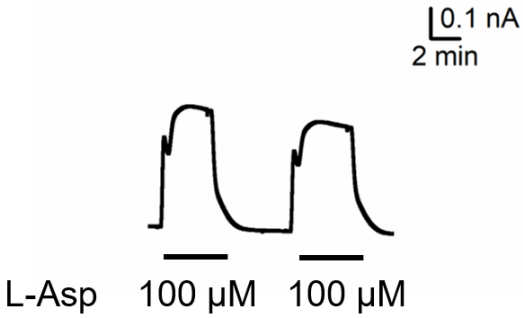

(b)

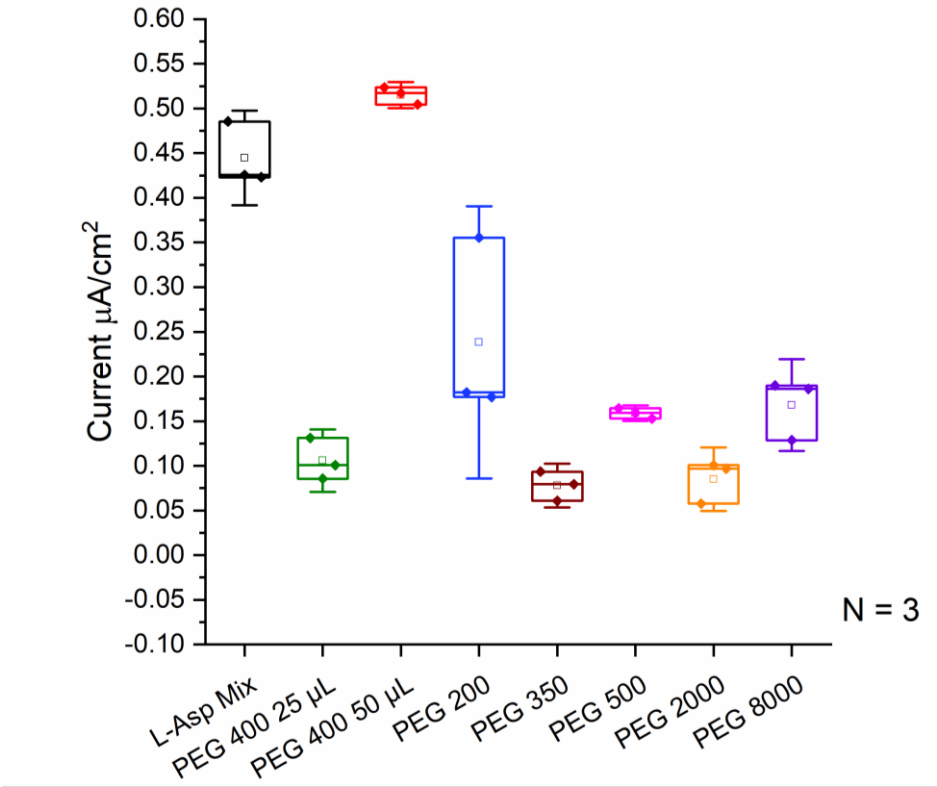

Figure 3-8. Addition of FAD and reducing PEG 400 improved sensor response.

(a) Current-time curve for sensor with reduced PEG 400. (b) Comparison of responses from different conditions tested in the mix. L-Asp mix with 50 µM FAD and PEG 40 reduced to 50 µl gave the best response at 0.52 µA/cm^2.

Table 3-3: L-Asp sensor mix: Final mix with 50mM PIPES, 50µl of 30% PEG 400 and 50 µM FAD in ageing mix.

Silanes	Ageing/ Storage buffer
TMOS - 60 µl	10 mM Sodium phosphate buffer pH 7.4
APTMOS - 20 µl	1mM $MgCl_2$
GOPTMOS - 20 µl	0.1M NaCl
	2.5 mM Glycerol
Additives	
50 mM PIPES pH 7.0 - 100 µl	
5 M Glycerol - 50 µl	
5% PEI - 100 µl	
30% PEG 400 - 50 µl	
2 M NaCl - 60 µl	

3.3.5 L-Asp sensor characterisation: sensor performance

The biosensor gave a linear response to increasing L-Asp concentrations. The 10-90% rise-time of the sensor was 15 seconds. The amperometric current-time curve for different concentrations of L-Asp, recorded on the sensor is shown in Figure 3-9 (a). Figure 3-9 (b) shows the calibration plot for L-Asp sensor, for concentration range of 3 µM to 300 µM, with 3 µM being the lower detection limit for the sensor. Mean current was determined to be 0.0016 µA/µM/cm^2 (R^2 = 0.99). L-Asp sensor measurements were also used to determine enzyme-substrate kinetics. The linear fitting of Lineweaver-Burk equation (Figure 3-10) was used to determine the apparent K_m^{App} and I_{max} as 131.6 µM and 0.61 nA respectively (K_m^{App} is the apparent K_m while I_{max} is the maximum current recorded by the sensor). Since one molecule

of L-Asp would generate one molecule of H_2O_2, and assuming that all H_2O_2 would be sensed by the L-Asp sensor, apparent V_{max} was calculated to be 3.16 fmol/sec.

(a)

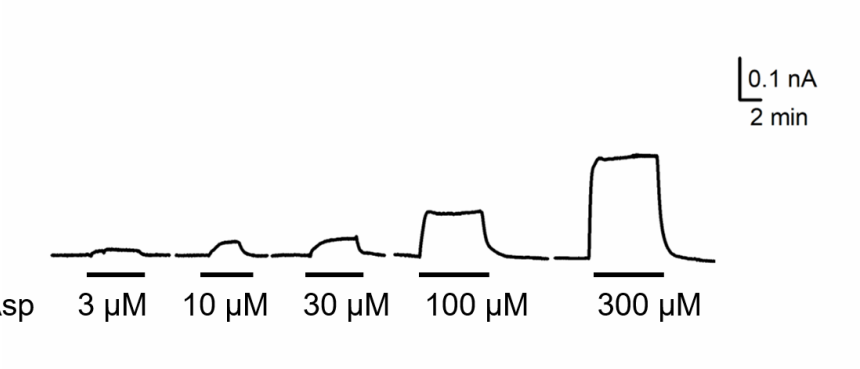

(b)

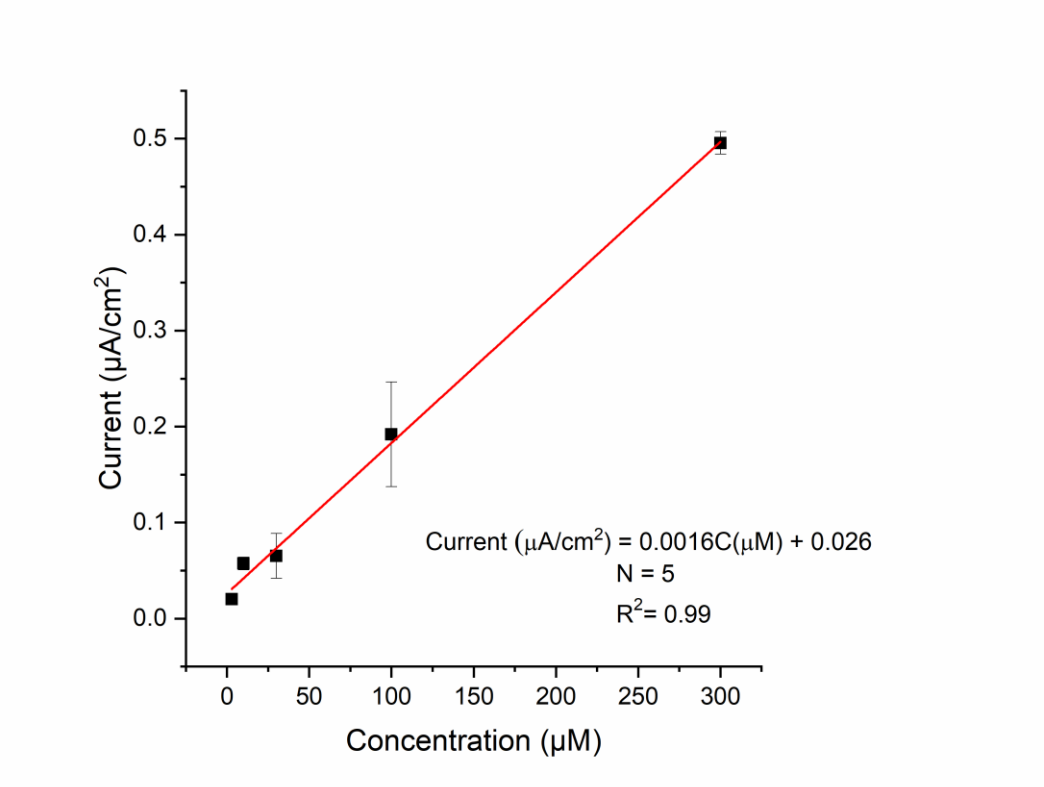

Figure 3-9. L-Asp sensor performance.

(a) Current-time curve for L-Asp sensor. (b) Calibration curve of L-Asp sensor with the linear regression equation.

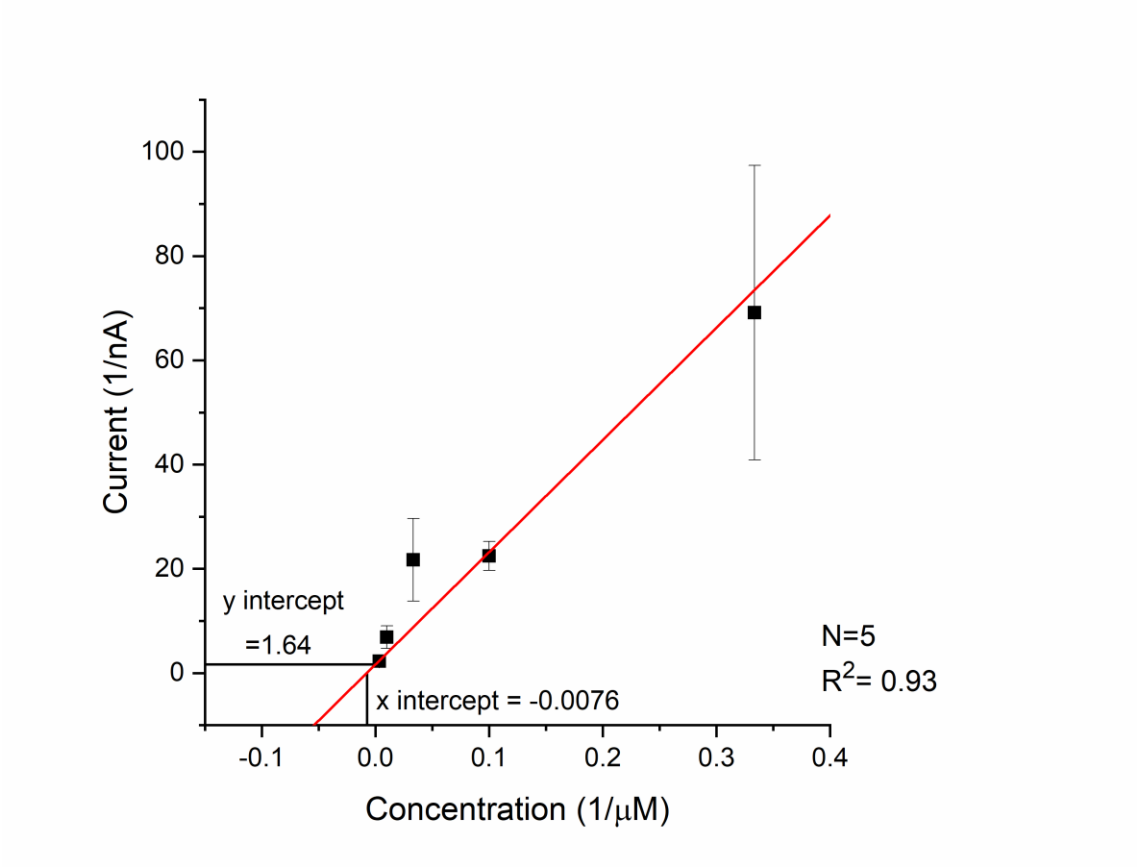

Figure 3-10. Linear fitting of Lineweaver-Burk equation.
y intercept of 1.64, and x intercept of -0.0076, are displayed.

The Eadie-Hofstee plot (Figure 3-11) was also used the determine the apparent K_m^{App} and I_{max} as 74 µM and 0.48 nA (R^2 = 0.73) respectively. This method gave a very low K_m^{App} while the I_{max} was very similar to that obtained from Lineweaver-Burk plot. Using the Imax value, and assuming that all H_2O_2 would be sensed by the L-Asp sensor, apparent V_{max} was calculated to be 2.5 fmol/sec. The coefficient of determination, R^2 for the Eadie-Hofstee equation was found to be low, this could be because in the Eadie-Hofstee plot both the x and y axis are dependent on the reaction rate and any experimental error would be present on both axes.

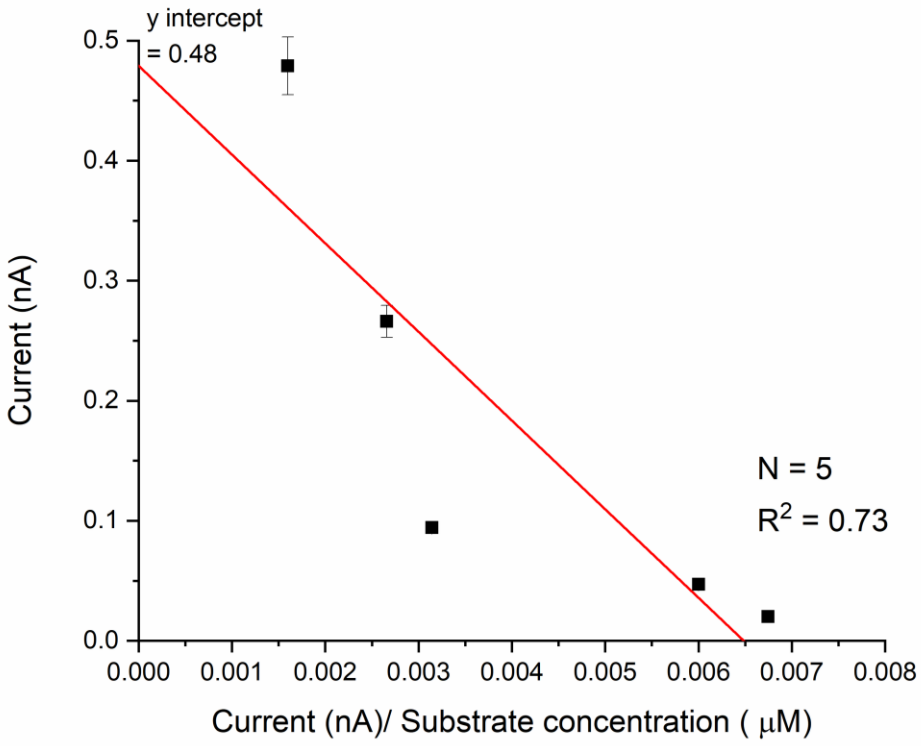

Figure 3-11. Linear fitting of Eadie-Hofstee equation.

y intercept which is the Imax of 0.48 nA is displayed and the slope of the line, represents Km which is 74 μM

3.3.6 Effect of pH on sensor response

The effect of pH on L-Asp biosensor response was studied at 100 μM L-Asp solutions, buffered to pH range from 6.8 – 8.0. The sensor response was lower from pH 6.8-7.2. It increased from pH 7.2 (0.12 μA/cm^2), to pH 8.0 (0.4 μA/cm^2). The response at physiologically relevant pH of 7.4 was mid-range at 0.19 μA/cm^2 (Figure 3-12).

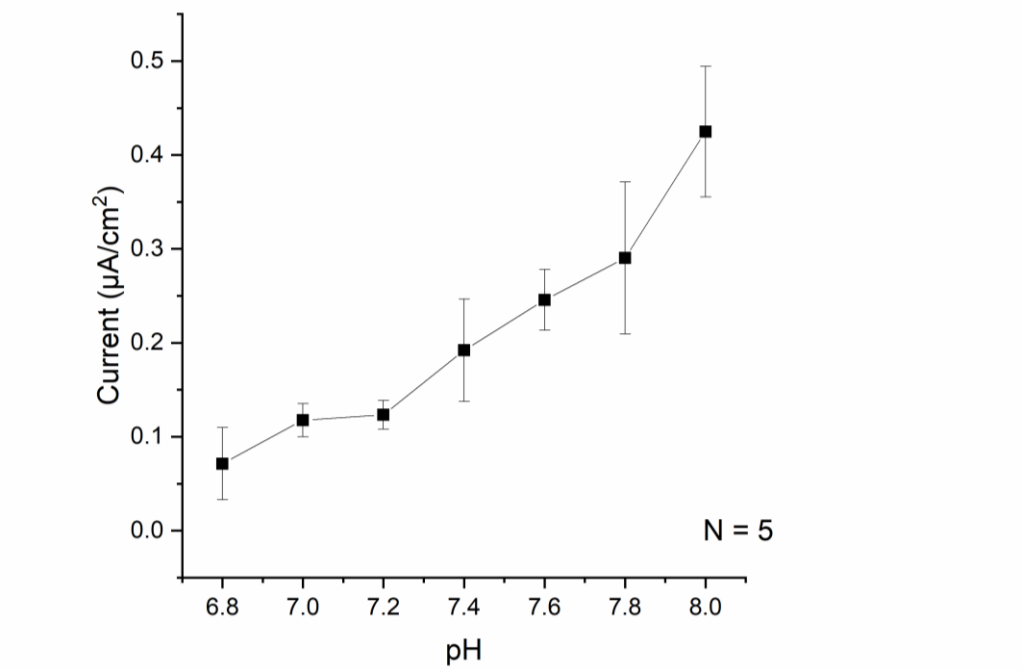

Figure 3-12. Effect of pH on L-Asp sensor response.

Solutions of L-Asp buffered to different pH were tested at 100 μM.

3.3.7 Selectivity and substrate specificity of L-Asp sensor

As there are potential interferents present in physiological samples, the selectivity of L-Asp sensor was tested towards 100 μM of 5-HT, ascorbate and urate. The high response towards ascorbate and urate was seen in L-Asp as well as null sensor. (Figure 3-13 (a)). The sensor response towards 5-HT was lower compared to the response observed for other two interferents for both null and L-Asp sensor (Figure 3-13 (a) and (b)).

(a)

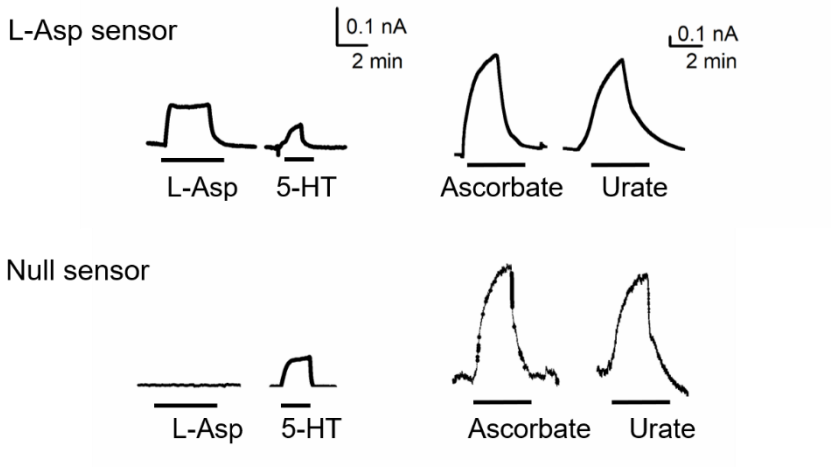

(b)

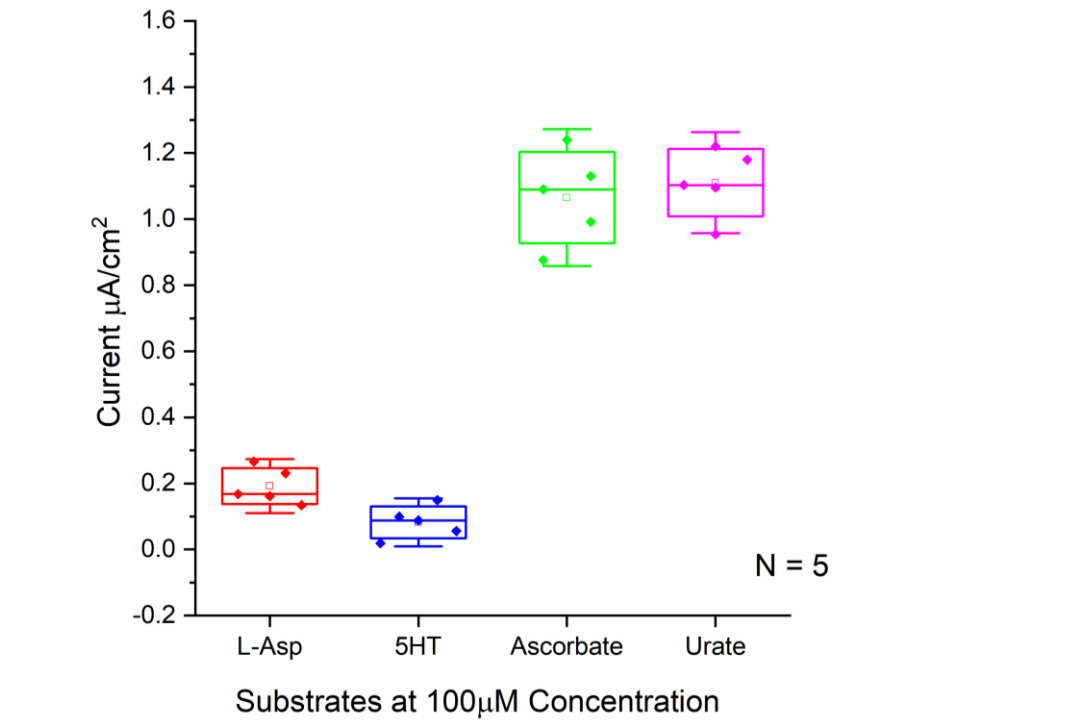

Figure 3-13. Selectivity of L-Asp sensor.

(a) Current-time curves for L-Asp and null sensors. Both sensors give a high response for ascorbate and urate. (b) L-Asp sensor response to different interferents at 100 µM concentration. Lowest response recorded for 5-HT.

Figure 3-14 (a) and (b) shows the response of L-Asp sensor towards L-Asp and other amino acids: L-Glu, L-Gln, L-Asn, D-Asp and amino acid

derivatives: NAA and gamma amino butyric acid (GABA) at equivalent concentration of 100 µM. The sensor did not respond to NAA, L-Glu, D-Asp and GABA. The sensor gave a response of 0.11 µA/cm^2 for L-Asn, while a small response of 0.05 µA/cm^2 was seen for L-Gln.

(a)

(b)

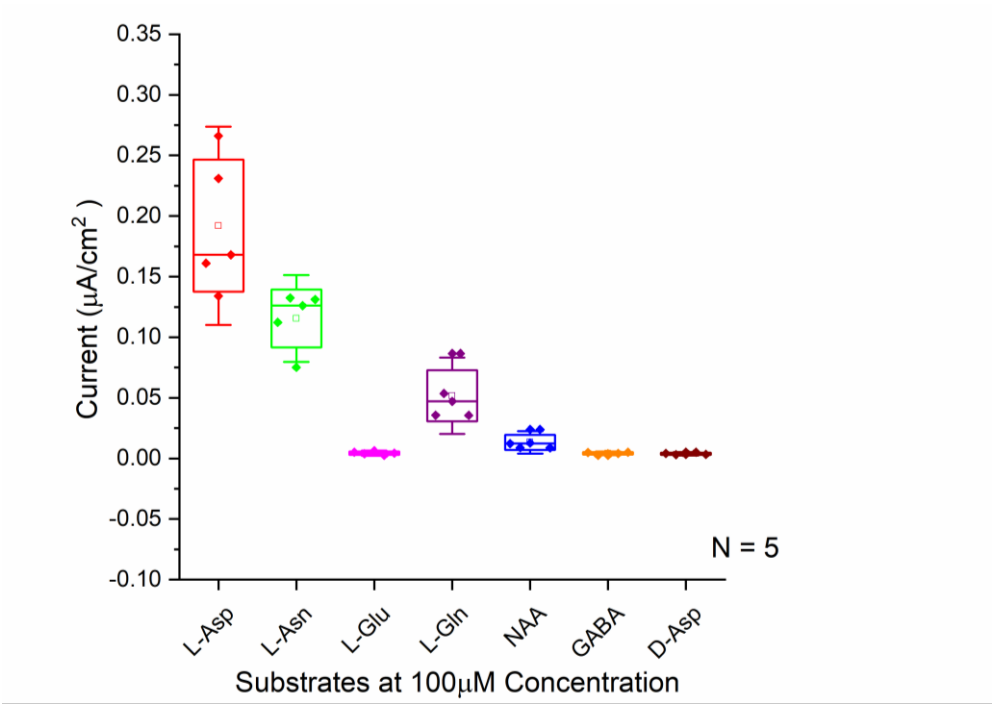

Figure 3-14. Specificity of L-Asp sensor.

(a) Current-time curves for L-Asp sensor for different substrates. Null sensor response to L-Asp, L-Asn and L-Gln. (b) L-Asp sensor response to different substrates at 100 µM concentration

3.4 Discussion

By using the proven technique of sol-gel method for enzyme encapsulation, PpLAO enzyme was immobilised on the surface of microelectrode to make the L-Asp sensor. The gel mix and ageing buffer solution optimised for L-Asp sensor allowed for fabrication of sensors that were reproducible and had a stable gel layer. The L-Asp sensor linear range was found to be like that observed for PpLAO enzyme in the spectrophotometric assay (from 3 µM- 300 µM). No response was seen for 1 µM of L-Asp, like the enzyme assay where no activity could be recorded for that concentration. Interestingly, the K_m of PpLAO from the assay was higher (222.2 µM) than the K_m^{App} value obtained from the L-Asp sensor (131.6µM); while the V_{max} value was much lower (6.67 µmol/min/mg vs 3.4 nmol/min/mg). The values obtained from L-Asp sensor were also lower than the reported values (K_m = 2.26 mM, specific activity = 10 µmol/min/mg) (Leese et al. 2013). These differences can be attributed to the fact that sol-gel method does not change the kinetic mechanism but does influence the magnitude of kinetic parameters. A similar decrease in K_m was observed for L-glutamate oxidase (LGO), where reported K_m was 5.0 mM, while K_m^{App} was 776 µM (Arima et al. 2003; Tian et al. 2009). An increase in K_m and decrease in V_{max} values has been reported for enzymes encapsulated by sol-gel methods for e.g., a four-fold decrease in V_{max} and k_{cat} accompanied by increase in K_m has been reported for pig kidney fructose-1,6-bisphosphatase encapsulated in SiO_2 gels (Pierre 2004).

It was also noted that the L-Asp sensor was much less sensitive than L-Glu sensor with a lower detection limit of 3 µM compared to 5 nM for L-Glu, the I_{max} for L-Asp sensor was also less than L-Glu sensor (0.61 nA vs 141 nA). The lower sensitivity of L-Asp sensor could be because of the lower activity of PpLAO than LGO. LGO is a much faster enzyme with a V_{max} of 26 mol/min/mg. The overall efficiency of the sensor is directly affected by the enzyme activity and the amount of enzyme that can be entrapped in the gel layer, without causing precipitation.

There was an increase in signal for 100 µM L-Asp, from pH 7.2 to pH 8.0. This change is more likely to be a characteristic of the enzyme, as LAOs in general have a higher activity at pH 8.0 (Bifulco et al. 2013; Tedeschi et al. 2010). Furthermore, changes in secondary structure have been reported for enzymes upon immobilization (Guzik, Hupert-Kocurek, and Wojcieszynska 2014). Structure of *E.coli* LAO (EcLAO) revealed that the enzyme prefers a dimeric state at alkaline pH, which is also active. PpLAO shares a 65% sequence identity with EcLAO and comparison with EcLAO showed the presence of many conserved residues (Leese et al. 2013). As the gel formation is induced with increase in pH, it is possible that it would also cause a change in the state of the enzyme, pushing it to a catalytically active dimeric state with a preference for alkaline pH. Thus, the increase in signal at higher pH is most probably because of structural change upon immobilisation. The sensor would be used in physiological pH range which is generally 7.2-7.5, therefore any responses recorded under these conditions would have to be accompanied with recordings from the null sensor, which is identical to L-Asp sensor but lacks the enzyme, for accurate interpretation.

In terms of L-Asp sensor selectivity, the screening layer was able to screen 5-HT, but a high response was observed for ascorbate and urate. One of the limitations of using microelectrode biosensors is that they have to be operated at a positive potential (+500 mV - + 700 mV), necessary for oxidation of H_2O_2. Certain chemicals naturally present in physiological samples will also oxidise at this potential and generate current which is non-specific to the analyte. Since the null sensor also gives similar response, it could be used to make differential recordings. As extracellular concentration of ascorbate is in the range of 200-400 µM (Rice 2000), it is expected to generate high background current. However, Llaudet *et al* reported a mean current of 293 pA while making purine measurements from brain slices, indicating that this background current might actually be lower than expected (Llaudet et al. 2005).

The specificity of L-Asp sensor towards L-Asp was very similar to that observed in the enzyme assay, with the exception of L-Gln. No activity was detected for NAA, L-Glu, GABA and D-Asp. NAA and L-Glu levels are very high in the brain (Moffett et al. 2014; Moussawi et al. 2011) and since the aim is to use the L-Asp sensor in brain slices, the absence of a response against 100 µM concentration of these substrates was very encouraging. As L-Asn is also considered a natural substrate of LAO, responses were seen for this amino acid (Bifulco et al. 2013; Leese et al. 2013). The response to L-Gln was unexpected as any activity to L-Gln has not been studied. As the null sensor did not respond to L-Gln, this response must arise from the enzyme interacting with the substrate in the sol-gel. The active-site cleft of EcLAO and PpLAO is formed by arginine (Arg) residues at positions 263, 290 and 386, which is a proton donor. The structural/conformational changes because of immobilisation (as noted for pH) raise the possibility of arginine-glutamine interaction in the gel environment that result in changes to substrate specificity. As the amide groups of L-Asn and L-Gln have a higher propensity for hydrogen bonding with Arg (Ippolito, Alexander, and Christianson 1990), it would account for the response obtained for L-Gln, as well as the slightly higher response observed for L-Asn, compared to the enzyme assay. This response to L-Gln might be problematic as L-Gln is also released from the astrocytes and would interfere with the L-Asp sensor response (Schousboe et al. 2014).

These limitations of the L-Asp sensor emphasize the fact that the null sensor as reference control must always be used in all experiments. It would be used to make differential recordings and check for the validity of the L-Asp sensor responses. L-Asp sensor would be calibrated before and after each experiment to check for sensitivity. Furthermore, L-Asp and null sensor would be routinely checked for screening layer when being used in the brain slices. Owing to the low sensitivity of the sensor, a higher stimulation of neurons or drugs that directly interfere with L-Asp physiology and possibly increase levels of L-Asp might be needed in order to record a response from the sensor.

The sol-gel method employed for L-Asp sensor was able to preserve the catalytic activity of PpLAO, as the sensor was responding in the micromolar range, which was one of the primary goals. However, the sensor does have drawbacks which need to be considered when designing experiments and making measurements from L-Asp sensor in physiological samples in vitro.

Chapter 4

Aspartoacylase purification and NAA sensor fabrication

4.1 Introduction

N-acetyl aspartate (NAA), is the second most abundant metabolite in the brain, with concentration up to 10 mM reported in neurons (Baslow 2018). NAA has emerged as an important biomarker for ischemic stroke and traumatic brain injury (TBI), however the exact physiological function of NAA is not fully understood (Moffett et al. 2013; Stovell et al. 2017). I have used the same principles as employed for the L-Asp biosensor to fabricate an NAA sensor (microelectrode sensors coated with enzymes immobilised on the surface by using the sol-gel method). The required enzyme cascade for NAA detection comprises a combination of the NAA metabolising enzyme – aspartoacylase (ASPA) and PpLAO (Figure 4-1). The cascade will give an increase of H_2O_2 proportional to the concentration of NAA, which can be detected at the surface of the sensor. Of course, such a biosensor would also be sensitive to L-Asp.

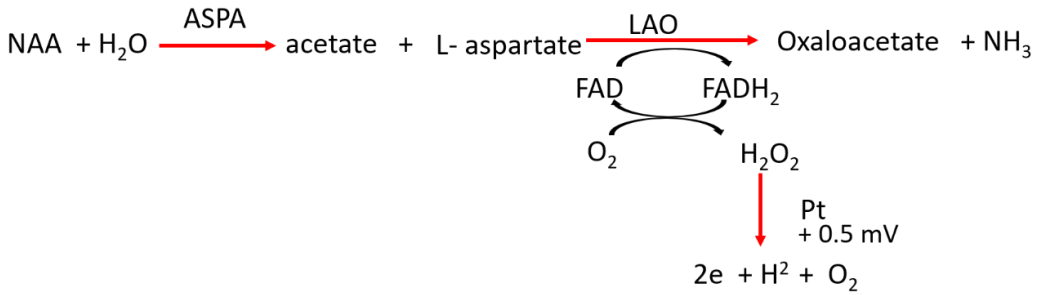

Figure 4-1: Enzyme cascade for NAA sensor.

The NAA sensor would enable real-time recording of the release of this metabolite in brain slices and help elucidate the functions of NAA. In addition,

the principle and methodology involved in the fabrication of an NAA sensor would pave the way for making integrated electrochemical sensor array such as the SMARTChip. The SMARTChip system is built on the concept of enzyme based amperometric detection technology. It is of the size of a glucose strip and enables faster detection of the analyte. The SMARTChip has been developed for detection of purines and was used to make blood purine measurements in adult patients with epilepsy (Beamer et al. 2021). This technology can be expanded to develop SMARTChips for other biomarkers.

An optofluidic device enabling rapid and label free detection of NAA was recently reported. The device can detect biomarkers for TBI (NAA, serum S-100 calcium-binding protein B, glial fibrillary acidic protein) from blood plasma in picomolar range. As this device has been developed on the concept of surface-enhanced Raman scattering, it needs a miniaturized Raman system for collecting the spectra, which is then compared to established fingerprint spectra of biomarkers (Rickard et al. 2020). The SMARTChip technology is much more simplified and if designed specifically for NAA, it can be added to the repertoire of testing methods available. Thus, the NAA sensor was fabricated with the objective of obtaining proof of concept results.

4.1.1 Aspartoacylase (ASPA) enzyme characteristics

The enzyme aspartoacylase (ASPA, EC. 3.5.1.15) catalyses the breakdown of NAA. The enzyme has been mainly identified in mammals, with high expression in the brain (Namboodiri et al. 2000; Kaul et al. 1991; Hershfield et al. 2006). ASPA is localized to oligodendrocytes, where it is present in the nucleus and cytoplasm. The enzyme consists of 313 amino acids with a molecular weight of 36 kDa (Hershfield et al. 2006). One of the earliest ASPA enzymes to be extracted and purified was from bovine brain, with a low activity of 0.02 µmol/min/mg. Through recombinant expression and purification mouse (mASPA) and human ASPA (hASPA) encoded by ACY2 gene, have also been characterized. Moore et al. reported that histidine tagged mASPA and hASPA expressed in *E.coli*, exist as dimers and had an activity of 0.05 µmol/min/mg (Moore et al. 2003). The solved structure of hASPA and

rat ASPA (rASPA) showed the enzyme to be in dimeric form (Bitto et al. 2007). This dimeric state of ASPA was also reported in rat brain extracts (Klugmann et al. 2003). By using the yeast expression system Le coq et al were able to purify a glycosylated from of hASPA which was active (Le Coq et al. 2006). hASPA with glutathione S transferase (GST) fused at the N -terminus recorded the highest activity of 1557 µmol/min/mg (Herga et al. 2006).

hASPA has the desirable properties, of a high specific activity, and a low K_m of 0.12- 0.7 mM (Herga et al. 2006; Le Coq et al. 2006; Namboodiri et al. 2000), hence this enzyme was chosen for NAA sensor preparation. As there were differences in the enzyme purification reports, two different expression systems were simultaneously explored for the expression of hASPA. ASPA being a eukaryotic enzyme, the baculovirus system using Sf9 insect cells was tested as it was thought that it would support any post-translational modifications that might be required for proper folding and activity of the enzyme. The bacterial expression system where hASPA is expressed as a GST fusion protein was also investigated as it gave a highly active form of the enzyme.

The main aims for this chapter were to:

1. Express and purify hASPA
2. Test the activity of hASPA
3. Fabricate NAA sensor using silicate sol gel method: obtain proof of concept data.

4.2 Materials and Methods

4.2.1 Materials

All restriction enzymes, cells and plasmid purification kits were obtained from NEB. Antibodies were obtained from Cell Signalling Technologies. NEB pre stained protein marker (#P7712) was used for SDS PAGE. Magic marker XP (Invitrogen) was used in western blot as protein standard.

4.2.2 Cloning of hASPA into pFastBac vector

Codon optimised wild-type gene encoding hASPA (WT) designed with a hexa-histidine tag at the 3' end (ahead of the stop codon) was obtained from Integrated DNA Technologies. The gene and vector pFastBac (Invitrogen) were cut using restriction enzymes BamHI and NotI, followed by ligation with T4 DNA ligase. Sequence of pFastBac-hASPA(WT) was confirmed using pFastBac forward (5' GGATTATTCATACCGTCCCA 3') and pFastBac reverse primer (5' CAAATGTGGTATGGCTGATT 3').

4.2.3 Site directed mutagenesis of hASPA

Mutations in pFastBac-hASPA(WT) were introduced using the QuickChange SDM Kit (Agilent Technologies). For each mutation, two overlapping primers with corresponding nucleotide changes were designed (Table 4-1). Sequence of all mutated pFastBac-hASPA vectors was confirmed using pFastBac forward and reverse primers as before.

Table 4-1: Primer sequences for introducing mutation in pFASTBac:hASPA

Mutation	Primer sequences
Lys59GLn **Lys60Gln** **(aag → cag)**	F: 5' ccaagagccgtt**cagcag**tgcaccaggtac 3' R: 5' gtacctggtgca**ctgctg**aacggctcttgg 3'
Lys80Gln **Lys81Gln** **(aag → cag)**	F:5'gacttggagaacctgggt**cagcag**atgtctgaggacttg 3' R:5'caagtcctcagacat**ctgctg**acccaggttctccaagtc 3'

4.2.4 Transfection of pFastBac-hASPA(WT) and mutants

Sf9 insect cells were transfected with 1 µg and 5 µg of purified bacmid DNA. Bacmid DNA preparation, transfection and cell extraction protocol was performed by Dr.D Brotherton.

4.2.5 Western blot

The prepared cell lysates were diluted in 2X SDS loading buffer in 1:1 dilution. Samples were loaded on a 12% SDS-PAGE gel. Following electrophoresis, samples were transferred onto a PVDF membrane (Merck Life Science). Membranes were blocked for 1 hr at room temperature (RT) in 1x TBS-Tween with 5% milk, followed by overnight incubation at 4 °C with His-Tag mouse (27E8) mAB at 1:1000 dilution (1x TBS-T, 5% BSA). After washings in 1x TBS-T, membrane was incubated for 1 hr at RT with anti-mouse IgG HRP-linked secondary antibody in 1:2000 dilution (1xTBS-T, 5% milk). Following brief washing, membranes were developed using LuminataTM Classico western HRP substrate (Merck Millipore).

4.2.6 Test expression of hASPA in *E.coli*

Codon optimised Glutathione S-transferase (GST) tagged hASPA cloned into pGEX-6p-1 vector was obtained from Genscript USA (pGEX:GST-hASPA). Sequence of the plasmid was confirmed using pGEX 5' forward (5'-GGGCTGGCAAGCCACGTTTGGTG-3') and pGEX 3' reverse (5'-CCGGGAGCTGCATGTGTCAGAGG -3') primers. For expression trials of the protein the plasmid was transformed into E. coli BL21 (DE3) and BL21(DE3) pLysS cells using heat-shock, 42 °C for 45s. Cells were plated on selective LB-Agar plates: BL21(DE3) cells on kanamycin (Kan) (30 µg/ml) plates, while BL21(DE3) plysS on Kan (30 µg/ml) and chloramphenicol (Chlor) (35 µg/ml) plates.

25ml of LB media with respective antibiotics was inoculated with a single transformed colony. Cells were grown at 25 °C, 18 °C or 15 °C with shaking at 180 rpm till they reached OD 600 of 0.6, upon which they were induced with IPTG to a final concentration of 1mM. Samples were collected after 3 hrs and after 16 hrs of induction. Cells were then harvested by centrifugation in bench top centrifuge (Eppendorf centrifuge 5424) at 11000g for 10 minutes. For analysis of total protein expression, soluble and insoluble fractions, samples were prepared as per method used for PpLAO samples. All samples were analysed on 12% SDS-PAGE gels.

4.2.7 Purification of ASPA

pGEX:GST-hASPA was transformed into chemically competent E.coli BL21 (DE3) pLysS cells using heat-shock, 42 °C for 45s. Cells were plated on Kan/Chlor selective LB-Agar plates. Two 50 ml LB media, starter cultures were inoculated with a single transformed colony. Cells were grown at 25 °C overnight with shaking at 180 rpm. Two 500 ml cultures with 30 μg/ml of Kan and 35 μg/ml of Chlor were inoculated with the 50 ml starter cultures. Cells were then grown at 18 °C with shaking at 180 rpm, till they reached OD 600 of 0.6, upon which they were induced with IPTG to a final concentration of 1mM. After 16 hrs of induction cells were harvested by centrifugation at 8000g for 20 minutes using JA-10 rotor (Beckman Coulter centrifuge). Harvested cells were snap frozen in liquid N2 and stored in -80 °C.

The cell pellet was thawed on ice, weighed and re-suspended (4 ml/gm of pellet) in resuspension buffer (50 mM Tris/HCl, 300 mM NaCl, 0.2 mg/ml protease inhibitor AEBSF, 10 μg/ml DNAseI, 5mM Dithiothreitol (DTT), pH 7.5). After placing on ice for 15 minutes, cells were sonicated on ice (6 times for 30 seconds at 60% power, with 1-minute cooling in between). Sonicated cell suspension was then spun in JA 25.5 rotor (Beckman Coulter), at 24000g for 45 minutes. Collected supernatant was filtered through a 0.45 μm and 0.2 μm syringe filter (Acrodisc) and adjusted to 0.4 M NaCl (final concentration). A 5 ml GSTraptm FF column (GE Healthcare) connected to a peristaltic pump and maintained at 4 °C was used for purification. The column was washed with 5 column-volumes (CV) of water and then pre-equilibrated with 5 CVs of equilibration buffer (50 mM Tris/HCl, 300 mM NaCl, 5 mM DTT pH 7.5). It was then loaded with the filtered supernatant at flow rate of 1 ml/min. The flow-through (FT) was collected and again loaded on the column. This procedure was repeated three times for complete binding of the protein. After washing the unbound protein with equilibration buffer, bound protein was eluted with 10 CVs of elution buffer (50 mM Tris/HCl, 300 mM NaCl, 5 mM DTT,10 mM reduced glutathione, pH 7.5). 2 ml fractions were collected and analysed on SDS-PAGE. Fractions showing the protein (correct molecular weight of ~62

kDa) were pooled together and dialysed against the dialysis buffer (50 mM Tris/HCl, 300 mM NaCl, 50% glycerol, pH 7.5). Dialysed protein was further concentrated using the Vivaspin 500 MWCO 10000 (GE Life sciences) column, by centrifugation at 3000g (Eppendorf centrifuge 5804R). Final protein concentration was measured on Implen NanoPhotometer N60/N50. Purified protein was then flash cooled in liquid N2 and stored in -80°C. Protein gel bands were quantified using ImageJ (Schneider, Rasband, and Eliceiri 2012).

4.2.8 Activity assay

1,2-Diamino-4,5-methylenedioxybenzene Dihydrochloride (DMB) was used as a derivatising reagent for the product oxaloacetate (OAA). ASPA activity was measured by measuring the initial rate of OAA formation in DMB fluorescent dye/ PpLAO coupled assay. OAA formation was measured in a spectrophotometre with DMB at 367 nm (ε = 2266.7 $M^{-1}cm^{-1)}$. All solutions were freshly prepared. The assay mixture contained 3 µl of PpLAO (55 mg/ml), 3 µl of 0.1 mM DMB or 1 mM DMB in PBS, pH 7.4. 2 µl of purified ASPA (1.32 mg/ml) was added and activity was measured against increasing concentrations of NAA (6 µM,10 µM, 60 µM,100 µM and 600 µM). Data was analysed using Origin (Pro) 2019b. All data presented as mean and SD from three independent assays, performed in triplicate.

4.2.9 NAA sensor fabrication and amperometric detection of NAA

The NAA sensor was prepared in the L-Asp sol-gel mix (Table 4-2) as per method described for L-Asp sensor optimisation. The microelectrodes were not coated with MPD prior to sol-gel deposition. The detection of NAA was performed in a flow system as per method for amperometric detection of L-Asp using L-Asp sensor. Sensors were tested against 100 µM concentration of NAA and L-Asp. The average current was normalised against the surface area of the electrode and is reported in µA/cm^2. Origin Pro 2019, Origin 9.6

was used for data analysis. All data presented as mean and standard deviation.

Table 4-2: sol-gel mix for NAA sensor.

Silanes	**Ageing/ Storage buffer**
TMOS - 60 μl	10 mM Sodium phosphate buffer pH 7.4
APTMOS - 20 μl	1mM $MgCl_2$
GOPTMOS - 20 μl	0.1M NaCl
	2.5 mM Glycerol
	50 μM FAD
Additives	
50 mM PIPES pH 7.0 - 100 μl	
5 M Glycerol - 50 μl	
5% PEI - 100 μl	
30% PEG 400 - 50 μl	
2 M NaCl - 60 μl	

4.3 Results

4.3.1 Expression of ASPA in Sf9 cells

The vector pFASTBac: hASPA (WT) (Figure 4-2) was sequenced using pFASTBac primers showed the gene to be inserted correctly and in frame. The translated sequence aligned with the amino acid sequence for ACY2 gene from the Uniprot Consortium (Figure 4-3).

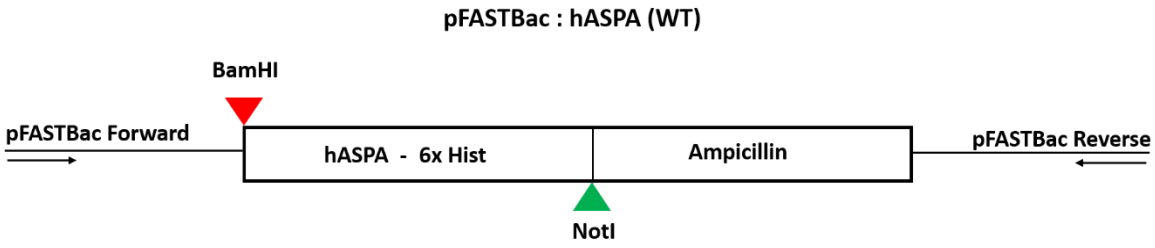

Figure 4-2: pFASTBac vector with hASPA (WT) and 6X-His tag at 3' end, cloned between BamHI and NotI.

pFASTBac forward and reverse primers were used for sequencing.

```
ACY2_human      MTSCHIAEEHIQKVAIFGGTHGNELTGVFLVKHWLENGAEIQRTGLEVKPFITNPRAVKK 60
hASPA           MTSCHIAEEHIQKVAIFGGTHGNELTGVFLVKHWLENGAEIQRTGLEVKPFITNPRAVKK 60
                ************************************************************

ACY2_human      CTRYIDCDLNRIFDLENLGKKMSEDLPYEVRRAQEINHLFGPKDSEDSYDIIFDLHNTTS 120
hASPA           CTRYIDCDLNRIFDLENLGKKMSEDLPYEVRRAQEINHLFGPKDSEDSYDIIFDLHNTTS 120
                ************************************************************

ACY2_human      NMGCTLILEDSRNNFLIQMFHYIKTSLAPLPCYVYLIEHPSLKYATTRSIAKYPVGIEVG 180
hASPA           NMGCTLILEDSRNNFLIQMFHYIKTSLAPLPCYVYLIEHPSLKYATTRSIAKYPVGIEVG 180
                ************************************************************

ACY2_human      PQPQGVLRADILDQMRKMIKHALDFIHHFNEGKEFPPCAIEVYKIIEKVDYPRDENGEIA 240
hASPA           PQPQGVLRADILDQMRKMIKHALDFIHHFNEGKEFPPCAIEVYKIIEKVDYPRDENGEIA 240
                ************************************************************

ACY2_human      AIIHPNLQDQDWKPLHPGDPMFLTLDGKTIPLGGDCTVYPVFVNEAAYYEKKEAFAKTTK 300
hASPA           AIIHPNLQDQDWKPLHPGDPMFLTLDGKTIPLGGDCTVYPVFVNEAAYYEKKEAFAKTTK 300
                ************************************************************

ACY2_human      LTLNAKSIRCCLH-----         313
hASPA           LTLNAKSIRCCLHHHHHH         318
                *************
```

Figure 4-3: Sequence alignment for ASPA.

ACY2_human: sequence of ASPA from the UniProt consortium. hASPA: translated sequence obtained after sequencing with pFASTBac primers. Both sequences show perfect alignment.

Sf9 cells expressing hASPA (WT) were collected at different time points to analyse protein expression (Figure 4-4). Cells were also transfected with pFASTBac: HK vector that gave a high and stable expression of a 26 kDa control protein - HK standard (HK). A western blot (WB) was performed to confirm hASPA and HK protein expression (Figure 4-5)

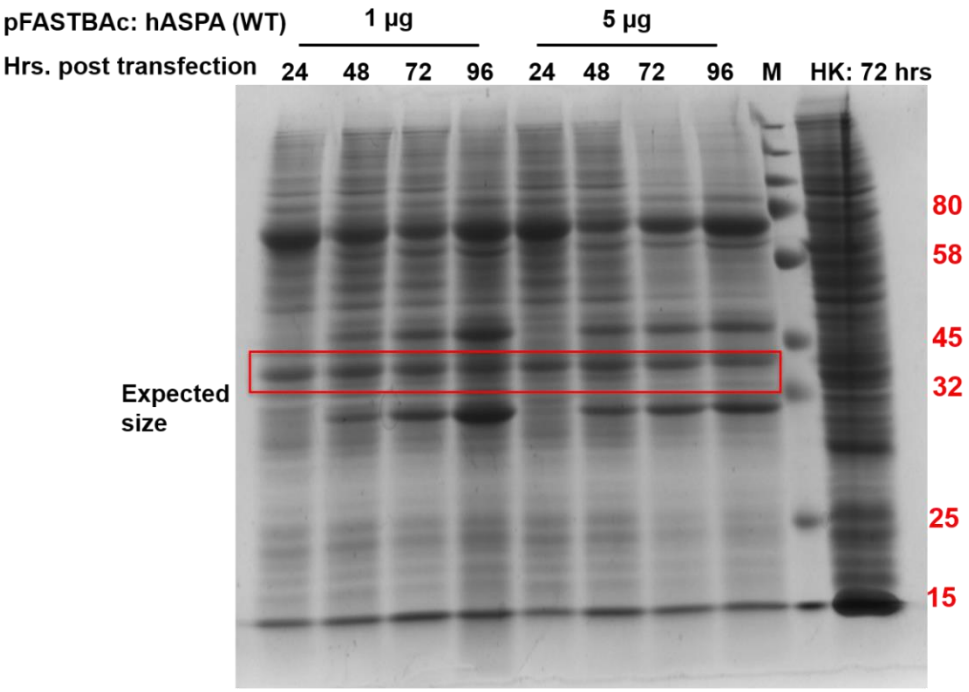

Figure 4-4: Expression of hASPA(WT) in Sf9 cells.

1 µg and 5 µg: Concentration of bacmid used for transfection of cells. Cells were harvested at different time points as indicated: hrs post transfection. M: molecular weight marker. HK: control protein HK harvested 72 hrs post transfection. Several protein bands were observed in the region of 32 kDa -45 kDa, instead of a single protein band.

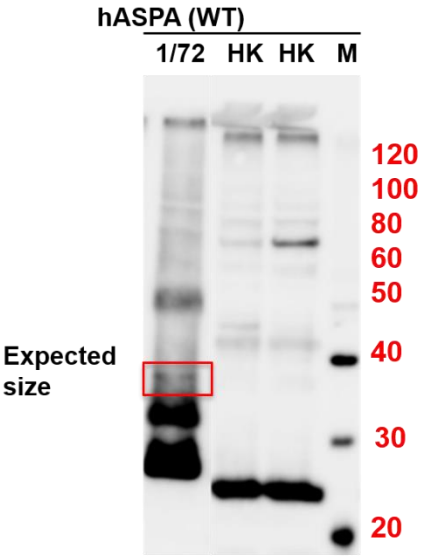

Figure 4-5: Western blot for hASPA (WT).

Sf9 cells transfected with 1 µg of bacmid virus and harvested at 72 hrs was used. M: WB magic marker. HK: control protein.

There was not much difference in expression between cells transfected with 1 µg or 5 µg of virus. A protein band of expected size (36 kDa) could be seen on the gel, however there were additional bands of equal intensity. Therefore, a WB was performed for the 72-hr sample transfected with 1 µg of virus as this sample had sufficient expression and the smaller band of 32 kDa was less pronounced. The WB indicated that the protein was less than 36 kDa (closer to 30 kDA, with another band of approximately 25 kDa) suggesting that there might be some proteolytic cleavage going on during expression. The amino acid sequence of hASPA showed that there were several lysine residues present in the protein with two adjacent lysine groups present at positions 59/60, 80/81 and 291/292 (Figure 4-6). Expression of several different proteases had been reported in Sf9 cells, which got expressed upon transfection with bacmids and affected the overall yield (Gotoh et al. 2002; Naggie and Bentley 1998; Slack, Kuzio, and Faulkner 1995). Since lysine or arginine was one of the preferred primary cleavage sites for serine proteases (Di Cera 2009), and lysine residues are also substrates for ubiquitin proteasomal complex (Mattiroli and Sixma 2014; Martensen and Justesen 2001), tandem lysine residues would pose a problem in protein expression. Therefore, these lysine residue pairs were mutated. As lysine at positions 291/292 were part of the C-terminal domain that was involved in maintaining a positive potential required for guiding NAA into the active site, these residues could not be mutated (Bitto et al. 2007). Furthermore, the cleaved ASPA appeared to be in the range of 30-25 kDa indicating that the cleavage might be occurring within the first 90 amino acids. These Lysine residues were part of a highly polar residue cluster (Bitto et al. 2007), hence they were mutated to glutamine, as glutamine was a polar amino acid with side chain length like lysine. It was thought that glutamine would help maintain the polar cluster and the overall protein fold of ASPA.

```
1       10         20         30         40         50
MTSCHIAEEHIQKVAIFGGTHGNELTGVFLVKHWLENGAEIQRTGLEVKP
        60         70         80         90         100
FITNPRAVKKCTRYIDCDLNRIFDLENLGKKMSEDLPYEVRRAQEINHLF
       110        120        130        140        150
GPKDSEDSYDIIFDLHNTTSNMGCTLILEDSRNNFLIQMFHYIKTSLAPL
       160        170        180        190        200
PCYVYLIEHPSLKYATTRSIAKYPVGIEVGPQPQGVLRADILDQMRKMIK
       210        220        230        240        250
HALDFIHHFNEGKEFPPCAIEVYKIIEKVDYPRDENGEIAAIIHPNLQDQ
       260        270        280        290        300
DWKPLHPGDPMFLTLDGKTIPLGGDCTVYPVFVNEAAYYEKKEAFAKTTK
       310   313
LTLNAKSIRC CLH
```

Figure 4-6. Amino acid sequence of hASPA. Tandem lysine residues at positions 59/60, 80/81 and 292/293 are highlighted in red.

Mutagenesis reactions were performed on pFastBac-hASPA(WT) vector to generate pFASTBac: hASPA (59/60) and pFASTBac: hASPA (80/81) mutants. Sequence of all mutated plasmids was confirmed. Sf9 cells were transfected and samples were analysed by WB to check for protein expression (Figure 4-7).

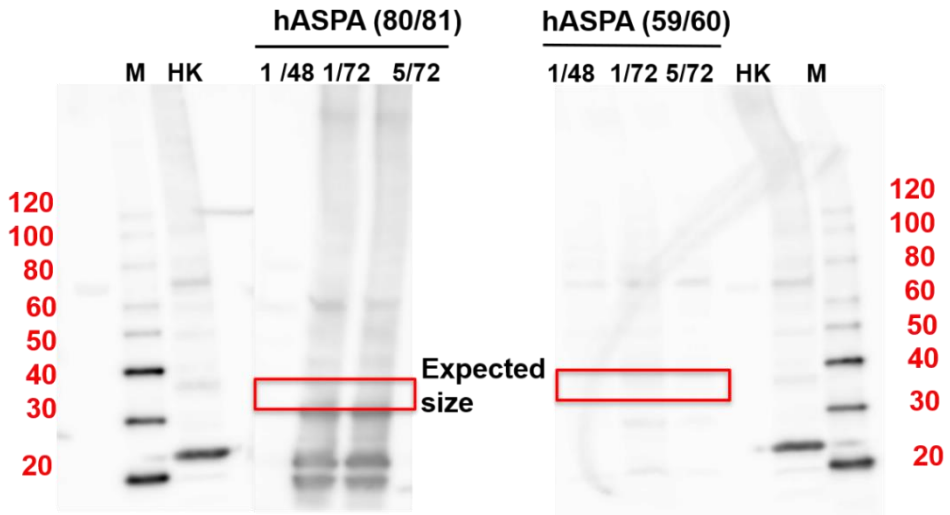

Figure 4-7. Expression of hASPA (59/60) and hASPA (80/81) mutants in Sf9 cells.

M: WB magic marker, HK: control protein. 1/48 and 1/72: Sf9 cells transfected with 1 µg of bacmid and harvested at 48 hrs and 72 hrs respectively, 5/72: Sf9 cells transfected with 5 µg of bacmid and harvested at 72 hrs. Region of expected size of the protein is highlighted. hASPA(59/60) did not express; Expression of hASPA(80/81) was reduced with protein band similar to the WT.

The hASPA(59/60) mutant did not express, while the hASPA(80/81) mutant showed reduced expression of protein which aligned with 30 kDa marker, similar to hASPA(WT). The expression profiles of hASPA (WT) and the mutants in Sf9 cells suggested that there might be some proteolytic/degradative mechanism in these cells that was not amenable for successful expression of hASPA.

4.3.2 Expression of hASPA (WT) in *E.coli*

The 3' hexa-histidine tagged hASPA cloned into pGEX-6p-1 (Figure 4-88) was sequenced using pGEX primers. Sequencing of the plasmid showed that the gene was inserted correctly, and the translated sequence aligned with the amino acid sequence of hASPA.

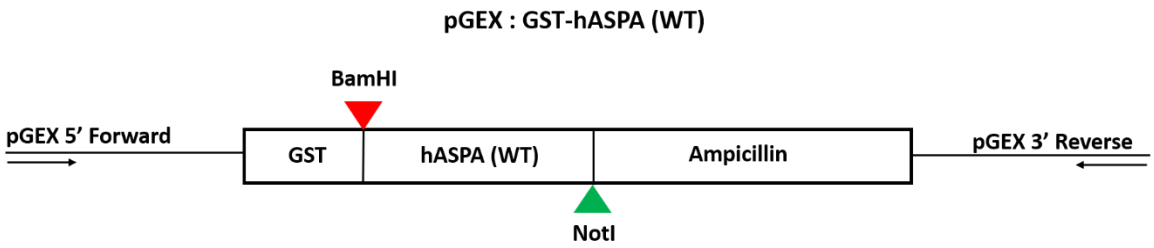

Figure 4-8. pGEX: GST-hASPA(WT).

GST Tag is at 5' end, hASPA(WT) cloned between BamHI and NotI. pGEX 5' forward and pGEX 3' reverse primer used for sequencing.

In order to obtain the best expression of hASPA, different cell strains and temperature conditions were tested. SDS PAGE analysis of the protein fractions from expression in BL21(DE3) and BL21(DE3) pLysS cells indicated that the protein was present in both soluble and insoluble fractions, and the percentage of expressed protein in the soluble fraction was higher after 16 hrs of induction in BL21(DE3) pLysS cells. (Figure 4-9).

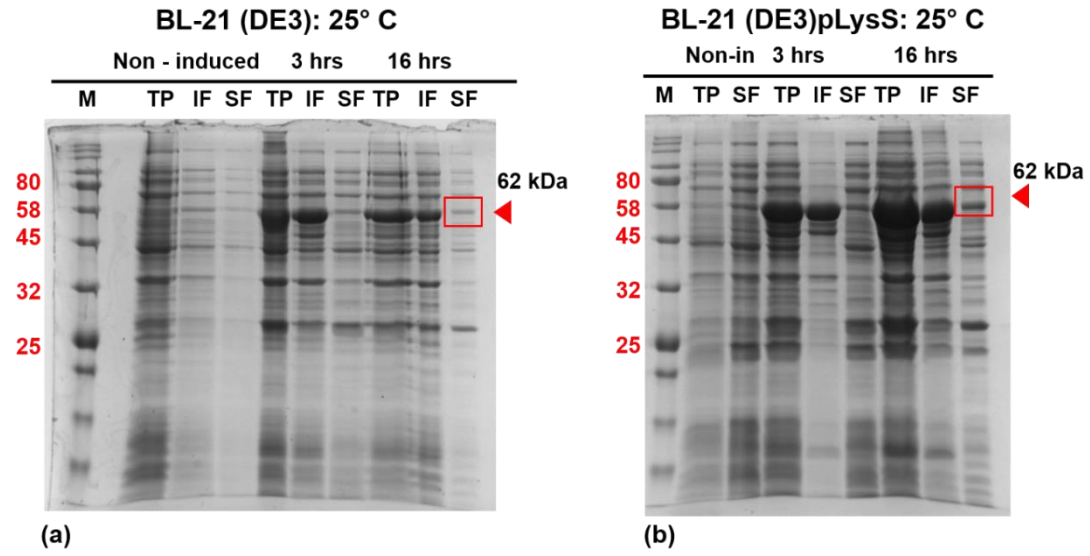

Figure 4-9. Expression of hAPSA(WT) in (a) Bl21(DE3) and (b) Bl21(DE3)pLysS at 25 °C after 3 hrs and 16 hrs of induction.

M: NEB pre-stained marker, TP: Total protein, IF: Insoluble fraction, SF: soluble fraction. Expression of hASPA is higher after 16 hrs of induction at 25 °C in BL21(DE3)pLysS cells.

BL21(DE3)pLysS cells were also tested at 18 °C, to see if lowering the temperature had any effect on overall protein expression and solubility(Figure 4-10). Expression at 18 °C after 16 hrs of induction was slightly better than at 25 °C cells, (ratio of protein in soluble fraction: total protein was higher at 18 °C as calculated by imageJ: 0.35 compared to 0.24 at 25 °C). Thus, large scale expression was done at 18 °C.

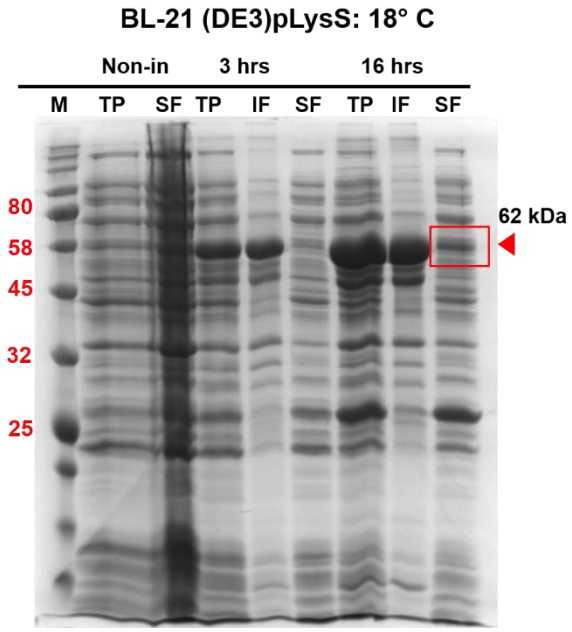

Figure 4-10. Expression of hASPA in Bl21(DE3) pLysS at 18 °C after 3 hrs and 16 hrs of induction.

M: NEB pre-stained marker, TP: Total protein, IF: Insoluble fraction, SF: Soluble fraction. Expression after 16 hrs of induction was slightly improved.

hASPA(WT) was purified from the soluble fraction of BL21(DE3)pLysS cells. The protein was purified on a GST column. Because of the slow binding kinetics of GST tagged proteins, a peristaltic pump was used with the loading of the protein at a slow rate of 1ml/min. The protein was eluted with 10mM reduced glutathione and fractions analysed on the gel (Figure 4-11 (a)) showed that the eluted protein was of the expected size of 62 kDa (36 kDa hASPA attached to 26 kDA GST). These fractions were pooled together and dialysed to remove reduced glutathione and DTT. ImageJ analysis of the gels showed that it was >85% pure (Figure 4-11 (b)). Protein yield after dialysis was 0.9 mg/ml from 2L culture, and it was further concentrated to 1.32 mg/ml (final volume 1 ml). 100µl aliquots of the protein were flash cooled in liquid N_2 and stored in -80° C until use.

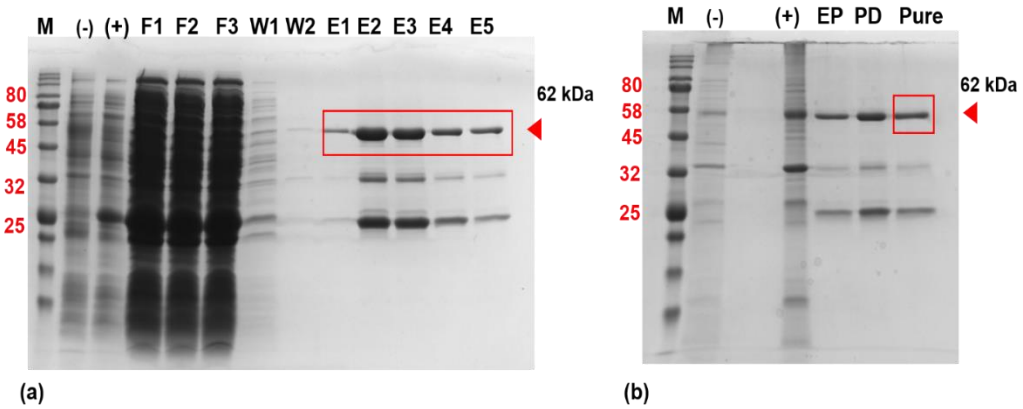

Figure 4-11. hASPA (WT) purification gels.

(a) M: NEB pre-stained marker, (-): non-induced SF, (+): induced SF, F1-F3: Flow through fractions, W1-W2: column washes, E1-E5 : eluted protein. (b) M: marker, (-): non-induced SF, (+): induced SF, EP : protein pooled from eluted protein fractions E1-E5, PD: protein after dialysis, Pure: hASPA(WT) pure protein.

4.3.3 Activity of hASPA

The activity of hASPA towards NAA was measured using the DMB/PpLAO coupled assay system. DMB is a fluorogenic derivatising reagent used for detection of alpha keto acids such as pyruvate and alpha keto glutarate. The compound can react with alpha keto acids to form a quinoxalinol derivative (Fujiwara et al. 2020) (Figure 4-12) which can be measured at 367 nm. As the hASPA/PpLAO enzyme coupled reaction produced oxaloacetate (OAA), which is also an alpha keto acid, this reagent was used to determine the activity of hASPA. Rate of formation of OAA-quinoxalinol derivative was measured at 367 nm and depended on the rate of formation of OAA by hASPA/PpLAO.

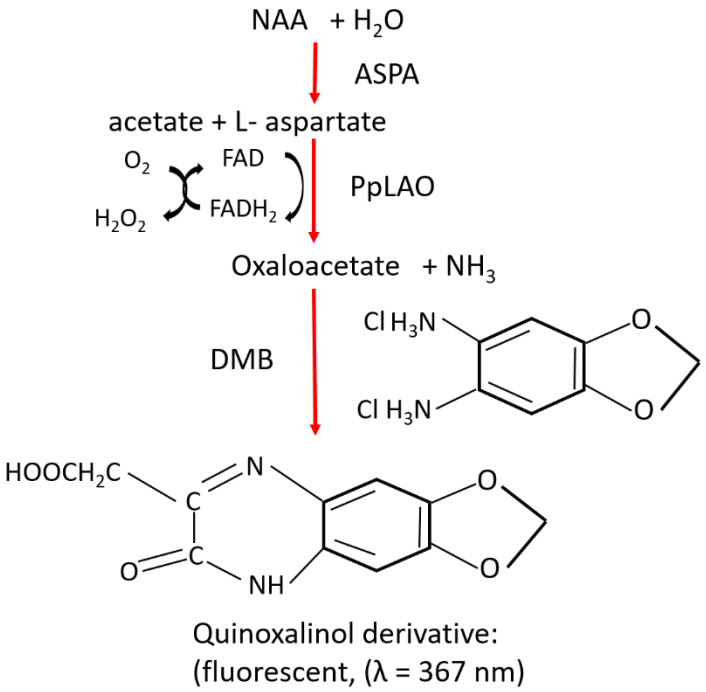

Figure 4-12. DMB/PpLAO coupled assay system for determination of hASPA activity. OAA can react with DMB to form a fluorescent derivative which can be measured at 367 nm.

This assay required optimisation as the DMB reagent had not been used before as a detection reagent in a spectrophotometer-fluorescence based enzyme assay system. DMB has been used for development of rapid and highly sensitive methods for detection of neuraminic acids (Hara et al. 1987) and alpha keto acids (Wang, Zaitsu, and Ohkura 1988) in serum samples. A DMB derived substrate had been used in another assay to study the kinetics of enzyme polysialyltransferase (Guo et al. 2020). This DMB substrate was used in the concentration range of 10-300 µM. So-far all assays with DMB have been performed in HPLC, however the reagent on its own has never been used for any reactions in a spectrophotometer. The reported assays indicated that DMB was a sensitive dye and could be adapted for fluorometric detection of OAA.

Based on previous reported values, for the hASPA assay optimisation 3µl of 1mM and 0.1mM DMB concentrations were initially used with 100 µM NAA as substrate concentration. The concentration of both enzymes was kept

constant during optimisation. 1 mM DMB in the reaction resulted in high background fluorescence and did not give consistent recordings, while 0.1 mM DMB gave reduced background fluorescence (Table 4-3), thus this concentration was used in the assay. Additional controls (Table 4.3.1) were used to check the validity of the assay. The rate of change of absorbance was recorded for all the controls and test sample.

Table 4-3: Control and test reactions for DMB/PpLAO assay.

Controls 1-4: Reaction components were successively eliminated from each control, as any missing enzyme/reagent/substrate would not result in a reaction rate. Control 5: buffer and enzymes only. Control 6: buffer and DMB only. Test sample: all reaction components are present, 100 µM NAA used as test concentration. ΔA: rate of change of absorbance min^{-1}.

	PBS	ASPA	PpLAO	DMB	NAA (100 µM)	ΔA min^{-1}
Control 1	+	—	+	+	+	0.0032
Control 2	+	+	—	+	+	0.0035
Control 3	+	+	+	—	+	0.000293
Control 4	+	+	+	+	—	0.0034
Control 5	+	+	+	—	—	0.000169
Control 6	+	—	—	+	—	0.0034
Test sample	+	+	+	+	+	0.048

As there were four components in the reaction, each one of them was successively eliminated in four different controls (control 1-4). The idea being that the reaction rate should be observed only when all components are present in the reaction mixture. Two additional controls, one with enzymes only (control 5) and another with DMB only (control 6) were also included. ΔA for controls 3 and 5 was very low as there was no DMB present. All other controls had a very similar ΔA.

Following optimisation, the DMB/PpLAO assay was used to measure specific activity of hASPA against increasing substrate concentrations. By performing a non-linear fitting of Lineweaver-Burk plot, K_m and V_{max} of hASPA

was determined to be 192.3 µM and 454.54 µmol/min/mg (R^2 = 0.97) respectively (Figure 4-13)

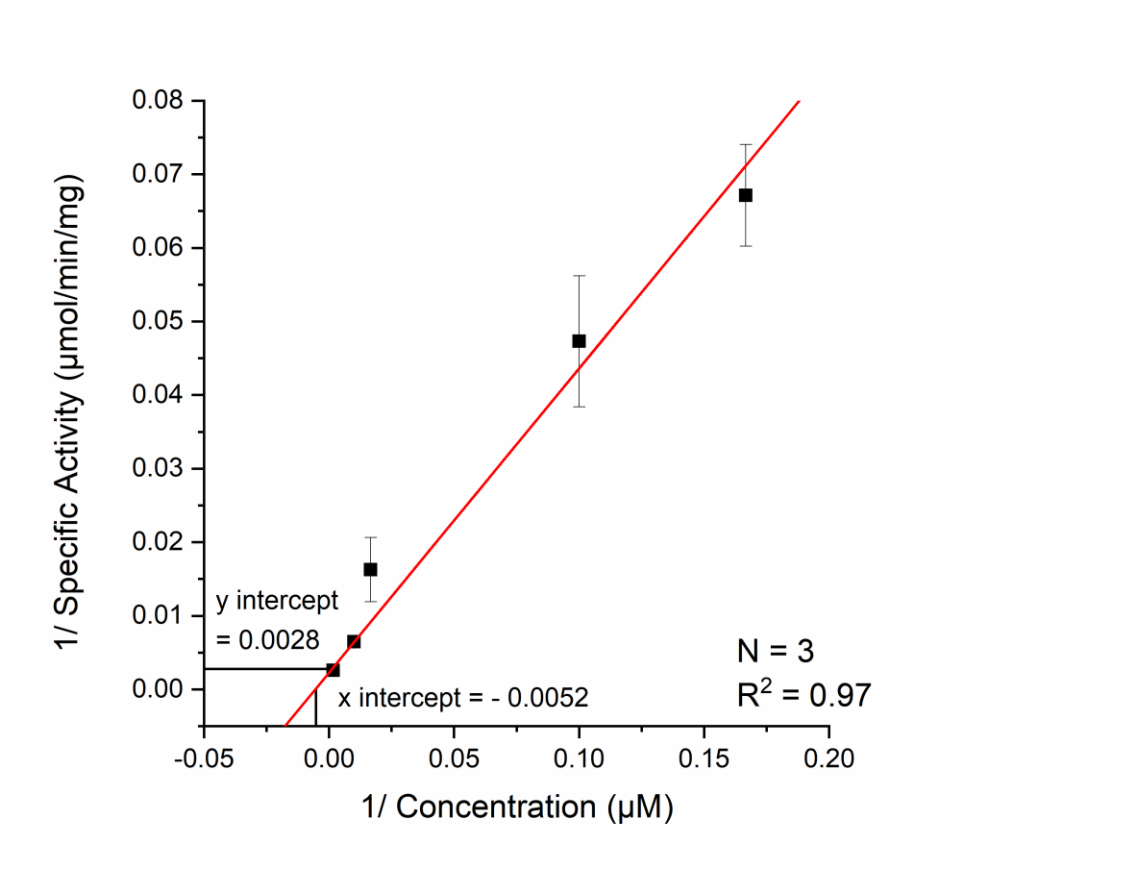

Figure 4-13. Lineweaver-Burk plot of initial velocity of hASPA.

For each assay, activity was measured at fixed enzyme concentraion and increasing NAA concentration (6 µM, 10 µM, 60 µM, 100 µM, 600 µM). V_{max} is 1/y intercept = 454.54 µmol/min/mg, while K_m = 1/ x intercept = 192.3 µM

4.3.4 NAA sensor fabrication

The L-Asp sensor mix was used to make the NAA sensor. NAA sensor was made using the same concentration of enzymes as in the assay (2 µl of 1.32 mg/ml hASPA and 3 µl of 55 mg/ml PpLAO), which corresponded to 1 unit of hASPA and 1.2 units of PpLAO (appoximately 1:1 ratio). NAA sensors prepared using this mix were tested against 100 µM NAA and L-Asp and gave the response of 0.16 µA/cm^2 and 0.15 µA/cm^2 respectively (Figure 4-14 (a) and (b)). A higher ratio of 1:2 (hASPA:PpLAO) was also tested but it did not change the sensor response, while lower ratios did not give any response. Ratios higher than 1:2 could not be tested as there is a limit to the amount of enzyme that can be added to the gel mix as it results in precipitation.

The NAA sensor was fabricated using the sol-gel method and by immobilisation of ASPA and PpLAO. The sensor responses show proof of principle result for the use of this method. However, further characterization of the NAA sensor could not be achieved because of time constraints.

(a)

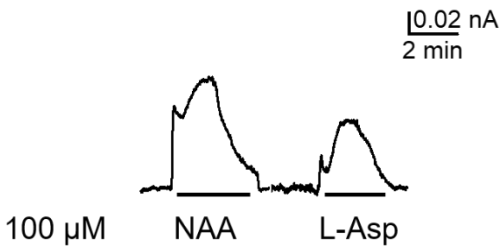

(b)

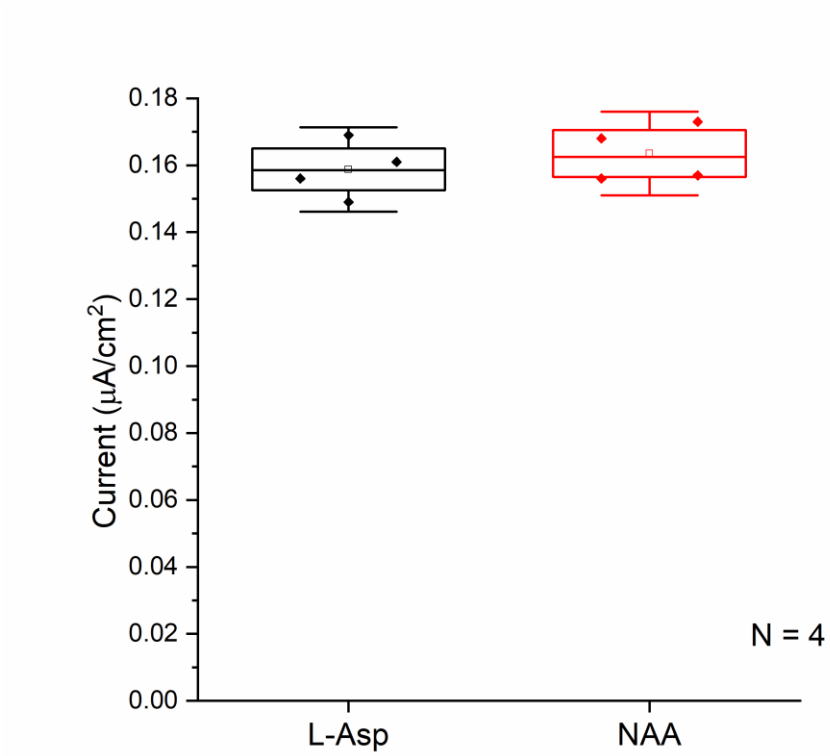

Figure 4-14. NAA sensor response.

(a) Amperometric current-time curve for NAA sesnor. (b) Average response for four NAA sesnors recorded against 100 µM NAA: 0.16 µA/cm^2 and L-Asp: 0.15µA/cm^2.

4.4 Discussion

The recombinant expression of hASPA was explored in insect Sf9 cells as ASPA is a eukaryotic enzyme, and it was thought that a eukaryotic expression system might work better for its expression. The baculovirus expression system has been used for expression of many mammalian enzymes (Kim et al. 2003; Fogal et al. 2015) in active form and was tested alongside the bacterial expression system for expression of hASPA.

Although the expression of hASPA in Sf9 cells was high, it was accompanied with proteolytic cleavage. As lysine residues are targeted by serine proteases and ubiquitin proteasomal complex (Mattiroli and Sixma 2014; Di Cera 2009), mutation of these residues was performed to eliminate the possibility of lysine induced degradation. However, the cleavage of hASPA could not be resolved with mutations of the lysine residues indicating that there might be other proteases or mechanisms interfering with the expression of hASPA. Though the proteases cleavage could have been addressed by addition of several protease inhibitors (Gotoh et al. 2002; Gotoh et al. 2001), this process would have required extensive optimization and been extremely time consuming, moreover as expression of GST-hASPA seemed promising, this method was not investigated further.

GST tagged hASPA has been successfully expressed and purified in active form before (Herga et al. 2006). The purification method I developed, differed from the previous method mainly with respect to use of a different buffer system, elimination of detergents (sarkosyl and triton x-100) from the purification process and no cleavage of GST tag from the enzyme. GST-hASPA was purified from the soluble fraction and resulted in the production of an enzyme which was of the expected size (62 kDa) and had comparable yield: 0.6 mg of enyme compared to the reported yield of about 1 mg from 1L of culture.

The activity of GST-hASPA was meaured using the DMB fluorescent dye. Several methods have been reported for determining the specfic activity of hASPA after recombinant expression and purrification. These include use of trinitrobenze-sulfonic acid (Herga et al. 2006), use of a coupled enzyme - aspartate ammonia lyase, (which converts L-Asp to fumarate and the rate of formation of fumarate is measured) (Le Coq et al. 2006) and HPLC based method (Di Pietro et al. 2008). All these methods are for determination of hASPA activity, however since my main goal was to not only determine hASPA activity, but also show that it works when coupled with PpLAO, these methods were not entirely suitable.

The Ared/HRP coupled assay used for PpLAO could not be used either as the presence of DTT and reduced glutathione (present in elution buffer), even in trace amounts results in very high levels of H_2O_2, giving false positives (Li and Imlay 2018; Votyakova and Reynolds 2004). Thus for determination of hASPA activity, coupled to PpLAO, DMB was suitable as the reagent could react with OAA, which was one of the end procuts of hASPA/PpLAO coupled reaction. It was very sensitive and could detect acitivty with very low enzyme concentraions (Guo et al. 2020).

Using this assay the enzyme activity was determined to be 454.54 µmol/min/mg, compared to the reported activity of 1557 µmol/min/mg. Presence of the GST tag did not seem to interfere with hASPA activity, and the reduced activity could be because of PpLAO which is rate limiting in this reaction. The K_m was found to be 192.3 µM or 0.19 mM which is very close to the reported K_m of hASPA: 0.24 mM (Herga et al. 2006). The K_m was also within range of K_m values reported from other assays (0.12 mM (Le Coq et al. 2006), 0.16 mM (Di Pietro et al. 2008)).

As the concentrations of hASPA and PpLAO required to record activity of hASPA, had been adjusted in the enzyme assay, the same concentrations were used to make the NAA sensor. Furthermore, as the L-Asp gel mix had been optimised for PpLAO and it was used to make the NAA sensor to obtain proof of principle data. The sensor responded to both L-Asp and NAA, which

was important as with multi-enzyme sensors, all enzymes should respond to their respective substrates. The limiting factor of NAA sensor was the enzyme PpLAO which is slow and limits the sensitivity of the sensor, similar to L-Asp sensor.Although the sensor response was low, it did show that both enzymes are working together. As it is a two enzyme sesnor, it would require further exploration to determine the best sol-gel mix that would allow both enzymes to work efficiently. The NAA levels in the brain are reported to be very high – upto 10 mM, so the sensor still might work in that range when used for detection of real-time release of NAA in brain slices.

Overall, purification of hASPA in active form was achieved. A new DMB/PpLAO asasy was validated. Finally, hASPA was used in conjuction with PpLAO to make the NAA sensor. This principle and methodology for NAA sensor holds potential and can be extended to make integrated electrochemical sensor array such as the SMARTChip (Beamer et al. 2021). These chip based sensors could prove useful for detection of NAA in samples of whole blood or plasma as it is an important biomarker for stroke and TBI.

Chapter 5

Real-time measurement of L-Aspartate release in the hippocampus

5.1 Introduction

The direct measurement of neuroactive compounds such as purines and neurotransmitters such as L-glutamate (L-Glu) has been made possible because of microelectrode biosensors (Llaudet et al. 2003; Tian et al. 2009). The sensors allow for real-time measurements of the release of these compounds along with simultaneous recording of synaptic activity. Thus, after the fabrication and characterization of L-Aspartate (L-Asp) sensor, the next goal was to test the sensor in brain slices to detect L-Asp release. L-Asp release was studied in the hippocampus as there was substantial literature support demonstrating presence of L-Asp in this area.

5.1.1 L-Asp is released in the hippocampus and is a N-methy-D-aspartate (NMDA) receptor agonist

One of the earlier studies on release of L-Asp and L-Glu in the rat hippocampus was done by Nadler et al.(Nadler et al. 1976; Nadler et al. 1978). The authors demonstrated that L-Asp release was reduced when lesions were introduced in commissural fibres of area CA1. Light and quantitative electron microscopy analysis of immunostained rat hippocampal slices by Gundersen *et al.* showed that at normal [K^+], L-Asp and L-Glu colocalized in nerve terminals forming asymmetrical synapses in stratum radiatum of CA1. After depolarization with high K^+, there was loss of immunoreactivity for both L-Asp and L-Glu, with simultaneous increase in immunoreactivity in glia cells. Furthermore, immunohistochemical localization of L-Asp was very strong in the Schaffer collateral -commissural pathway in areas CA1 and CA3 (Gundersen, Ottersen, and Storm-Mathisen 1991; Gundersen et al. 1998). By exposing rat hippocampal synaptosomes (from area CA1) to 25 mM K^+ or 300 µM 4-aminopyridine (4-AP) Zhou et al. (Zhou et al. 1995) and later Bradford

and Nadler(Bradford and Nadler 2004) studied the mechanism of release of L-Asp and L-Glu. Additionally, Zhou *et al* in 1995 gave the first demonstration of L-Asp release from synaptosomes upon application of 4-AP. These studies also demonstrate Ca^{2+} dependent release of L-Asp. K^{+} evoked release of L-Asp from rat hippocampal synaptosomes was reduced upon loading of light chain of tetanus toxin and botulinum neurotoxins A, B or C indicating an exocytotic mechanism for L-Asp release (Wang and Nadler 2007). Holten *et al* in 2008 also presented evidence for vesicular release of L-Asp from hippocampal nerve terminals (Aleksander Talgøy Holten 2008).

In contrast to this evidence supporting L-Asp as a neurotransmitter, Herring et al. studied the excitatory synaptic transmission in hippocampus in vesicular glutamate transporter -1 (VGLUT1) knock out (KO) mice and concluded that glutamate alone accounts for excitatory transmission (Herring et al. 2015). Thus, if L-Asp really does act as a neurotransmitter it is not as the main excitatory transmitter in the hippocampus. However, Herring et al. studied VGLUT-1 KO mice and VGLUT1 and -2 are considered specific markers for glutamatergic neurons with absolute specificity for L-Glu versus L-Asp. A third transporter, VGLUT-3, which can also transport L-Asp into vesicles, has been identified in neurons that are not exclusively glutamatergic, and that these synapses release L-Glu as a co-transmitter (El Mestikawy et al. 2011; Stensrud, Sogn, and Gundersen 2015). An overlooked possibility is that they may also release L-Asp.

It has been shown that L-Asp selectively activates the NMDA receptors. Patneau and Mayer recorded the dose response curves for activation of excitatory amino acid receptors on cultured mouse embryonic hippocampal neurons for several different amino acids and their isomers. Their data showed that L-Glu was the most potent receptor agonist for both NMDA and quisqualate or α-amino-3-hydroxy-5-methyl-4-isoxazole-propionic acid (AMPA) receptors, but L-Asp was highly selective for NMDA with an EC50 of 16.9 µM. L-Asp did not activate AMPA receptors, with concentrations as high as 5 mM (Patneau and Mayer 1990). Fleck et al. also examined the activity of

released L-Glu and L-Asp in area CA1 of rat hippocampal slices and found that both amino acids had affinity for NMDA receptors, while only L-Glu had affinity for AMPA receptors (Fleck et al. 1993).

In addition to all the supporting evidence in favour of L-Asp in the hippocampus, it is also one of the most investigated structures in the brain. Because of its distinct anatomy, regular arrangement of neuronal population and afferent fibre pathways, the hippocampus is an ideal region of the brain to initiate the study of L-Asp release. It is highly susceptible to damage from epilepsy, hypoxia or ischemia, and there are several protocols that can be adopted. it provides diverse avenues of investigation and is an established model of study (Anand and Dhikav 2012; Knierim 2015).

The main aim of this chapter was to study L-Asp release for which the following methods were used:

1. Standard model of seizure induction: application of 4-AP and 8-cyclopentyltheophylline (8-CPT), in Mg^{2+} -free aCSF.
2. Focal Stimulation of Schaffer collaterals in area CA3 of hippocampus
3. Application of DL-threo-β-Benzyloxyasparticacid (TBOA), to block the excitatory amino acid transporters (EAATs) and study its effect on L-Asp release (Shimamoto et al. 1998).
4. Ca^{2+} dependence of L-Asp release: studied in combination with TBOA application in Ca^{2+} -free aCSF
5. Study the release of L-Asp by application of L-albizziine (L-Alb), a competitive inhibitor of enzyme asparagine synthetase (ASNS). ASNS is the enzyme that synthesizes asparagine (L-Asn) from L-Asp and glutamine (L-Gln) (Lomelino et al. 2017).
6. NMDA receptor activation by L-Asp: by application of L-Alb in presence of D-(-)-2-amino-5-phosphonopentanoic acid (D-AP5), which is NMDA receptor antagonist (Zhou et al. 1995).

Finally, as an extension to this study,

7. Changes in ASNS expression levels were checked by immunohistochemistry in mouse brain slices from epileptic mice, and by western blot on mice and human epileptic tissue.

5.2 Material and Methods

5.2.1 Drugs

L-Asp, 5-Hydroxytryptamine (5-HT), ethylene glycol-bis(β-aminoethyl ether)-N,N,N′,N′-tetraacetic acid (EGTA), 8-cyclopentyltheophylline (8-CPT) and 4-aminopyridine (4-AP) were obtained from Sigma. D-(-)-2-amino-5-phosphonopentanoic acid (D-AP5) and DL-threo-β-Benzyloxyasparticacid (TBOA) were obtained from Tocris Biosciences. L-Albizziine (L-Alb) was obtained from Bachem. Stock solutions of all the drugs were prepare and stored frozen. On the day of the experiment solutions were thawed and diluted in aCSF. All chemicals were dissolved in water except TBOA and 4-AP which were dissolved in DMSO.

5.2.2 Preparation of hippocampal slices

Parasagittal hippocampal slices (400 µm) were prepared from 4-5-week-old C57 BL/6 mice. Mice were killed by cervical dislocation and decapitated according to Schedule 1 of the UK Government Animals Act (Scientific Procedures) 1986 and Local Ethical Review procedures. The brain was quickly removed and put into ice cold high Mg^{2+}, low Ca^{2+} artificial cerebrospinal fluid (aCSF) containing in mM: 127 NaCl, 1.9 KCl, 8 $MgCl_2$, 0.5 $CaCl_2$, 1.2 KH_2PO_4, 26 $NaHCO_3$, 10 D-glucose, at pH 7.4 when bubbled with 95% O_2 and 5% CO_2. The brain was cut along the median line and the two halves were stuck on their medial surface. Hippocampal slices were cut in high Mg^{2+} aCSF on a vibratome (Microm HM650 V microslicer). Slices were kept in standard aCSF (1mM $MgCl_2$, 2mM $CaCl_2$, pH 7.4) at 34 °C for 1 h before use.

5.2.3 Electrophysiological recordings

After the recovery period, an individual slice was transferred to a recording chamber, was perfused with oxygenated aCSF at rate of 6-7 ml/min

and was maintained at 32 °C throughout the experiment. To elicit a response, trains of stimuli : high frequency stimulations (HFS, 100 stimuli per train at 100 Hz frequency, each pulse of 2 ms, with 10 ms interval) were delivered by a DS3 isolated stimulator (Digitimer Ltd., UK) via a concentric bipolar metal stimulating electrode (FHC, Greenville, PA, USA) placed on the surface of area CA3 of the hippocampus. aCSF-filled glass microelectrode was placed in stratum radiatum of CA1 to make extracellular recordings (10 kHz sampling and 1Hz to 3kHz filtering). Extracellular field excitatory postsynaptic potentials (fEPSPs) and physiological activity was recorded and analysed using Spike2 software (v 7.08) (Cambridge Electronic Design, Cambridge, UK). All drugs used in the experiments were bath applied.

Experiments involving 4-AP and 8-CPT: Drugs were applied in Mg^{2+} -free ACSF: 0 $MgCl_2$, 2mM $CaCl_2$,1.4 mM KCl, pH 7.4 at 34 °C. Experiments with Ca^{2+}-free aCSF: 0 $CaCl_2$, 3 mM $MgCl_2$, 1mM EGTA, pH 7.4 at 34 °C.

5.2.4 Biosensor measurements

Screened L-Asp and null sensors were prepared as per methods in chapter 3 (section 3.2.2- sensor characterisation). The biosensors were calibrated with bath application of 300 µM L-Asp before the slice was present in the perfusion chamber and after each experiment when the sensors had been withdrawn from the slice. The screening layer of the sensors, which reduces the interference from electroactive substances was also routinely checked by applying 100 µM 5-HT.

L-Asp and null sensors were fully inserted into the stratum radiatum of the CA1 area. The slice was left to recover for at least 30 minutes after insertion of the sensors, for any signal associated with the sensor insertion to dissipate before each experiment. Sensor recordings were made on Spike2 software (v 7.08) at sampling rate of 1kHz.

All data analysed using Origin pro 9.6 and presented as mean and standard deviation. The decay time course was determined from exponential fits in Origin pro 9.6, made on individual currents after removal of baseline.

5.2.5 Immunohistochemistry

Induction of epilepsy, mouse brain slice preparation and imaging was performed by Dr Amol Bhandare. Epilepsy was induced in 8-10 weeks old C57BL/6 male mice through kainic acid injection procedure (Benson, Manzanero, and Borges 2015). After 14 weeks of induction of status epilepticus (SE), mice were humanely killed and the brains were removed and postfixed in paraformaldehyde (4°C) overnight, 40 µm slices were used for immunohistochemistry.

Slices were blocked for 1 hr with 4% bovine serum albumin (BSA) in PBS with 0.1% triton. Slices were then incubated for 16 hrs at room temperature (RT) in primary antibodies prepared in 4% BSA in PBS with 0.1% triton, as per the dilutions stated: glial fibrillary acidic protein (GFAP, abcam, ab4674,1:1000), asparagine synthetase (ASNS, recombinant rabbit monoclonal antibody 2H11L12, Thermo fisher,1:500) and neuron specific protein (NeuN, MAB377- Sigma, 1:500). After brief washing in PBS, slices were incubated for 1 hr at RT with secondary antibodies prepared in 4% BSA in PBS with 0.1% triton at 1:250 dilution: Alexa Fluor 488, Alexa Fluor 594 and Alexa Fluor 680 (Thermo Fisher). Pots were covered with foil to protect from light during the incubation period. After washing in PBS, slices were mounted on a clean slide and stored in 4 °C until imaging. Images were examined using a Zeiss 880 confocal microscope with ZEN acquisition software (Zeiss, Oberkochen, Germany).

5.2.6 Western Blot

Western blot (WB) was performed by Dr Aida Menendez Mendez at the Royal College of Surgeons, Dublin, Ireland. Expression of ASNS was probed using ASNS primary antibody. Mice were 8-weeks old when SE was induced. The mice were sacrificed at 4, 8 or 24-hours following SE (acute) or 4 weeks after epilepsy induction (epileptic mice). WB was also performed on excised human tissue from patient with temporal lobe epilepsy (TLE).

5.3 Results

5.3.1 Sensor performance in the recording chamber

In order to check the performance of the L-Asp and null sensor in the same solutions as those used for the experiments, sensors were placed in the recording chamber and calibrated with 300 µM of L-Asp and 100 µM of 5-HT. The calibration was performed before inserting the sensors in the slice and after withdrawing the sensors from the slice after each experiment. The response was recorded in normal aCSF by bath application of the analytes. As the null sensor is the sensor without the enzyme, it is the control to check for the response generated by electroactive interferents and any changes in temperature and pH. The signal from the null sensor was digitally subtracted and the differential recording was considered as the true response generated by application of L-Asp. Figure 5-1(a) and (b) shows the sensor calibrations before and after the experiment (averaged from 5 independent recordings).

The response to L-Asp before inserting the sensor into the slice was 0.56 ± 0.15 nA, while for 5HT it was 0.040 ± 0.0086 nA. After the withdrawal of the senor, the L-Asp response was recorded as 0.38 ± 0.065 nA, and for 5-HT it was 0.087 ± 0.023 nA. The 10-90% signal rise time was < 10 s.

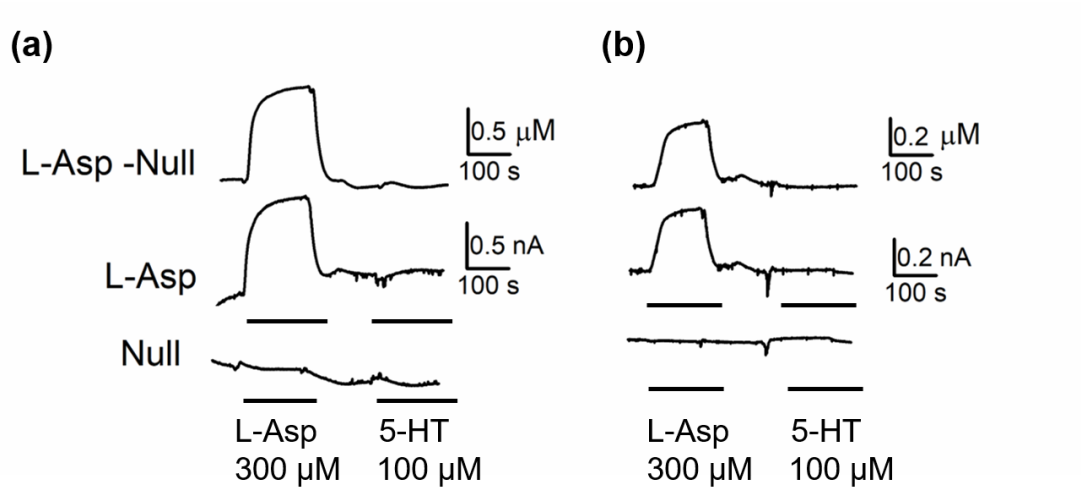

Figure 5-1. L-Asp sensor calibrations.

(a) Sensor calibration before inserting the sensor into the slice. Response to L-Asp: 0.56 ± 0.15 nA, 5-HT: 0.0405 ± 0.0086 nA. (b) Sensor calibration after the sensors were withdrawn from the slice. Response to L-Asp: 0.38 ± 0.065 nA, 5-HT: 0.087 ± 0.023 nA.

A 10-15% decrease in sensitivity was observed for the sensors after the experiments, because of interaction with the tissue and also because of the fouling of the platinum wire. In order to retain the sensitivity and minimize the effect of fouling, sensors were subjected to a process of “cycling”, where a cycling voltage ramp going from +500 mv to -500 mV was applied for about 10-12 cycles (Frenguelli and Wall 2016). In general, if the decrease in sensitivity was >15% and if the signal for 5-HT was higher than 0.1 nA, the senor was not used any further. The null sensor was included in all the experiments and the second calibration after sensor withdrawal was used for calculating the concentration of L-Asp released.

5.3.2 Placing of electrodes in the hippocampus

The L-Asp and null sensors were fully inserted into the stratum radiatum of the CA1 area of the hippocampus to detect the release of L-Asp. Sensors were held by micromanipulators and placed under optical magnification. Sensors were fully embedded into the tissue, through the entire thickness of the brain slices, so that the entire sensing surface was in contact with the tissue. Focal stimulation of the Shaffer collaterals was performed by placing the stimulating electrode gently on the surface of the CA3 area. The recording

electrode was also placed in the CA1 area, to record for fEPSP, in between the sensors and the stimulating electrode. Figure 5-2 illustrates the positioning of the sensors and the electrodes in the hippocampal slice. Care was taken to place the sensor away from the stimulator, so as to minimize effect of stimulus artifact.

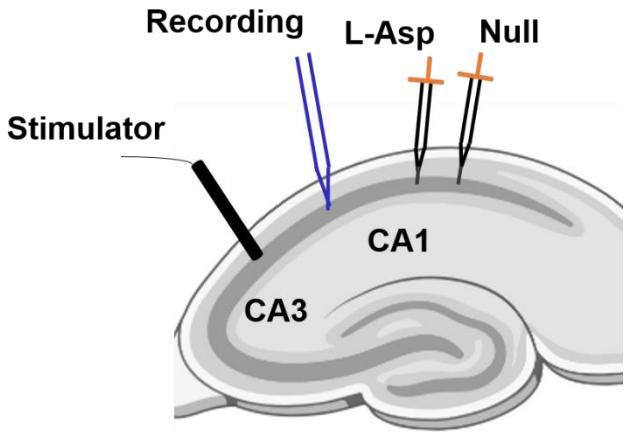

Figure 5-2. Diagram illustrating the positioning of sensors, recording electrode and stimulating electrode on the hippocampal slice.

5.3.3 Application of 4-AP, 8-CPT in Mg^{2+} -free aCSF does not evoke L-Asp release.

With the aim of recording L-Asp release, electrographic seizures were induced by the application of 4-AP (50 µM), 8-CPT (1 µM) in Mg^{2+} - free aCSF. Perfusion of hippocampal slices with Mg^{2+} - free aCSF provokes release of adenosine and also induces electrographic seizure activity. This activity is increased by the application of 4-AP which blocks the K^+ channels and promotes neuronal depolarization. In combination with the adenosine A1 receptor antagonist 8-CPT, the epileptiform activity is further enhanced (Hall and Frenguelli 2018). Thus, a combination of these drugs is a strong generator of increased activity in the hippocampus and it was thought that it would be a good starting point to evoke L-Asp release, however L-Asp release could not be detected upon the application of these drugs in Mg^{2+} - free aCSF *(n = 5)*. A representative recording is shown in Figure 5-3. Slice was perfused with

normal aCSF for 15 minutes. Seizure activity normally appeared within 4 minutes of drug application. Drugs were applied for 15- 20 minutes before switching to wash in normal aCSF.

The fEPSPs and activity could also be recorded on the slices indicating that the neuropil around the sensors had not been inactivated and the damage caused by sensor insertion does not affect the detection of neural activity in close vicinity of the sensors.

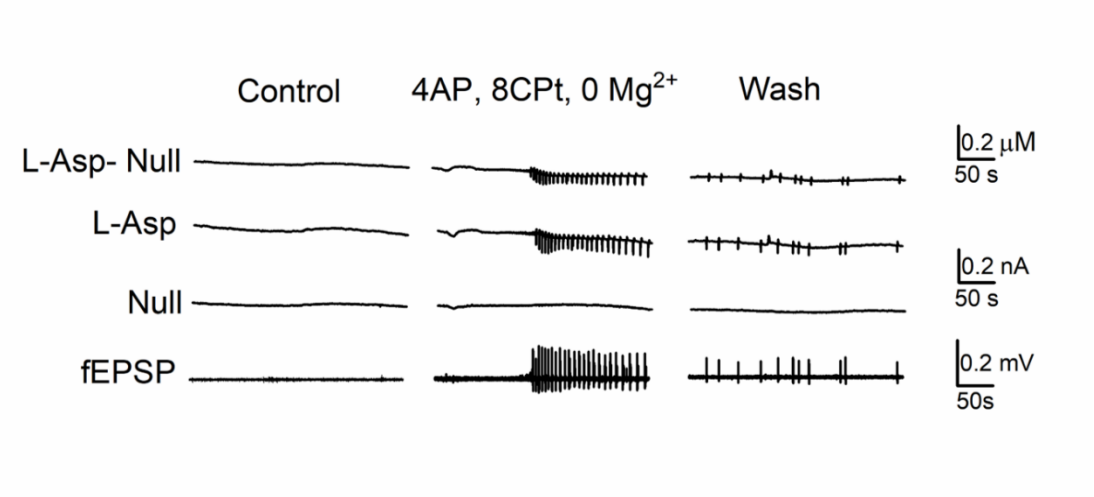

Figure 5-3. Application of 4-AP and 8-CPT in Mg^{2+} -free aCSF does not evoke L-Asp release.

A representative slice recording is shown. L-Asp- Null: differential recording, L-Asp and Null traces with corresponding fEPSP. 5 min recordings are shown for each section. All traces are on same time scale. The fast transients on the sensor traces are due to the sensors recording electrical activity within the slice (compare to fEPSP trace).

5.3.4 L-Asp release detected upon HFS

Since induction of seizure activity by application of drugs did not result in L-Asp release, another approach was used. Focal stimulation of Schaffer collaterals in the CA3 region was performed, in normal aCSF. Following 100 Hz stimulation (100 pulses, stimulus amplitude 10-15 µA) L-Asp release could be detected in 4 out of 6 slices. Stimuli were delivered at 4-5-minute intervals. No release was detected when the number of pulses was reduced to 4. Furthermore, there was a delay of about 8-10 s from the time the stimulus was applied to when the signal appeared (where it starts to rise above the

baseline), which indicated that it was a true release as opposed to a stimulus artifact. Average L-Asp concentration recorded from 4 slices (3 stimulations in each) was 71.3 ± 12.17 µM *(n = 4).* There was also an average delay of 22 ± 1.01 s *(n = 4)* from the stimulus to peak amplitude. This delay is much longer than that observed for glutamate release (Wall and Dale 2013).

5.3.4.1 Is L-Asp release Ca^{2+} dependent?

In order to check if the L-Asp release observed upon stimulation, was dependent on Ca^{2+}, slices were washed in Ca^{2+} -free aCSF for 10 minutes before applying stimulus. The L-Asp release in Ca^{2+} -free aCSF reduced to 28.7 ± 25.4 µM *(n = 2)*. A representative recording is shown in Figure 5-4. The fEPSP did not diminish in Ca^{2+}- free aCSF, this could be because it was not washed long enough.

The stimulus amplitude for these slices was high (10 -15 µA), thus for the next set of experiments, this amplitude was reduced to 1-5 µA, and the time for drug application and subsequent washings was also increased.

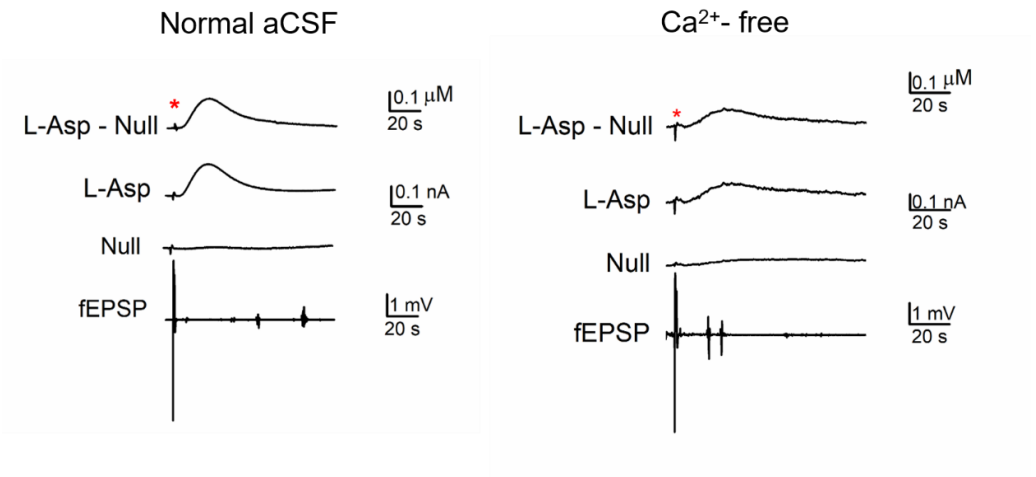

Figure 5-4. Focal Stimulation in CA3 region evoked L-Asp release recorded in CA1; L-Asp release is reduced in Ca^{2+} -free aCSF.

A representative trace is shown. Stimulus is denoted by red asterisk. L-Asp – Null: differential trace, L-Asp, null and corresponding fEPSP traces are shown on the same time scale. L-Asp release after 10 minutes in Ca^{2+} -free aCSF is shown on the right. Compared to normal aCSF, L-Asp release reduced.

Statistical analysis for Ca^{2+} sensitivity of L-Asp response is presented in Figure 5-5. Average peak amplitude reduced from 0.86 ± 0.10 nA to 0.65 ± 0.23 nA *(n = 3)* and was found to be significant (Paired T test, P < 0.05).

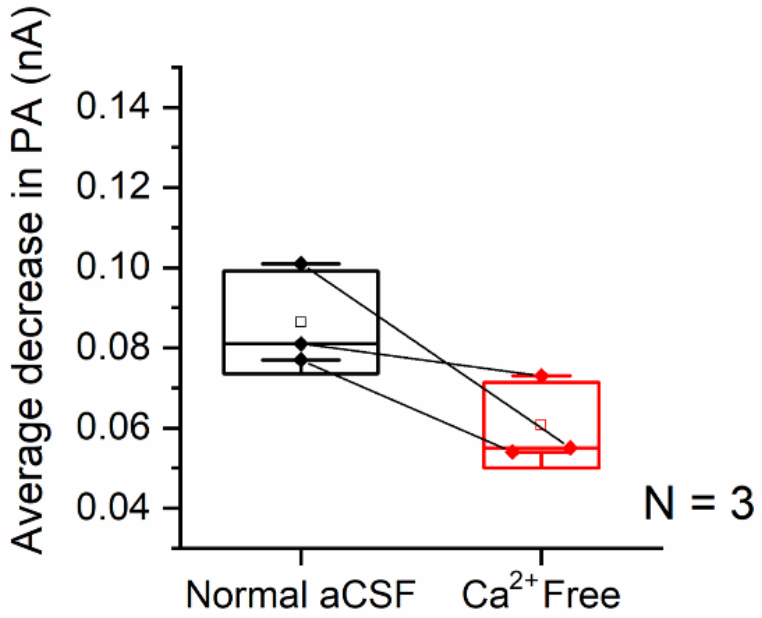

Figure 5-5. Ca^{2+} sensitivity of L-Asp release.

Ca^{2+} sensitivity of L-Asp release was observed in 3 slices. After 10 minutes in Ca^{2+} aCSF, the peak amplitude was reduced. Average peak amplitude reduced from 0.86 ± 0.10 nA to 0.55 ± 0.23 nA *(n = 3)*, and was found to be significant (Paired T test, P < 0.05)

5.3.5 Effect of TBOA on L-Asp release

As spontaneous release of L-Asp was observed upon stimulation with 100 pulses at 100 Hz, it was applied in combination with a glutamate transporter blocker TBOA, to see if it had any effect on L-Asp release. TBOA is a potent blocker of the glutamatergic transporters-excitatory amino acid transporters (EAATs). EAAT1 or L-glutamate/L-aspartate transporter (GLAST) has been identified as the transporter for L-Glu and L-Asp in the rodent brain, and TBOA is an effective blocker for this transporter (Storck et al. 1992; Shimamoto et al. 1998).

To observe the effect of TBOA on L-Asp release, slices were perfused in normal aCSF for 15 minutes(control), with application of stimuli. TBOA (200 µM) was applied for full 15 minutes before applying stimulus and finally washed for 10 minutes in normal aCSF. Three stimuli were applied in each segment at interval of 3-4 minutes.

Effect of TBOA on a representative slice is shown in Figure 5-6, where a spontaneous release of L-Asp was observed upon stimulation, with average L-Asp release of 10.8 µM (control). Upon application of TBOA, the average L-Asp release was recorded as 24 µM (TBOA). The effect of TBOA persisted after 10 minutes of washing, as L-Asp release was higher than control: 24.4 µM (wash). Time constant of decay (tau, τ) described by a single exponential was calculated and it increased from 28.2 s in control to 34 s in TBOA.

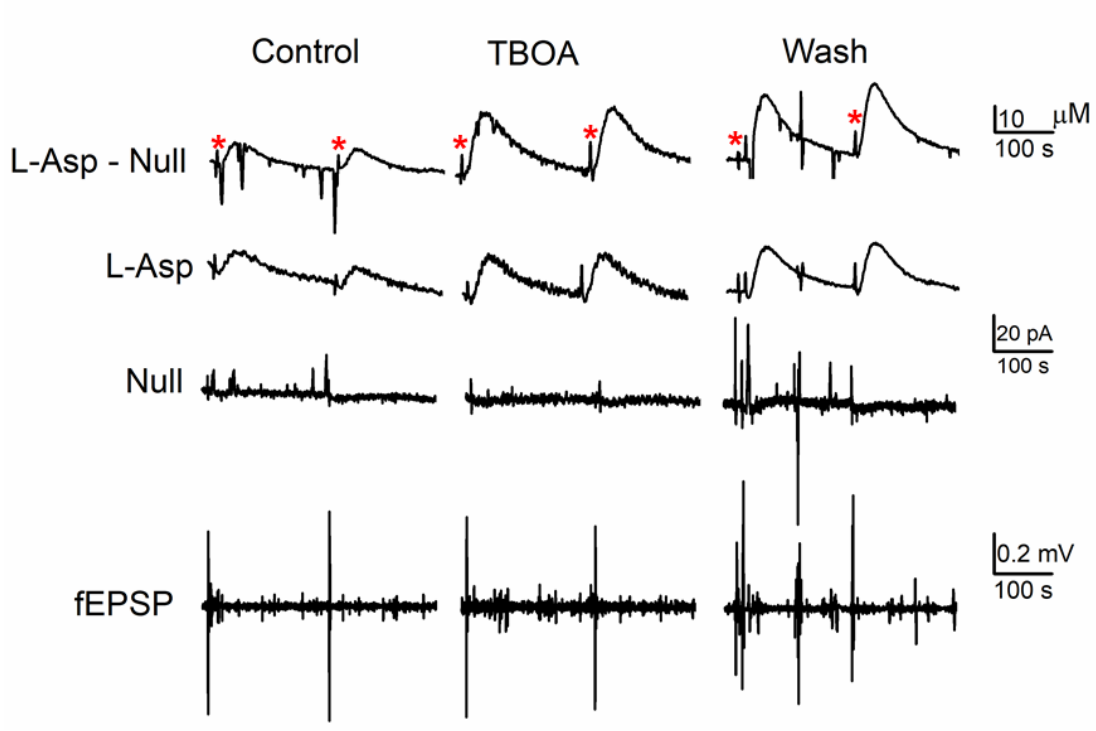

Figure 5-6. Effect of TBOA on L-Asp release.

Representative trace is shown, with full 6-minute recording for each segment. Stimulus is marked by red asterisk. L-Asp – Null: differential recording, L-Asp, null and corresponding fEPSP traces are shown, all on the same time scale. Application of TBOA increased L-Asp release from 10.8 µM to 24 µM. A longer decay of response was observed in TBOA going from 28.2 s to 34 s.

On three other slices where TBOA was applied, no spontaneous release of L-Asp was detected in the control. However, after application of TBOA, L-Asp release was observed which persisted in the wash. A representative slice is shown in Figure 5-7. Average L-Asp release for TBOA segment from all four slices was 9.9 ± 5.9 µM *(n = 4)*.

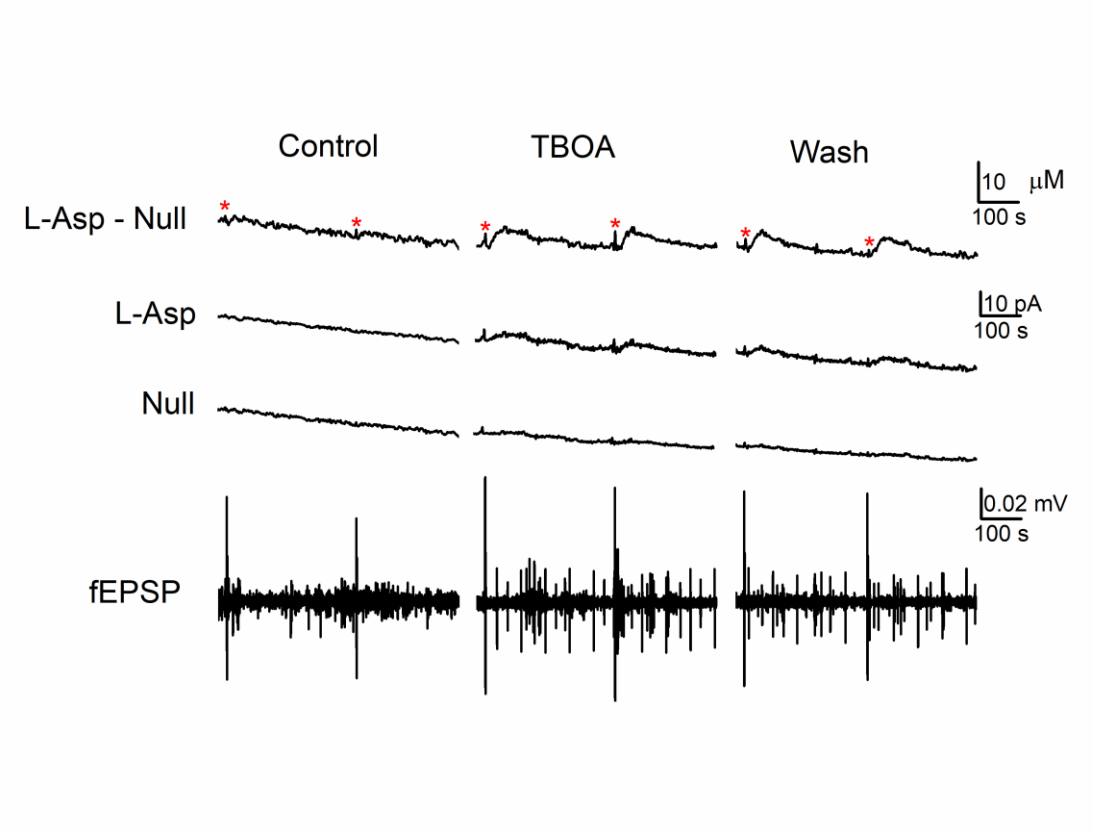

Figure 5-7. L-Asp signal appeared after application of TBOA.

After 15 minutes of TBOA application a signal for L-Asp could be detected which persisted in the wash. L-Asp – Null: differential recording, L-Asp, Null and fEPSP traces are shown. Stimulus is marked by red asterisk.

5.3.5.1 Effect of TBOA on L-Asp release: is the release Ca^{2+} dependent?

In order to check if L-Asp release was Ca^{2+} dependant, L-Asp release was checked in Ca^{2+} -free aCSF in combination with TBOA. Slices were first perfused in normal aCSF for 10 minutes, then TBOA was applied for another 15 minutes, followed by application of stimuli, and finally slices were washed in Ca^{2+} -free aCSF with TBOA present in the solution for 20 minutes.

Figure 5-8 shows a representative trace, where spontaneous release of L-Asp was observed upon stimulation with L-Asp release of 10.4 µM (control). After application of TBOA for 15 minutes, L-Asp release increased to 12.7 µM (TBOA segment). Average decay constants were calculated to be 52.6 s in control and 59.1 s in TBOA. L-Asp release reduced to 3 µM in Ca^{2+} -free aCSF with TBOA (wash).

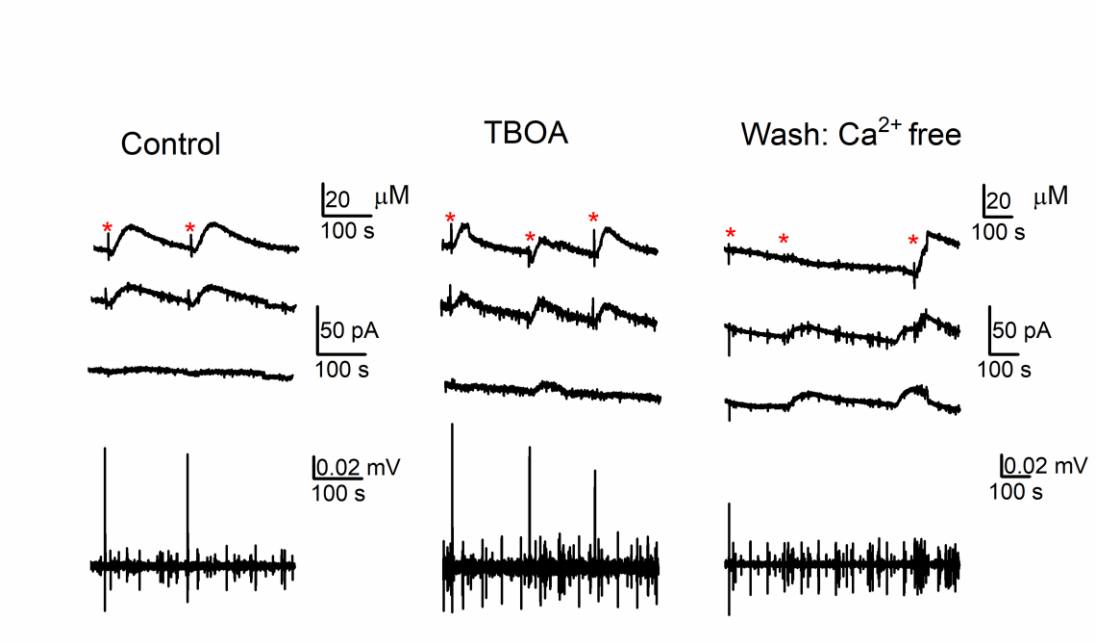

Figure 5-8. L-Asp release in Ca^{2+} -free aCSF with TBOA.

Representative trace is shown. Stimuli marked with red asterisk. L-Asp- Null differential recording, L-Asp, Null and corresponding fEPSPs are shown. Control segment is an 8-minute recording in normal aCSF. TBOA segment and Ca^{2+}-free wash segments are 12-minute recordings. Ca^{2+} -free segment: first stimulus applied after 12 minutes in wash, second stimulus was after 15 minutes and the final stimulus was after 22 minutes in Ca^{2+} -free aCSF. L-Asp release was reduced in Ca^{2+} -free aCSF. There were fluctuations of the baseline, which were recorded on both L-Asp and null traces.

The effect of Ca^{2+} -free aCSF was checked on two other slices, where on one slice again there was spontaneous release upon stimulation, while on a third slice L-Asp release was observed only upon TBOA application. L-Asp release was reduced upon application of Ca^{2+} -free aCSF. Average release of L-Asp from the three slices in TBOA segment only was 13.5 ± 1.6 µM *(n = 3)*, while for Ca^{2+} - free segment was 5.3 ± 1.8 µM.

A Friedman ANOVA test was conducted, for L-Asp release on application of TBOA, followed by wash in normal aCSF (degrees of freedom = 2, α = 0.005) which rendered χ^2 = 11.25, which was significant (P = 0.002).

In order to check if L-Asp release was Ca^{2+} dependant, L-Asp release was checked in Ca^{2+} -free aCSF in combination with TBOA. Average peak amplitude decreased Ca^{2+} free aCSF wash. A Friedman ANOVA test was conducted, (degrees of freedom = 2, α = 0.05) which rendered χ^2 = 6.2, which was significant (P = 0.03). Figure 5-9 shows the average changes in peak amplitude on application of TBOA, followed by normal wash (a) or Ca^{2+} wash (b).

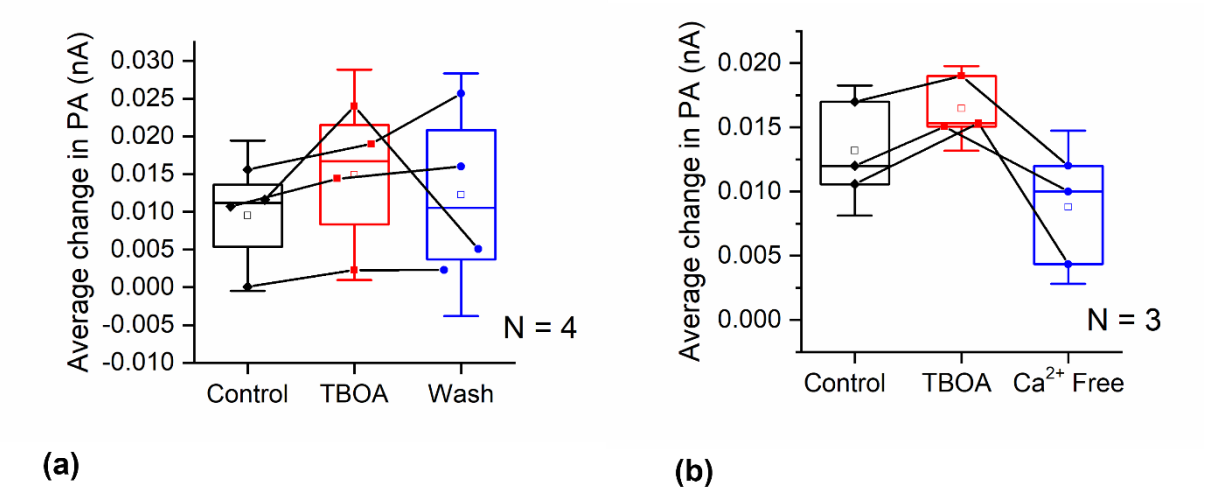

Figure 5-9. Average changes in peak amplitude observed for TBOA in normal aCSF and Ca^{2+} free aCSF.

(a) Increase in peak amplitude was observed after application of TBOA, which persisted in 3 out of 4 slices in the normal aCSF wash segment. (b) A decrease in peak amplitude was observed on all 3 slices upon application of Ca^{2+} free aCSF.

Effects of TBOA on the decay and peak amplitude are summarised in Figure 5-10 ((a) and (b)). The average decay constant and increase in peak amplitude, from control and TBOA segments was calculated from three slices, where spontaneous release of L-Asp was observed (one washed in normal aCSF and other two in Ca^{2+} free aCSF) to be 42.3 ± 12.6 s for control and 48.2

± 12 s in TBOA segment *(n = 3)*. The time constant of decay was significantly higher in the TBOA segment (paired T-test, P = 0.003).

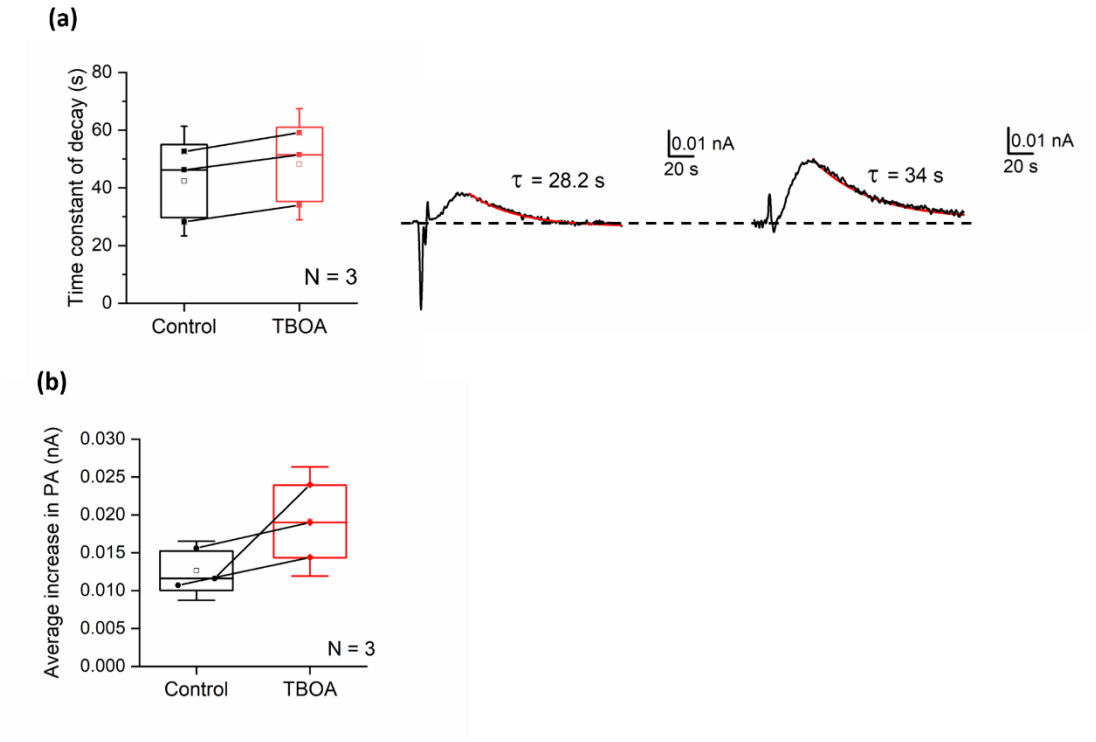

Figure 5-10. Effect of TBOA on time constant and peak amplitude.

(a) Graph summarising the effect of TBOA on time constant of decay, average decay constant for control was 42.3 ± 12.6s and in TBOA segment was 48.2 ± 12 s. Traces on the right from a representative slice with the decay fitted with a single exponential (shown in red). (b) Effect of TBOA on peak amplitude, an increase in peak amplitude was observed upon application of TBOA, in slices where spontaneous L-Asp release occurred on stimulation.

5.3.6 Effect of L-Alb on L-Asp release

L-Asp release was also studied by the application of L-Alb which is a competitive inhibitor of the enzyme ASNS (Deng et al. 2020). ASNS synthesizes L-Asn in the brain in an ATP dependent manner from L-Asp and L-Gln. This reaction is central to synthesis of L-Asn and is completely dependent on presence of L-Asp and ASNS activity (Lomelino et al. 2017). Inhibition of ASNS was a direct intervention in one of the key metabolic pathways involving L-Asp (Figure 5-11).

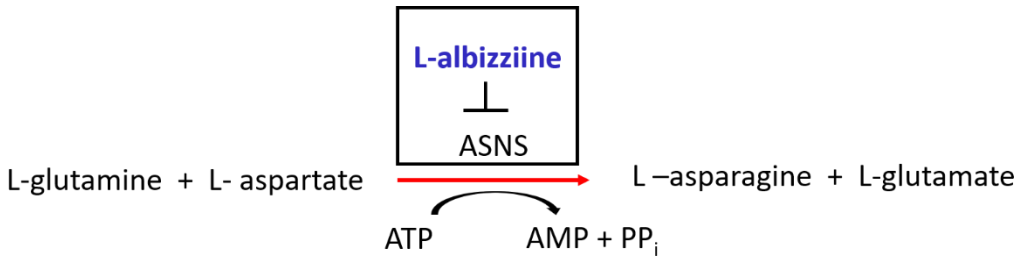

Figure 5-11. ASNS reaction and inhibition by L-Alb.

L-Alb is generally applied at concentrations of 2-4 mM in cell culture experiments (Deng et al. 2020), thus for application on hippocampal slices 2.5 mM of L-Alb was used. Slices were perfused in normal aCSF for 15 minutes with accompanying application of stimuli. This was followed by application of L-Alb in normal aCSF for another 15-20 minutes and application of stimuli. Finally, slices were washed in normal aCSF for 20 minutes.

A representative image from a continuous recording is shown in Figure 5-12. Each segment is a 700 s recording (11.67 minutes). Spontaneous release of L-Asp was observed in the slice, with L-Asp release of 28.8 µM (control). After application of L-Alb electrographic seizure- like activity appeared within 4 minutes. This electrical activity was evident both on the field electrode recordings and the L-Asp and Null sensor recordings. The appearance of this seizure-like activity was accompanied by an increase in L-Asp release- 41.3 µM (L-Alb segment). The seizure activity lasted for the entire length of L-Alb application. Upon washing in normal aCSF, frequency of seizures diminished in 5 minutes, but the L-Asp release remained high, 38.5 µM (Wash 1). After 10 minutes of washing, the L-Asp release decreased to 20.9 µM (Wash 2).

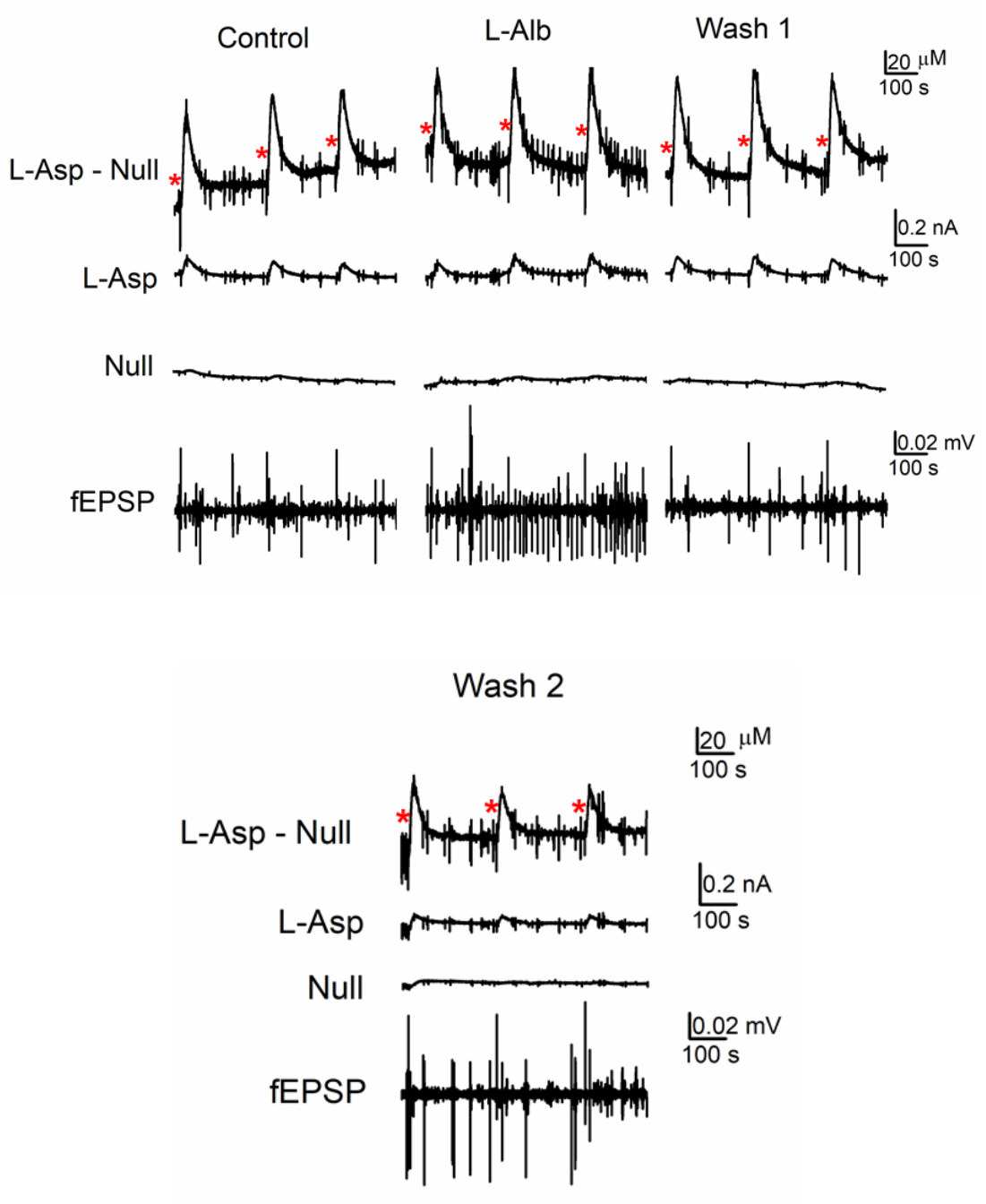

Figure 5-12. Effect of L-Alb on L-Asp release.

A representative slice is shown. Each segment is 700 s. Stimuli are indicated by red asterisk. L-Asp – Null: differential recording, L-Asp, Null and corresponding fEPSPs are shown on the same time scale. Appearance of seizure activity with accompanying increase in L-Asp release was observed upon application of L-Alb. Peak amplitude increased by a factor of 0.026 nA after L-Alb application. L-Asp release continued to remain high in wash 1- after 5 minutes of washing. L-Asp release goes down after 10 minutes of washing- wash 2.

This effect of L-Alb was observed on 4 slices. Average peak amplitudes and L-Asp release for control, L-Alb and final wash (Wash -2) are shown in Table 5-1, and average increase in peak amplitudes for control, L-Alb and wash -2 are shown in Figure 5-13. A Friedman ANOVA test was conducted, (degrees of freedom = 2, α = 0.05) which rendered $\chi^2 = 6.5$, which was significant (P = 0.03).

Table 5-1. Average peak amplitudes and L-Asp release observed on 4 slices after application of L-Alb

N=4 (mean ± S.D)	Control	L-Alb	Wash-2
Peak amplitude	0.03 ± 0.02 nA	0.06 ± 0.03 nA	0.024 ± 0.012 nA
L-Asp	17.7 ± 13 µM	29 ± 15 µM	12.7 ± 8.5 µM

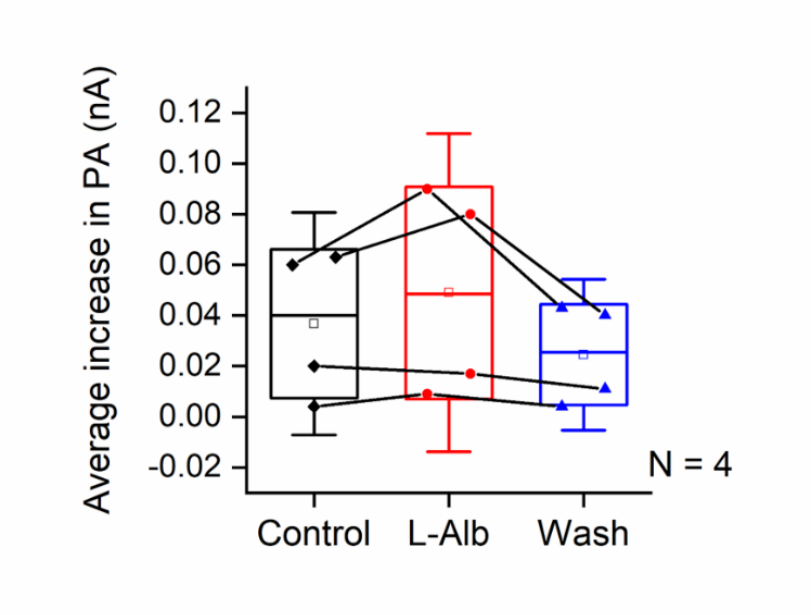

Figure 5-13. Increase in peak amplitude observed upon application of L-Alb.
Friedman ANOVA rendered $\chi^2 = 6.5$, which was significant (P = 0.03).

On one other slice, there was reduced epileptic activity, but L-Asp release increased from 39.3 µM to 42.2 µM. On yet another slice, spontaneous release of L-Asp was observed only after application of L-Alb with accompanying stimulation, and L-Asp release for this slice was: 47.1 µM

respectively. Average L-Asp release from L-Alb segment on all slices was 30.3 ± 19 µM *(n = 6)*.

Overall, effect of L-Alb, resulting in appearance of seizure-like activity was observed on 5 out of six slices with accompanying increases in peak amplitude and L-Asp release. A representative 40- minute fEPSP recording, is shown in Figure 5-14. The Ca^{2+} dependence of L-Asp release with L-Alb application was also checked on 3 slices, however because of unstable baseline the results were inconclusive (data not shown).

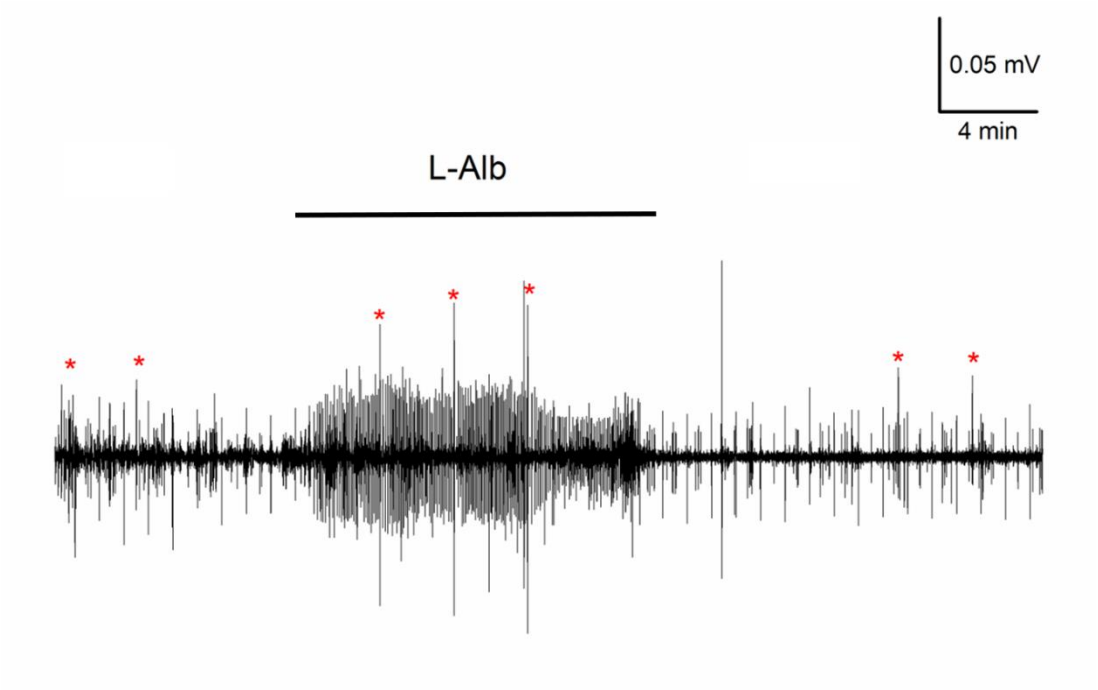

Figure 5-14. Inhibition of ASNS by L-Alb resulted in appearance of seizure-like activity.

Representative fEPSP recording is shown: 40- minute recording. Stimulus marked by red asterisk in each segment. Black bar: L-Alb application. Seizure-like activity appeared within 4-minutes and persisted for the entire time of L-Alb application.

5.3.7 Effect of D-AP5 and L-Alb on L-Asp release

As L-Asp is known to activate NMDA receptors (Patneau and Mayer 1990; Fleck et al. 1993), the epileptic seizure -like activity observed upon L-Alb application could be through activation of NMDA receptors caused by increased L-Asp release. Thus, if NMDA receptors are blocked, then L-Asp release should still be observed but there should be no epileptic activity. This

hypothesis was tested by applying the NMDA receptor antagonist D-AP5 (Zhou et al. 1995).

For these experiments, slices were first perfused in normal aCSF for 10 minutes, followed by application of 50 µM of D-AP5. L-Alb (2.5 mM) was introduced after 15 minutes. L-Alb was washed after 20 minutes followed by D-AP5 application for another 15 minutes before switching to wash in normal aCSF. Slices were stimulated in each segment at 3-5-minute intervals. Representative traces from a single continuous recording are shown in: Figure 5-15.

L-Asp release was not observed upon stimulation in control or upon D-AP5 application. On the representative slice, the release was seen after applying L-Alb with L-Asp release of 20.3 µM. L-Asp release persisted after 5 minutes of L-Alb wash with release of 15.3 µM. This release was not seen after further washing. Slice activity remained consistent throughout the recording, with no appearance of seizure- like activity.

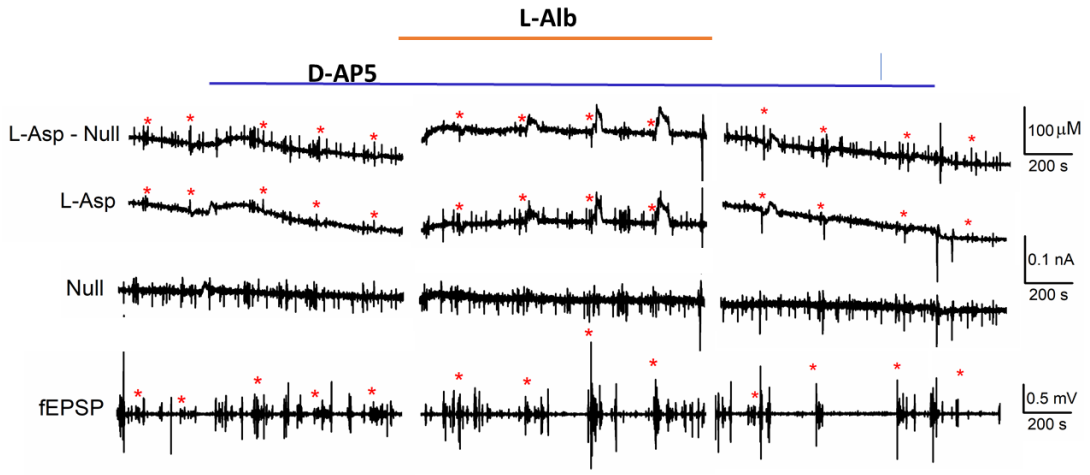

Figure 5-15. Effect of D-AP5 and L-Alb on L-Asp release.

L-Asp – Null : differential recording, L-Asp, Null and corresponding fEPSP traces are shown on same time scale. Stimuli are indicated by red asterisk. Blue bar: application of D-AP5 in the bath, a shift in baseline was observed for both null and L-Asp sensors. No spontaneous L-Asp release was observed. Orange bar: L-Alb application in the bath. L-Asp release was observed after 7 minutes of L-Alb application. L-Asp release persisted for 5 minutes after L-Alb wash.

No spontaneous release of L-Asp was seen on stimulation or upon D-AP5 application on all 3 slices. L-Asp was released only after L-Alb application. Average peak amplitude was 0.053 ± 0.05 nA in L-Alb segment in combination with D-AP5, which reduced to 0.034 ± 0.04 nA *(n = 3)*, when L-Alb was washed and was found to be significant (Paired T test, $P < 0.05$) (Figure 5-16).

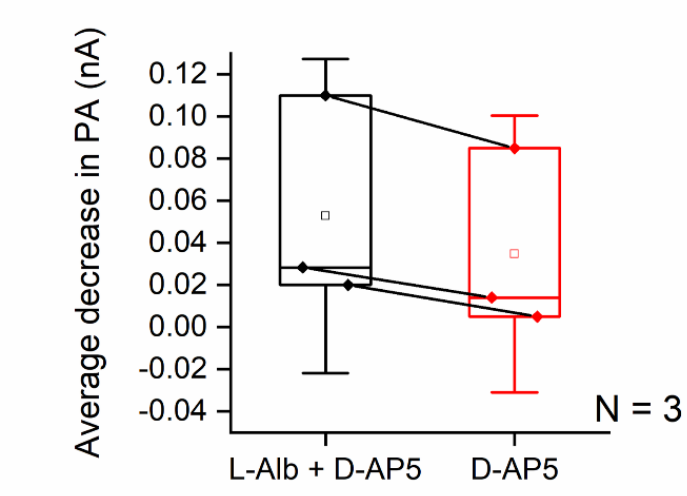

Figure 5-16. Average change in peak amplitude observed for D-AP5 application.

L-Asp release and signal was observed only after application of L-Alb, which persisted for 5 minutes after L-Alb wash. D-AP5 did not affect the release of L-Asp.

This effect of D-AP5 and L-Alb was observed in two more slices, where no spontaneous release of L-Asp was seen on stimulation or upon D-AP5 application. L-Asp was released only after L-Alb application. Average L-Asp release for three slices for D-AP5 and L-Alb segment was 35.5 ± 32 µM *(n = 3)*. L-Asp release persisted for 5-10 minutes after L-Alb was washed.

Thus, D-AP5 did not affect L-Asp release, but it successfully blocked the appearance of seizure-like activity, when applied in combination with L-Alb. A comparison of fEPSP recordings (54-minutes each) for two slices is shown in Figure 5-17.

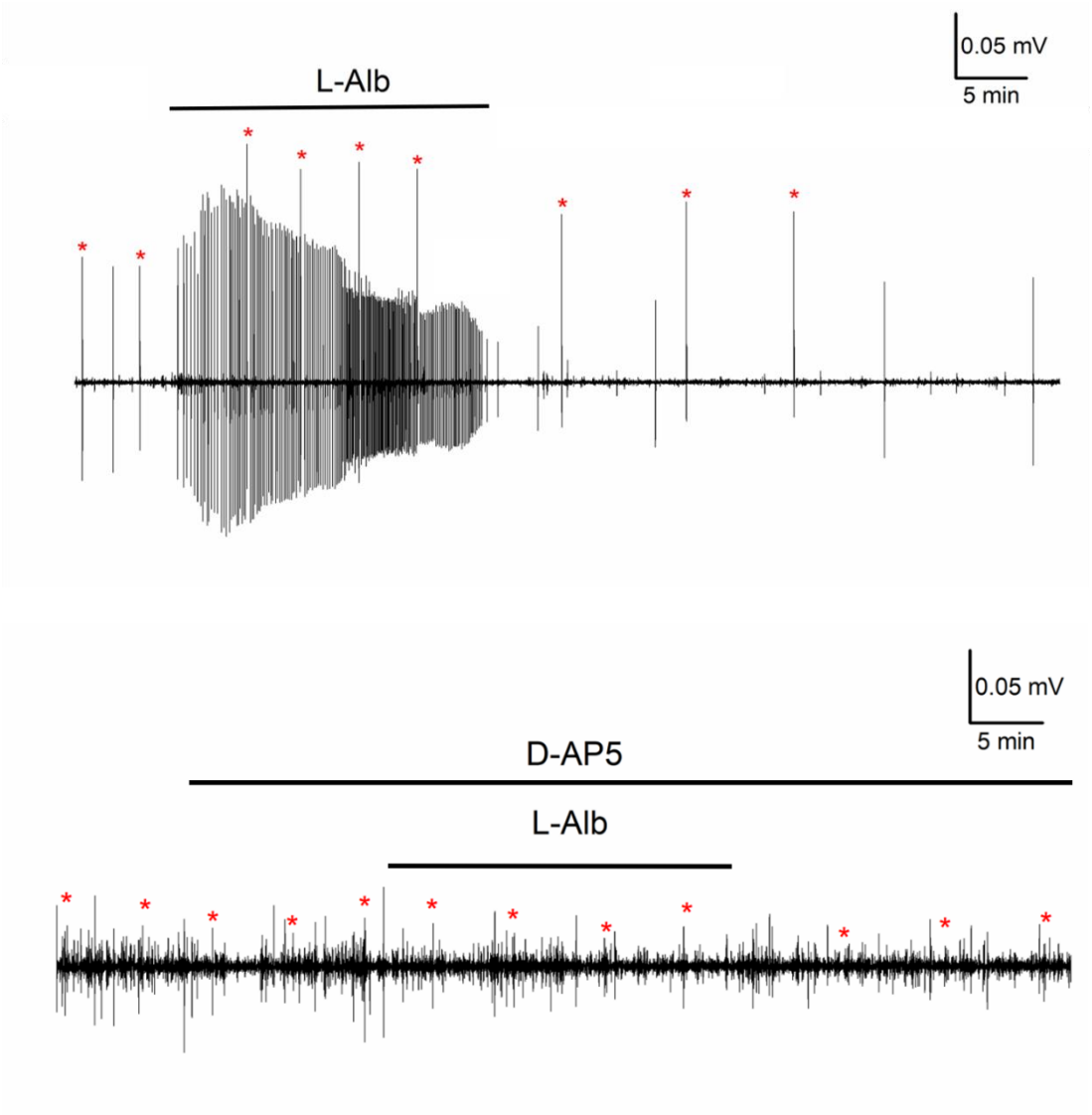

Figure 5-17. NMDA receptor antagonist D-AP5 blocked the appearance of seizure-like activity.

Stimulus denoted by red asterisk in both recordings. Top panel: representative 54- minute fEPSP recording from slice where only L-Alb was applied. Black bar: duration of L-Alb application. This activity was observed on 5 slices. Bottom panel: representative 54-minute fEPSP recording from slice where D-AP5 was applied on its own and in combination with L-Alb. Slice activity remained the same throughout the recording. The effect of D-AP5 was observed on 3 slices, with same result.

5.3.8 Changes in expression of ASNS upon induction of status epilepticus

The inhibition of ASNS by L-Alb resulted in seizure- like activity. Since epileptic seizures are observed in patients with ASNS deficiency (ASD) (Lomelino et al. 2017), the appearance of seizure- like activity upon enzyme

inhibition co-related with that symptom. To further explore if there are any changes in ASNS expression in epilepsy, immunohistochemistry was performed on brain slices from mice induced with SE.

Wild-type C57 BL/6 mice were induced with SE, spontaneous seizures were observed for 14 weeks before the mice were sacrificed. Staining with ASNS antibody showed that the enzyme co-localized with the neuronal layer in CA1, CA3 and in dentate gyrus (DG) and in the granule layer of DG in the control. In the epileptic mice, an upregulation of this enzyme in CA1 area on the ipsilateral side (where status was induced) was observed. Figure 5-18 shows the full brain slice, compared to the control. Hippocampal region from the ipsilateral side is shown in Figure 5-19.

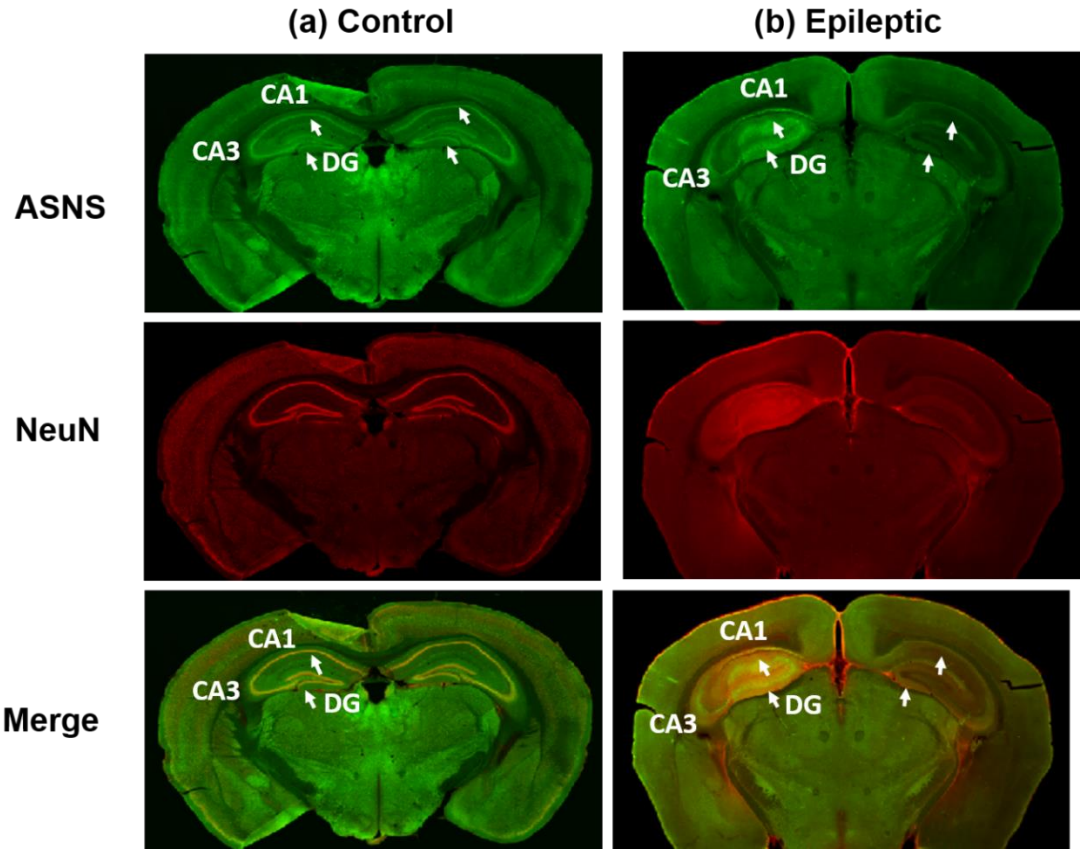

Figure 5-18. Changes in ASNS expression observed upon induction of epilepsy.

Full brain slices are shown for control and epileptic mice. ASNS co-localized with the neuronal layer in CA1, CA3 and DG. The enzyme is upregulated on the ipsilateral side while a diminished expression is observed on the contralateral side. Top panel: ASNS, middle panel: NeuN, bottom panel: merge of ASNS and NeuN.

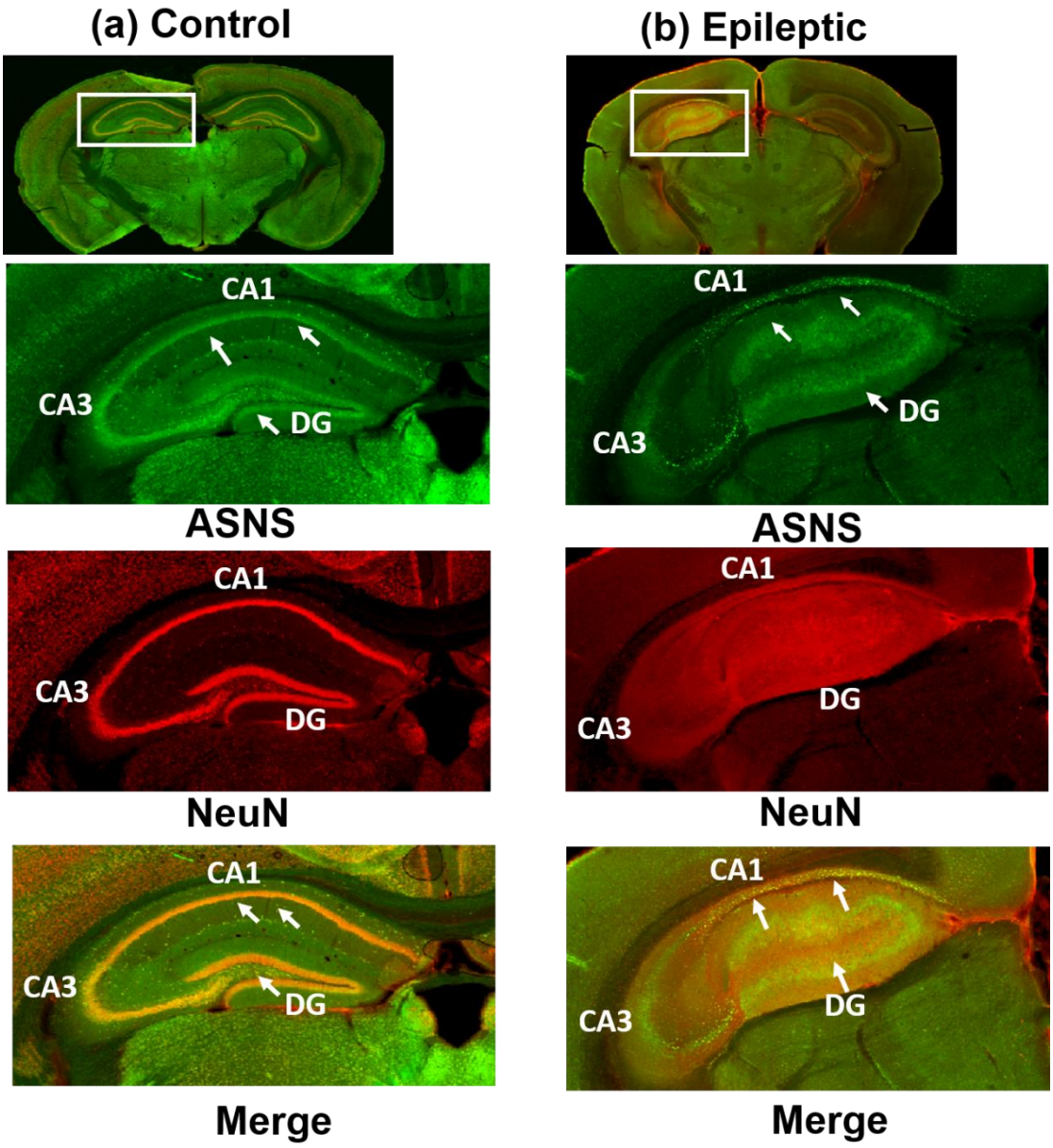

Figure 5-19. Upregulation of ASNS in area CA1 of hippocampus observed on the ipsilateral side.

Top panel: ASNS, middle panel: NeuN, bottom panel: merge. ASNS expression was upregulated in area CA1 – white arrows in top and bottom panel.

Based on these findings a request was made to Dr Tobias Engel and Dr Aida Menendez Mendez at the Royal College of Surgeons, Dublin, Ireland for WB on mice and human epileptic tissue. The ASNS antibody used for immunohistochemistry was provided. WB was performed on the ipsilateral side from mice with induced epilepsy to check for changes in ASNS expression levels. Mice were sacrificed after 4, 8 and 24 hours of status induction and after 4 weeks of epilepsy. No change in expression was observed after 4 and 8 hours, while an increase in ASNS levels could be seen after 24 hours (Figure 5-20 (a)). A clear upregulation was observed after 4 weeks (Figure 5-20 (b)). These observations were consistent with the immunohistochemistry data.

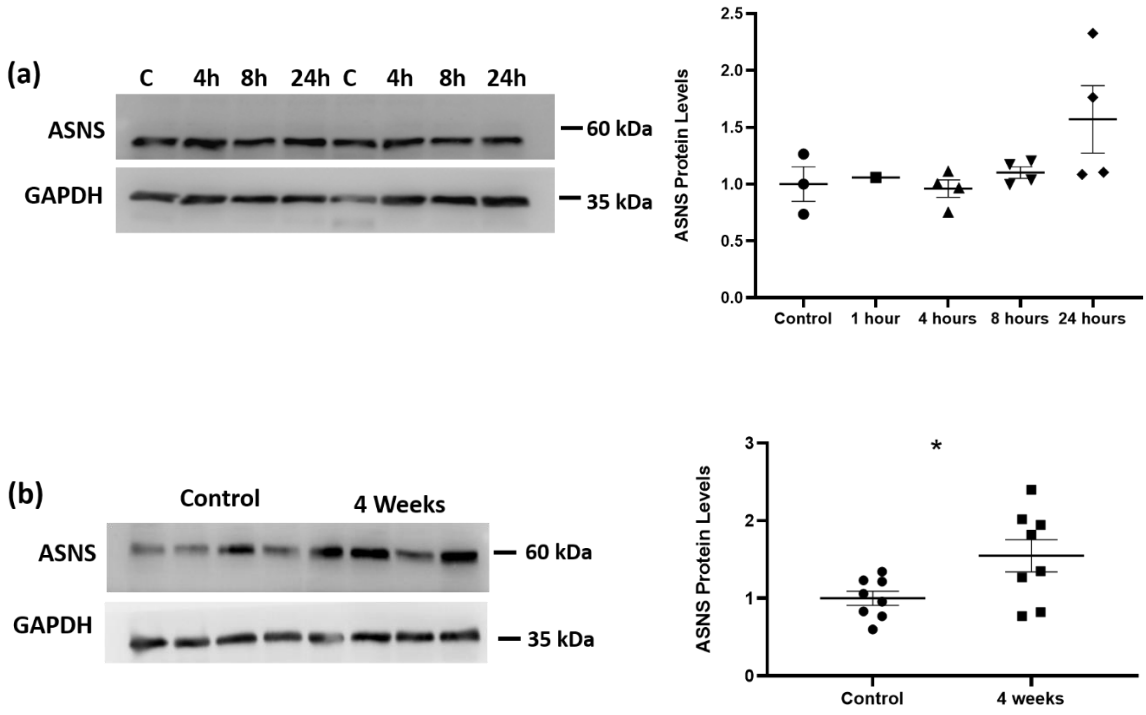

Figure 5-20. Changes in ASNS expression levels observed in mice hippocampal tissue: ipsilateral side.

WB and corresponding protein levels are shown. a) mice sacrificed after 4, 8 and 24 hours of status induction, ASNS levels are increased after 24 hours. (b) mice sacrificed after 4 weeks of status induction – ASNS levels are upregulated after 4 weeks.

Human tissue from patient with TLE was also probed with ASNS antibody and it showed upregulated levels of ASNS (Figure 5-21) in the hippocampus and cortex.

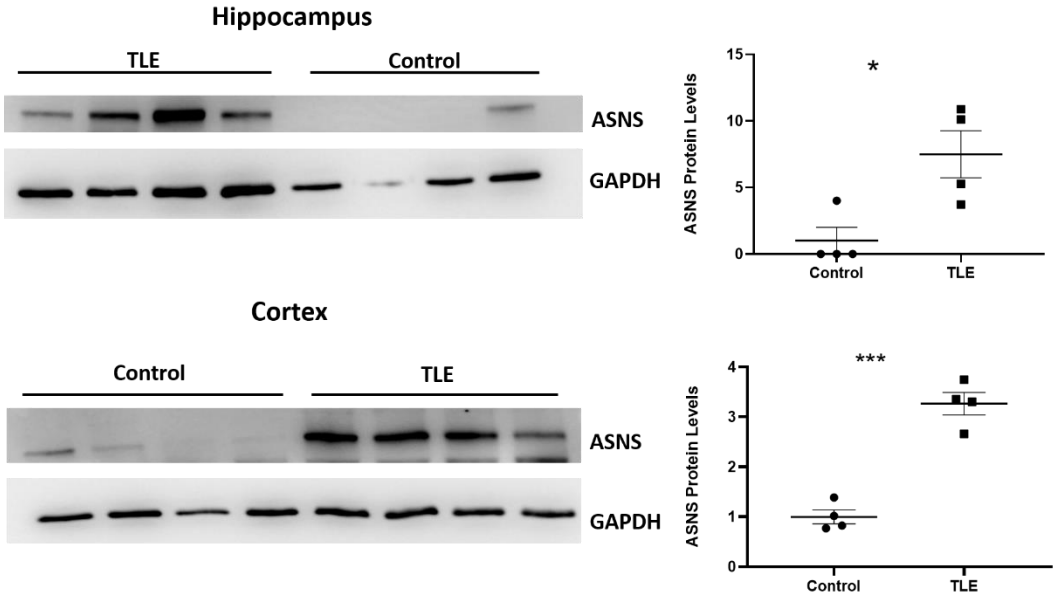

Figure 5-21. Changes in ASNS expression levels observed in human tissue.

WB and corresponding protein levels are shown. Tissue from patient with TLE: ASNS levels are upregulated in hippocampus and cortex.

5.4 Discussion

The L-Asp sensor in the recording chamber gave a fairly stable and consistent response during sensor calibrations. The sensor did not lose sensitivity at the higher temperature of 32° C, and the screening layer was also intact as response to 5-HT remained low. Upon insertion of the sensor into the slices, the sensors also picked up slice activity (as reported previously for purine sensors) (Frenguelli and Wall 2016) indicating that the sensors did not cause any extensive damage and did not impede the detection of neuronal activity around them.

The application of 4-AP and 8-CPT in Mg^{2+} -free aCSF did not result in L-Asp detection by the sensors. Previously, L-Asp release from synaptosomes has been studied by application of 300 µM of 4-AP (Bradford and Nadler

2004), which is very high compared to 50 µM used in this study. However, combination of 4-AP (at 50 µM) and 8-CPT (at 1 µM) is proven and effective model for generation of seizures (Hall and Frenguelli 2018), thus if no L-Asp was detected, it would suggest that it was not being released or the concentration of L-Asp released was below 3 µM, which is the lower limit of detection for L-Asp sensor.

As HFS of neurons in area CA3 resulted in L-Asp release, this method was pursued in combination with application of drugs that would interfere with L-Asp transport and metabolism. An average delay of 22 ± 1.01 s *(n = 4)* was observed for L-Asp release, which is much longer than the release of glutamate (3-5 s) (Wall and Dale 2013), indicating that there are differences in characteristics of release for L-Asp and L-Glu.

Excitatory amino acid transporters play an important role in transport of amino acids and termination of signals at the synapse. A 66-kDa glycoprotein, purified from rat brain was identified as L-glutamate/L-aspartate transporter (GLAST), which was inhibited by DL-threo-3-hydroxyaspartate (TBOA is a derivative of this compound) (Storck et al. 1992). Schmitt *et al.* detected a very high astrocytic immunolabelling for GLAST mRNA and protein (Schmitt et al. 1997) in rat central nervous system.

Indeed, application of TBOA affected L-Asp release by increasing the time constant of decay, by factor of 10 s. In slices where no spontaneous L-Asp release was observed, 15-minute application of TBOA resulted in appearance of L-Asp signal, this would suggest that the L-Asp being released and the blockade of reuptake by TBOA, increased the concentration of L-Asp allowing it to be detected.

Another important metabolic pathway for L-Asp utilization is the L-Asn synthesis by the enzyme ASNS. This reaction is important for synthesis of L-Asn in the brain and the only source of this amino acid. A deficiency of ASNS as a result of mutations, leads to asparagine synthetase deficiency (ASD), which has been characterized by microcephaly, intractable seizures and

progressive brain atrophy (Lomelino et al. 2017; Schleinitz et al. 2018). Application of L-Alb, a competitive inhibitor for ASNS was a direct inhibition of a key enzyme involved in metabolism of L-Asp.

L-Alb is a L-Gln analogue (Deng et al. 2020), and inhibits the first step of the reaction mechanism, which is L-Gln deamination and activation of L-Asp carboxylate in an ATP dependent manner. As this first step would not take place, the downstream reaction mechanisms would not occur either, causing an increase in the intracellular levels of L-Asp. As L-Asn and L-Glu are reaction products, they would not be formed (Lomelino et al. 2017).

Furthermore, ASNS is highly expressed in mouse brain, developing embryonic mouse brain and is particularly enriched in the neurons. ASNS mutations affect mitosis of neural progenitors and generally reduce the number of neurons (Ruzzo et al. 2013).

Thus, application of L-Alb not only increased the concentration of L-Asp, it also induced seizure- like activity which is associated with the neurological impairment resulting from ASD. Seizures appeared with 3-4 minutes of L-Alb application, similar to the 4-AP seizure model, and disappeared after 5 minutes of wash. Although the levels of L-Asp were high even after 5 minutes of wash, indicating that strong inhibition of ASNS must have caused a high accumulation of L-Asp which took time to clear. Where no spontaneous L-Asp release occurred on stimulation only, a signal could be detected upon L-Alb application accompanying epileptic activity.

Ca^{2+} dependent release of L-Asp was also examined, with stimulation only and in presence of TBOA and L-Alb. L-Asp release in Ca^{2+} -free aCSF with stimulations only and with TBOA was reduced, however because of unstable baseline and noise in the chamber, results from L-Alb- Ca^{2+} -free aCSF, could not be interpreted conclusively. Previous reports have shown that the release of L-Asp is Ca^{2+} dependent, however, L-Asp release depends only in part on influx of Ca^{2+} through voltage gated channel, suggesting that there might be independent mechanisms of release for L-Asp and L-Glu. (Zhou et

al. 1995; Bradford and Nadler 2004), hence this would be one result that would require further investigation.

Next, to confirm that the increased excitability was because of L-Asp acting on NMDA receptors, NMDA receptor antagonist D-AP5 was tested as it is potent NMDA receptor antagonist (Zhou et al. 1995; Wall and Dale 2013) D-AP5 was applied on its own and in combination with L-Alb. No epileptic activity was observed on all the three slices tested, while L-Asp release was still detectable in the presence of L-Alb, providing strong support in favour of L-Asp induced NMDA receptor activation (Patneau and Mayer 1990; Fleck et al. 1993).

Another interesting outcome was that the epileptic seizure activity was observed in the presence of 1 mM Mg^{2+}, which would suggest that L-Asp might be acting on a subtype of NMDA receptors that are less sensitive to Mg^{2+} (NMDA receptors containing the NR2C- or NR2D- subunit) (Chaffey and Chazot 2008; Cull-Candy, Brickley, and Farrant 2001).

Kubrusly et al. have also shown L-Asp induced release of [^{3}H] gamma amino butyric acid (GABA) in the presence of 1 mM Mg^{2+}, from cultured cells of avian retina (Kubrusly, de Mello, and de Mello 1998). Moreover, Gundersen et al. in 2004 presented immunogold electron microscopy results from hippocampal slices where L-Asp co-localized and co-exocytosed with GABA from synaptic vesicles in nerve endings that are thought to be inhibitory. The authors also show presence of NMDA receptors at GABAergic synapses in area CA1 pyramidal layer and granule cells. These synapses were low in L-Glu and high in L-Asp. Co-release of L-Glu and L-Asp has been demonstrated from GABAergic synaptosomes purified from cerebral cortex (Docherty, Bradford, and Wu 1987).Furthermore, there is emerging evidence that VGLUT-3 is expressed primarily in GABAergic/ non-glutametergic neurons, which are also enriched in NMDA receptors, suggesting that these neurons might also be releasing L-Asp (Gundersen, Holten, and Storm-Mathisen 2004; Stensrud, Sogn, and Gundersen 2015; Fasano et al. 2017).

As the appearance of epileptic seizures was because of inhibition of ASNS, as an extension to the study of L-Asp release, changes in ASNS expression levels were examined in epileptic tissue from mice and human patient with TLE.

From the immunohistochemistry and WB, it could be seen that ASNS levels were upregulated in the ipsilateral side. A clear down regulation was observed in the contralateral side from immunostained slices. The mutations associated with ASD, do not affect mRNA stability but affect the enzyme activity or protein stability. Moreover, ASNS expression is regulated by two inter-related pathways. Protein limitation in the cells initiates the amino acid response (AAR), while endoplasmic reticulum stress triggers the unfolded protein response (UPR), both these mechanisms induce ASNS gene expression (Lomelino et al. 2017). Thus, the upregulation on the ipsilateral side could be a compensatory mechanism. A WB performed on tissue from this side would be very useful and would give a better understanding of ASNS expression across the different regions of the brain and its associated role in epilepsy.

Overall, the L-Asp biosensor proved to be a useful tool for real-time detection of L-Asp release in the hippocampus. Although the biosensor is not perfectly selective, my pharmacological studies (the effect of TBOA, L-albizziine, and the ability of a selective NMDA receptor antagonist D-AP5 to block electrographic seizure activity evoked by L-albizziine) strongly support that the biosensor was measuring L-Asp in these experiments. Taken together, these findings highlight the role of L-Asp in enhanced excitability that is observed in ASD, and also a possible role in the development of epilepsy. These results warrant further exploration in understanding the role of L-Asp as a possible co-transmitter or neuromodulator in synaptic transmission.

Chapter 6

General Discussion

The sol-gel coating method for enzyme immobilization was used to fabricate microelectrode biosensors for L-Aspartate (L-Asp), and N-acetyl aspartate (NAA). The L-Asp sensor was fully characterized and used for detection of L-Asp in brain slices, while proof of concept data was obtained for NAA sensor.

6.1 L-aspartate oxidase (LAO) and L-Asp sensor

The L-Asp sensor was made by immobilising the enzyme PpLAO. *E.coli* expression system was used for the expression of N-terminal His-tagged PpLAO. This method of purification worked well as the enzyme was >90% pure and fairly active. The enzyme was also very specific for L-Asp. In terms of activity, the highest reported activity of LAO is 10 µmol/min/mg(Leese et al. 2013) and the activity I obtained was 6.67 µmol/min/mg. The activity of LAO is much lower compared to other oxidases like L-glutamate oxidase (26 mol/min/mg) (Arima et al. 2003) and this lower activity also reflected in the performance of L-Asp sensor.

Indeed, the performance of L-Asp sensor was not as good as biosensors previously fabricated with sol-gel method, with an I_{max} of 0.61 nA which is much lower than that for glutamate sensor (141 nA) (Tian et al. 2009). The sensor was also not completely selective or specific for L-Asp as it still picked-up signals for L-asparagine/L-glutamine and had a high response for ascorbate and urate. The sensor in these respects was an ‘imperfect tool’ but was still better than having no tool for direct measurement of L-Asp release.

An approach to improve L-Asp sensitivity could be to modify the enzyme in order to improve its activity. Directed protein engineering to improve activity and dynamic range of sensors has been reported and could be applied to improve LAO sensor performance (Campàs, Prieto-Simón, and Marty 2009)

6.2 Aspartoacylase (ASPA) and NAA sensor

The enzyme aspartoacylase (ASPA) in combination with LAO was used for making NAA sensor. GST fused ASPA was purified in *E.coli* and the enzyme was >85% pure. The purification of GST fused proteins requires the use of Dithiothreitol (DTT), which is a reducing agent. Presence of DTT might not interfere with the activity of ASPA but could be affecting the activity of LAO. This interpretation stems from the observation that L-Asp sensor did not give a good response during optimisation when fabricated in presence of thioglycerol (also a reducing agent). Hence for NAA sensor which requires both ASPA and LAO to be in active form, GST could either be completely cleaved off or replaced by another fusion protein for e.g. maltose binding protein (Sun, Tropea, and Waugh 2011). This change might help in improving NAA sensor response. Proof of principle data could be obtained for NAA sensor, indicating that both enzymes could work together.

The novel assay using 1,2-Diamino-4,5-methylenedioxybenzene Dihydrochloride (DMB) also proved useful in successfully determining the activity of ASPA. The dye had some intrinsic background fluorescence in PBS buffer, which can be investigated by testing in a different buffer system.

6.3 L-Asp release in hippocampus

The L-Asp sensor was used to study the release of L-Asp in hippocampus. The pharmacological treatments used in this study were specifically directed towards pathways that are known to block glutamate-aspartate transporters: using DL-threo-β-Benzyloxyasparticacid (TBOA) and inhibiting asparagine synthetase (ASNS) by L-Albizziine (L-Alb), an important enzyme in the metabolic pathway involving L-Asp. These interventions strongly support that it was L-Asp being measured. It was the stimulation induced release of L-Asp which actually led to these experiments where an increase in L-Asp release could be observed after pharmacological intervention.

This is the first ever real-time measurement of L-Asp release. L-Asp release was observed upon tetanic stimulation. A high frequency stimulation pattern was used in all the experiments; other patterns could also be tested. An interesting observation was that activation of AMPA receptors by application of AMPA was also tested on two slices but did not result in any release or seizure-like activity.

The results also indicate that the release was at least partially Ca^{2+} dependent as there was a decrease in L-Asp concentration in Ca^{2+}- free aCSF. This is in line with some previous observations that suggest that the release of L-Asp could be occurring at a distance from the synaptic cleft and by a different mechanism (Nadler 2011; Bradford and Nadler 2004).

The application of L-Alb was performed with the intention of blocking ASNS and thereby increasing L-Asp concentration so it could be detected. This experiment not only increased L-Asp release, but it also resulted in appearance of seizure-like activity which suggests that ASNS is an important enzyme involved in maintaining intracellular and extracellular concentrations of L-Asp and that there might be a continual cycle for L-Asp release, uptake and conversion to L-asparagine (L-Asn). This is similar to control of extracellular adenosine concentrations by adenosine kinase as inhibition of this enzyme also resulted in increase of adenosine (Wall, Atterbury, and Dale 2007).

ASNS deficiency (ASD) results from mutations in ASNS genes and is a recently characterized neurological disorder (Lomelino et al. 2017). Patients with ASD have epileptic seizures suggesting that ASNS may also be linked to epilepsy. The immunological studies in epileptic mice also showed that ASNS was upregulated on the ipsilateral side which could be a compensatory upregulation. ASNS expression and L-Asn metabolism in cancer has received attention, however a possible role in development of epilepsy could be further looked into.

These results indicate that there is a strong possibility of L-Asp co-release from GABA-positive terminals. One of the first studies to show the co-release of L-Asp, L-Glu and GABA from GABAergic synaptosomes purified from cerebral cortex was conducted by Docherty et al. in 1987 (Docherty, Bradford, and Wu 1987). Gundersen et al. demonstrated that L-Asp co-localised and co-exocytosed with GABA from GABA positive terminals in dentate granule cells and CA1 pyramidal cells. At these synapses there is also strong expression of NMDA receptors.(Gundersen, Holten, and Storm-Mathisen 2004). There is also emerging evidence that out of the three VGLUT (1-3) transporters for glutamate, VGLUT-3 is primarily found in neurons that are nonglutamatergic (El Mestikawy et al. 2011). A subset of GABAergic interneurons in the hippocampus co-express the GABA/glycine vesicular transporters (VIAAT) and also VLGUT-3 (Stensrud, Sogn, and Gundersen 2015). VGLUT-3 has been identified in cholecystokinin (CCK^{+}) expressing GABAergic basket cells. These findings have shown the co-release of glutamate and GABA. However, the release of L-Asp which was initially demonstrated from GABAergic neurons ((Docherty, Bradford, and Wu 1987; Gundersen, Holten, and Storm-Mathisen 2004), has largely been overlooked. VGLUT-3 could be a potential candidate for L-Asp vesicular loading. Based on these reports and results presented in this study, a possible model for L-Asp release could be (Figure 6-1):

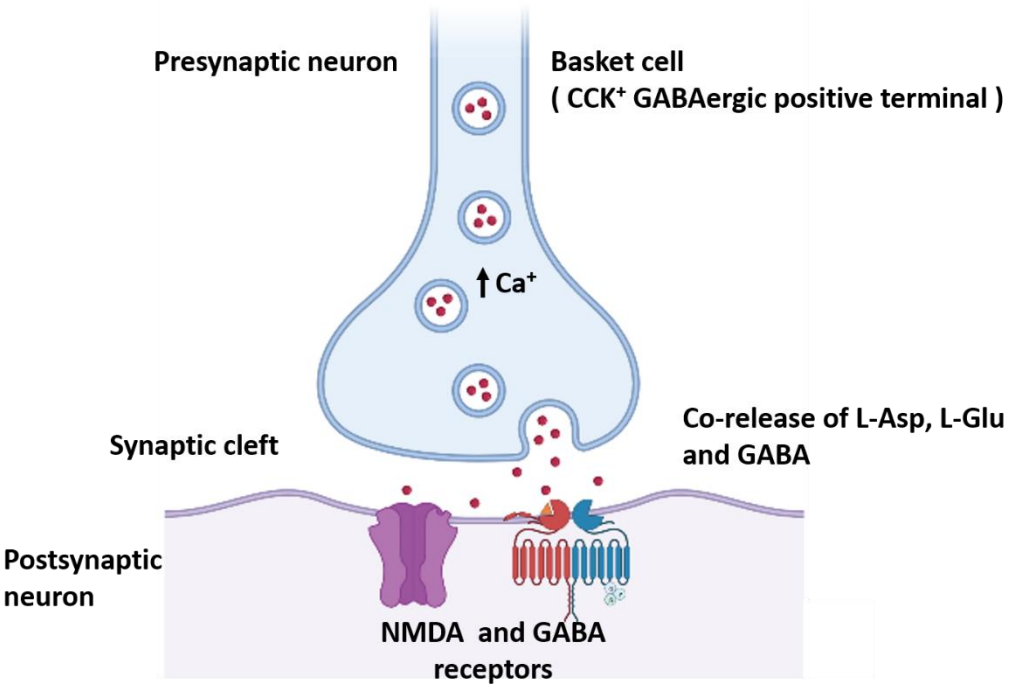

Figure 6-1: Proposed model for L-Asp release.

At the CCK^+ GABAergic basket cells, depolarization induced Ca^{2+} -dependent co-release of L-Asp, L- Glu and GABA. Released L-Asp would activate NMDA receptors. (Figure created using BioRender.com).

6.4 Future directions

An idea that was not explored and could be a potential model for studying L-Asp release is by inducing hypoglycaemia or hypoxia. Reduced glucose concentration led to an increase in K^+ induced depolarization L-Asp release (Fleck et al. 1993), and insulin-induced hypoglycaemia showed an enhanced L-Asp immunoreactivity in synaptic vesicles (Gundersen et al. 1998). A reduction in availability of glucose or O_2 would lead to conversion of oxaloacetate to L-Asp by the enzyme aspartate ammonia transferase which utilizes glutamate. Thus, the energetic state of the neurons would determine the L-Asp content and hence this concept could be explored.

Because of the low sensitivity of L-Asp sensor, all experimental studies should involve the use of the null sensor. It is absolutely imperative to include the null sensor in all experiments for authentic validation of the L-Asp signal. Furthermore, the experiments performed in this study could be repeated, with

additional experiments to completely verify the release of L-Asp. Since the seizure-like activity observed upon application of L-Alb was in the presence of Mg^{2+}, it suggests that L-Asp could be selectively acting on NR2C/NR2D subtypes of NMDA receptors which are less sensitive to Mg^{2+}. This can be further explored by using antagonists which are more potent against the NR2C/NR2D subtypes (Feng et al. 2004; Mosley et al. 2010).

Some additional studies could be to use the Cre-lox recombinase technology targeting ASNS in the brain, to study the effect on L-Asp release and seizure activity. Similarly, a Knock-out/knock down of VGLUT-3 could be made and may result in loss of L-Asp release. A possible experiment that could be developed and fine-tuned along the lines of immunolocalization studies would be to show co-localization of L-Asp and L-Glu with VGLUT-3 positive and VGLUT-3 negative GABAergic synaptosomes, insulin induced hypoglycaemia could be used to increase the L-Asp content (Gundersen et al. 1998). In VGLUT-3 positive synaptosomes both L-Asp and L-Glu would co-localize, If VGLUT-3 is loading L-Asp, then in VGLUT-3 negative synaptosomes immunoreactivity for both should diminish to equal extent.

The imperfect L-Asp sensor has drawn attention to hitherto unknown mechanisms of L-Asp release and action. It has definitely re-kindled the interest in studying the role of this amino acid in brain electrophysiology.

Bibliography

Albery, W. John, Martyn G. Boutelle, and Peter T. Galley. 1992. 'The dialysis electrode—a new method for in vivo monitoring', *Journal of the Chemical Society, Chemical Communications*: 900-01.

Aleksander Talgøy Holten, Cecilie Morland, Kaja Nordengen, Vidar Gundersen. 2008. 'Vesicular Release of L- and D-Aspartate from Hippocampal Nerve Terminals: Immunogold Evidence', *open Neuroscience Journal*, 2: 51:58.

Anand, K. S., and V. Dhikav. 2012. 'Hippocampus in health and disease: An overview', *Ann Indian Acad Neurol*, 15: 239-46.

Andreo-Vidal, A., A. Sanchez-Amat, and J. C. Campillo-Brocal. 2018. 'The Pseudoalteromonas luteoviolacea L-amino Acid Oxidase with Antimicrobial Activity Is a Flavoenzyme', *Mar Drugs*, 16.

Appu, A. P., J. R. Moffett, P. Arun, S. Moran, V. Nambiar, J. K. S. Krishnan, N. Puthillathu, and A. M. A. Namboodiri. 2017. 'Increasing N-acetylaspartate in the Brain during Postnatal Myelination Does Not Cause the CNS Pathologies of Canavan Disease', *Front Mol Neurosci*, 10: 161.

Arima, J., T. Tamura, H. Kusakabe, M. Ashiuchi, T. Yagi, H. Tanaka, and K. Inagaki. 2003. 'Recombinant expression, biochemical characterization and stabilization through proteolysis of an L-glutamate oxidase from Streptomyces sp. X-119-6', *J Biochem*, 134: 805-12.

Armenia, Ilaria, Riccardo Balzaretti, Cristina Pirrone, Chiara Allegretti, Paola D'Arrigo, Mattia Valentino, Rosalba Gornati, Giovanni Bernardini, and Loredano Pollegioni. 2017. 'l-aspartate oxidase magnetic nanoparticles: synthesis, characterization and l-aspartate bioconversion', *RSC Advances*, 7: 21136-43.

Baslow, M. H. 2018. 'Chasing N-acetyl-L-aspartate, a shiny NMR object in the brain', *NMR Biomed*, 31: e3895.

Bazzari, A. H., and H. R. Parri. 2019. 'Neuromodulators and Long-Term Synaptic Plasticity in Learning and Memory: A Steered-Glutamatergic Perspective', *Brain Sci*, 9.

Beamer, E., A. Lacey, M. Alves, G. Conte, F. Tian, L. de Diego-Garcia, M. Khalil, F. Rosenow, N. Delanty, N. Dale, H. El-Naggar, D. C. Henshall, and T. Engel. 2021. 'Elevated blood purine levels as a biomarker of seizures and epilepsy', *Epilepsia*, 62: 817-28.

Benson, M. J., S. Manzanero, and K. Borges. 2015. 'Complex alterations in microglial M1/M2 markers during the development of epilepsy in two mouse models', *Epilepsia*, 56: 895-905.

Bhakoo, Kishore K. 2012. 'N-Acetyl-Aspartate (NAA) Metabolism.' in In-Young Choi and Rolf Gruetter (eds.), *Neural Metabolism In Vivo* (Springer US: Boston, MA).

Bhalla, N., P. Jolly, N. Formisano, and P. Estrela. 2016. 'Introduction to biosensors', *Essays Biochem*, 60: 1-8.

Bifulco, D., L. Pollegioni, D. Tessaro, S. Servi, and G. Molla. 2013. 'A thermostable L-aspartate oxidase: a new tool for biotechnological applications', *Appl Microbiol Biotechnol*, 97: 7285-95.

Bitto, E., C. A. Bingman, G. E. Wesenberg, J. G. McCoy, and G. N. Phillips, Jr. 2007. 'Structure of aspartoacylase, the brain enzyme impaired in Canavan disease', *Proc Natl Acad Sci U S A*, 104: 456-61.

Bradford, S. E., and J. V. Nadler. 2004. 'Aspartate release from rat hippocampal synaptosomes', *Neuroscience*, 128: 751-65.

Brooks, H. B., S. Geeganage, S. D. Kahl, C. Montrose, S. Sittampalam, M. C. Smith, and J. R. Weidner. 2004. 'Basics of Enzymatic Assays for HTS.' in G. S. Sittampalam, A. Grossman, K. Brimacombe, M. Arkin, D. Auld, C. P. Austin, J. Baell, B. Bejcek, J. M. M. Caaveiro, T. D. Y. Chung, N. P. Coussens, J. L. Dahlin, V. Devanaryan, T. L. Foley, M. Glicksman, M. D. Hall, J. V. Haas, S. R. J. Hoare, J. Inglese, P. W. Iversen, S. D. Kahl, S. C. Kales, S. Kirshner, M. Lal-Nag, Z. Li, J. McGee, O. McManus, T. Riss, P. Saradjian, O. J. Trask, Jr., J. R. Weidner, M. J. Wildey, M. Xia and X. Xu (eds.), *Assay Guidance Manual* (Eli Lilly & Company and the National Center for Advancing Translational Sciences: Bethesda (MD)).

Campas M., Marty JL. 2006. 'Encapsulation of Enzymes Using Polymers and Sol-Gel Techniques.' in Guisan J.M. (ed.), *Immobilization of Enzymes and Cells. Methods in Biotechnology™* (Humana Press).

Campàs, M., B. Prieto-Simón, and J. L. Marty. 2009. 'A review of the use of genetically engineered enzymes in electrochemical biosensors', *Semin Cell Dev Biol*, 20: 3-9.

Cavallero, A., A. Marte, and E. Fedele. 2009. 'L-aspartate as an amino acid neurotransmitter: mechanisms of the depolarization-induced release from cerebrocortical synaptosomes', *J Neurochem*, 110: 924-34.

Chae, Hee Jeong, Eui Yong Kim, and Man-Jin In. 2000. 'Improved immobilization yields by addition of protecting agents in glutaraldehyde-induced immobilization of protease', *Journal of Bioscience and Bioengineering*, 89: 377-79.

Chaffey, Heather, and Paul L. Chazot. 2008. 'NMDA receptor subtypes: Structure, function and therapeutics', *Current Anaesthesia & Critical Care*, 19: 183-201.

Chantranupong, L., J. L. Saulnier, W. Wang, D. R. Jones, M. E. Pacold, and B. L. Sabatini. 2020. 'Rapid purification and metabolomic profiling of synaptic vesicles from mammalian brain', *Elife*, 9.

Citri, A., and R. C. Malenka. 2008. 'Synaptic plasticity: multiple forms, functions, and mechanisms', *Neuropsychopharmacology*, 33: 18-41.

Cosnier, S., C. Innocent, L. Allien, S. Poitry, and M. Tsacopoulos. 1997. 'An electrochemical method for making enzyme microsensors. Application to the detection of dopamine and glutamate', *Anal Chem*, 69: 968-71.

Cull-Candy, S., S. Brickley, and M. Farrant. 2001. 'NMDA receptor subunits: diversity, development and disease', *Curr Opin Neurobiol*, 11: 327-35.

Curras, M. C., and R. Dingledine. 1992. 'Selectivity of amino acid transmitters acting at N-methyl-D-aspartate and amino-3-hydroxy-5-methyl-4-isoxazolepropionate receptors', *Mol Pharmacol*, 41: 520-6.

Curtis, D. R., and J. C. Watkins. 1963. 'Acidic amino acids with strong excitatory actions on mammalian neurones', *J Physiol*, 166: 1-14.

Dalangin, R., A. Kim, and R. E. Campbell. 2020. 'The Role of Amino Acids in Neurotransmission and Fluorescent Tools for Their Detection', *Int J Mol Sci*, 21.

Dale, N. 1998. 'Delayed production of adenosine underlies temporal modulation of swimming in frog embryo', *J Physiol*, 511 (Pt 1): 265-72.

Dale, N., and B. G. Frenguelli. 2012. 'Measurement of purine release with microelectrode biosensors', *Purinergic Signal*, 8: 27-40.

Dale, N., S. Hatz, F. Tian, and E. Llaudet. 2005. 'Listening to the brain: microelectrode biosensors for neurochemicals', *Trends Biotechnol*, 23: 420-8.

Dave, Bakul C., Bruce Dunn, Joan Selverstone Valentine, and Jeffrey I. Zink. 1994. 'Sol-gel encapsulation methods for biosensors', *Anal Chem*, 66: 1120A-27A.

Deng, L., P. Yao, L. Li, F. Ji, S. Zhao, C. Xu, X. Lan, and P. Jiang. 2020. 'p53-mediated control of aspartate-asparagine homeostasis dictates LKB1 activity and modulates cell survival', *Nat Commun*, 11: 1755.

Di Cera, E. 2009. 'Serine proteases', *IUBMB Life*, 61: 510-5.
Di Pietro, V., A. Gambacurta, A. M. Amorini, A. Finocchiaro, S. D'Urso, L. Ceccarelli, B. Tavazzi, B. Giardina, and G. Lazzarino. 2008. 'A new T677C mutation of the aspartoacylase gene encodes for a protein with no enzymatic activity', *Clin Biochem*, 41: 611-5.
Docherty, M., H. F. Bradford, and J. Y. Wu. 1987. 'Co-release of glutamate and aspartate from cholinergic and GABAergic synaptosomes', *Nature*, 330: 64-6.
El Mestikawy, S., A. Wallén-Mackenzie, G. M. Fortin, L. Descarries, and L. E. Trudeau. 2011. 'From glutamate co-release to vesicular synergy: vesicular glutamate transporters', *Nat Rev Neurosci*, 12: 204-16.
Escobar, Sindy, Claudia Bernal, Juan M. Bolivar, Bernd Nidetzky, Fernando López-Gallego, and Monica Mesa. 2018. 'Understanding the silica-based sol-gel encapsulation mechanism of Thermomyces lanuginosus lipase: The role of polyethylenimine', *Molecular Catalysis*, 449: 106-13.
Fasano, C., J. Rocchetti, K. Pietrajtis, J. F. Zander, F. Manseau, D. Y. Sakae, M. Marcus-Sells, L. Ramet, L. J. Morel, D. Carrel, S. Dumas, S. Bolte, V. Bernard, E. Vigneault, R. Goutagny, G. Ahnert-Hilger, B. Giros, S. Daumas, S. Williams, and S. El Mestikawy. 2017. 'Regulation of the Hippocampal Network by VGLUT3-Positive CCK- GABAergic Basket Cells', *Front Cell Neurosci*, 11: 140.
Feng, B., H. W. Tse, D. A. Skifter, R. Morley, D. E. Jane, and D. T. Monaghan. 2004. 'Structure-activity analysis of a novel NR2C/NR2D-preferring NMDA receptor antagonist: 1-(phenanthrene-2-carbonyl) piperazine-2,3-dicarboxylic acid', *Br J Pharmacol*, 141: 508-16.
Fleck, M. W., G. Barrionuevo, and A. M. Palmer. 2001. 'Synaptosomal and vesicular accumulation of L-glutamate, L-aspartate and D-aspartate', *Neurochem Int*, 39: 217-25.
Fleck, M. W., D. A. Henze, G. Barrionuevo, and A. M. Palmer. 1993. 'Aspartate and glutamate mediate excitatory synaptic transmission in area CA1 of the hippocampus', *J Neurosci*, 13: 3944-55.
Fogal, S., M. Carotti, L. Giaretta, F. Lanciai, L. Nogara, L. Bubacco, and E. Bergantino. 2015. 'Human tyrosinase produced in insect cells: a landmark for the screening of new drugs addressing its activity', *Mol Biotechnol*, 57: 45-57.
Frenguelli, B. G., E. Llaudet, and N. Dale. 2003. 'High-resolution real-time recording with microelectrode biosensors reveals novel aspects of adenosine release during hypoxia in rat hippocampal slices', *J Neurochem*, 86: 1506-15.
Frenguelli, B. G., and M. J. Wall. 2016. 'Combined electrophysiological and biosensor approaches to study purinergic regulation of epileptiform activity in cortical tissue', *J Neurosci Methods*, 260: 202-14.
Fujiwara, T., A. Hattori, T. Ito, T. Funatsu, and M. Tsunoda. 2020. 'Analysis of intracellular α-keto acids by HPLC with fluorescence detection', *Anal Methods*, 12: 2555-59.
Garguilo, Michael G., and Adrian C. Michael. 1994. 'Quantitation of Choline in the Extracellular Fluid of Brain Tissue with Amperometric Microsensors', *Anal Chem*, 66: 2621-29.
Georganopoulou, D. G., R. Carley, D. A. Jones, and M. G. Boutelle. 2000. 'Development and comparison of biosensors for in-vivo applications', *Faraday Discuss*: 291-303; discussion 35-51.
González-Espinosa, Claudia, and Fabiola Guzmán-Mejía. 2014. '8 - Basic Elements of Signal Transduction Pathways Involved in Chemical Neurotransmission.' in Alfredo Meneses (ed.), *Identification of Neural Markers Accompanying Memory* (Elsevier: San Diego).

Gotoh, T., Y. Miyazaki, K. Chiba, and K. Kikuchi. 2002. 'Significant increase in recombinant protein production of a virus-infected Sf-9 insect cell culture of low MOI under low dissolved oxygen conditions', *J Biosci Bioeng*, 94: 426-33.

Gotoh, T., Y. Miyazaki, W. Sato, K. Kikuchi, and W. E. Bentley. 2001. 'Proteolytic activity and recombinant protein production in virus-infected Sf-9 insect cell cultures supplemented with carboxyl and cysteine protease inhibitors', *J Biosci Bioeng*, 92: 248-55.

Gundersen, V., F. A. Chaudhry, J. G. Bjaalie, F. Fonnum, O. P. Ottersen, and J. Storm-Mathisen. 1998. 'Synaptic vesicular localization and exocytosis of L-aspartate in excitatory nerve terminals: a quantitative immunogold analysis in rat hippocampus', *J Neurosci*, 18: 6059-70.

Gundersen, V., A. T. Holten, and J. Storm-Mathisen. 2004. 'GABAergic synapses in hippocampus exocytose aspartate on to NMDA receptors: quantitative immunogold evidence for co-transmission', *Mol Cell Neurosci*, 26: 156-65.

Gundersen, V., O. P. Ottersen, and J. Storm-Mathisen. 1991. 'Aspartate- and Glutamate-like Immunoreactivities in Rat Hippocampal Slices: Depolarization-induced Redistribution and Effects of Precursors', *Eur J Neurosci*, 3: 1281-99.

Guo, X., J. R. Malcolm, M. M. Ali, G. Ribeiro Morais, S. D. Shnyder, P. M. Loadman, L. H. Patterson, and R. A. Falconer. 2020. 'An efficient assay for identification and quantitative evaluation of potential polysialyltransferase inhibitors', *Analyst*, 145: 4512-21.

Guzik, U., K. Hupert-Kocurek, and D. Wojcieszynska. 2014. 'Immobilization as a strategy for improving enzyme properties-application to oxidoreductases', *Molecules*, 19: 8995-9018.

Hall, J., and B. G. Frenguelli. 2018. 'The combination of ribose and adenine promotes adenosine release and attenuates the intensity and frequency of epileptiform activity in hippocampal slices: Evidence for the rapid depletion of cellular ATP during electrographic seizures', *J Neurochem*, 147: 178-89.

Hara, S., Y. Takemori, M. Yamaguchi, M. Nakamura, and Y. Ohkura. 1987. 'Fluorometric high-performance liquid chromatography of N-acetyl- and N-glycolylneuraminic acids and its application to their microdetermination in human and animal sera, glycoproteins, and glycolipids', *Anal Biochem*, 164: 138-45.

Herga, S., J. G. Berrin, J. Perrier, A. Puigserver, and T. Giardina. 2006. 'Identification of the zinc binding ligands and the catalytic residue in human aspartoacylase, an enzyme involved in Canavan disease', *FEBS Lett*, 580: 5899-904.

Herring, B. E., K. Silm, R. H. Edwards, and R. A. Nicoll. 2015. 'Is Aspartate an Excitatory Neurotransmitter?', *J Neurosci*, 35: 10168-71.

Hershfield, J. R., C. N. Madhavarao, J. R. Moffett, J. A. Benjamins, J. Y. Garbern, and A. Namboodiri. 2006. 'Aspartoacylase is a regulated nuclear-cytoplasmic enzyme', *Faseb j*, 20: 2139-41.

Hussain, Mohammad Musarraf, Abdullah M. Asiri, and Mohammed M. Rahman. 2020. 'Simultaneous detection of l-aspartic acid and glycine using wet-chemically prepared Fe3O4@ZnO nanoparticles: real sample analysis', *RSC Advances*, 10: 19276-89.

Huynh, K., and C. L. Partch. 2015. 'Analysis of protein stability and ligand interactions by thermal shift assay', *Curr Protoc Protein Sci*, 79: 28 9 1-14.

Hyman, S. E. 2005. 'Neurotransmitters', *Curr Biol*, 15: R154-8.

Ippolito, J. A., R. S. Alexander, and D. W. Christianson. 1990. 'Hydrogen bond stereochemistry in protein structure and function', *J Mol Biol*, 215: 457-71.

Izidoro, L. F., J. C. Sobrinho, M. M. Mendes, T. R. Costa, A. N. Grabner, V. M. Rodrigues, S. L. da Silva, F. B. Zanchi, J. P. Zuliani, C. F. Fernandes, L. A. Calderon, R. G. Stábeli, and A.

M. Soares. 2014. 'Snake venom L-amino acid oxidases: trends in pharmacology and biochemistry', *Biomed Res Int*, 2014: 196754.

Karamitros, C. S., J. Lim, and M. Konrad. 2014. 'An Amplex Red-based fluorometric and spectrophotometric assay for L-asparaginase using its natural substrate', *Analytical Biochemistry*, 445: 20-22.

Kaul, R., J. Casanova, A. B. Johnson, P. Tang, and R. Matalon. 1991. 'Purification, characterization, and localization of aspartoacylase from bovine brain', *J Neurochem*, 56: 129-35.

Kim, H. G., S. M. Yang, Y. C. Lee, S. I. Do, I. S. Chung, and J. M. Yang. 2003. 'High-level expression of human glycosyltransferases in insect cells as biochemically active form', *Biochem Biophys Res Commun*, 305: 488-93.

Klugmann, M., C. W. Symes, B. K. Klaussner, C. B. Leichtlein, T. Serikawa, D. Young, and M. J. During. 2003. 'Identification and distribution of aspartoacylase in the postnatal rat brain', *Neuroreport*, 14: 1837-40.

Knierim, J. J. 2015. 'The hippocampus', *Curr Biol*, 25: R1116-21.

Kubrusly, R. C., M. C. de Mello, and F. G. de Mello. 1998. 'Aspartate as a selective NMDA receptor agonist in cultured cells from the avian retina', *Neurochem Int*, 32: 47-52.

Kueng, A., C. Kranz, and B. Mizaikoff. 2004. 'Amperometric ATP biosensor based on polymer entrapped enzymes', *Biosens Bioelectron*, 19: 1301-7.

Kulagina, N. V., L. Shankar, and A. C. Michael. 1999. 'Monitoring glutamate and ascorbate in the extracellular space of brain tissue with electrochemical microsensors', *Anal Chem*, 71: 5093-100.

Le Coq, J., H. J. An, C. Lebrilla, and R. E. Viola. 2006. 'Characterization of human aspartoacylase: the brain enzyme responsible for Canavan disease', *Biochemistry*, 45: 5878-84.

Leese, Charlotte, Ian Fotheringham, Franck Escalettes, Robert Speight, and Gideon Grogan. 2013. 'Cloning, expression, characterisation and mutational analysis of l-aspartate oxidase from Pseudomonas putida', *Journal of Molecular Catalysis B: Enzymatic*, 85–86: 17-22.

Li, X., and J. A. Imlay. 2018. 'Improved measurements of scant hydrogen peroxide enable experiments that define its threshold of toxicity for Escherichia coli', *Free Radic Biol Med*, 120: 217-27.

Llaudet, E., N. P. Botting, J. A. Crayston, and N. Dale. 2003. 'A three-enzyme microelectrode sensor for detecting purine release from central nervous system', *Biosens Bioelectron*, 18: 43-52.

Llaudet, E., S. Hatz, M. Droniou, and N. Dale. 2005. 'Microelectrode biosensor for real-time measurement of ATP in biological tissue', *Anal Chem*, 77: 3267-73.

Lomelino, C. L., J. T. Andring, R. McKenna, and M. S. Kilberg. 2017. 'Asparagine synthetase: Function, structure, and role in disease', *J Biol Chem*, 292: 19952-58.

Lopatář, J., N. Dale, and B. G. Frenguelli. 2015. 'Pannexin-1-mediated ATP release from area CA3 drives mGlu5-dependent neuronal oscillations', *Neuropharmacology*, 93: 219-28.

Lowry, J. P., M. Miele, R. D. O'Neill, M. G. Boutelle, and M. Fillenz. 1998. 'An amperometric glucose-oxidase/poly(o-phenylenediamine) biosensor for monitoring brain extracellular glucose: in vivo characterisation in the striatum of freely-moving rats', *J Neurosci Methods*, 79: 65-74.

Lowry, J. P., R. D. O'Neill, M. G. Boutelle, and M. Fillenz. 1998. 'Continuous monitoring of extracellular glucose concentrations in the striatum of freely moving rats with an implanted glucose biosensor', *J Neurochem*, 70: 391-6.

Marinesco S., Frey O. 2013. ' Microelectrode Designs for Oxidase-Based Biosensors.' in Dale N. Marinesco S. (ed.), *Microelectrode Biosensors.* (Humana Press: Totowa, NJ).

Martensen, P. M., and J. Justesen. 2001. 'Specific inhibitors prevent proteolytic degradation of recombinant proteins expressed in High Five cells', *Biotechniques*, 30: 782-4, 86, 88 passim.

Marvizón, J. G., F. Mayor, Jr., M. C. Aragón, C. Giménez, and F. Valdivieso. 1981. 'L-Aspartate transport into plasma membrane vesicles derived from rat brain synaptosomes', *J Neurochem*, 37: 1401-6.

Mattiroli, F., and T. K. Sixma. 2014. 'Lysine-targeting specificity in ubiquitin and ubiquitin-like modification pathways', *Nat Struct Mol Biol*, 21: 308-16.

Mehrotra, Parikha. 2016. 'Biosensors and their applications – A review', *Journal of Oral Biology and Craniofacial Research*, 6: 153-59.

Mishin, V., J. P. Gray, D. E. Heck, D. L. Laskin, and J. D. Laskin. 2010. 'Application of the Amplex red/horseradish peroxidase assay to measure hydrogen peroxide generation by recombinant microsomal enzymes', *Free Radic Biol Med*, 48: 1485-91.

Miyaji, T., H. Omote, and Y. Moriyama. 2011. 'Functional characterization of vesicular excitatory amino acid transport by human sialin', *J Neurochem*, 119: 1-5.

Moffett, J. R., P. Arun, P. S. Ariyannur, and A. M. Namboodiri. 2013. 'N-Acetylaspartate reductions in brain injury: impact on post-injury neuroenergetics, lipid synthesis, and protein acetylation', *Front Neuroenergetics*, 5: 11.

Moffett, J. R., M. A. Namboodiri, C. B. Cangro, and J. H. Neale. 1991. 'Immunohistochemical localization of N-acetylaspartate in rat brain', *Neuroreport*, 2: 131-4.

Moffett, John R., Prasanth Ariyannur, Peethambaran Arun, and Aryan M. A. Namboodiri. 2014. 'Chapter 2.1 - N-Acetylaspartate and N-Acetylaspartylglutamate in Central Nervous System Health and Disease.' in Charlotte Stagg and Douglas Rothman (eds.), *Magnetic Resonance Spectroscopy* (Academic Press: San Diego).

Moore, R. A., J. Le Coq, C. R. Faehnle, and R. E. Viola. 2003. 'Purification and preliminary characterization of brain aspartoacylase', *Arch Biochem Biophys*, 413: 1-8.

Morland, C., K. Nordengen, M. Larsson, L. M. Prolo, Z. Farzampour, R. J. Reimer, and V. Gundersen. 2013. 'Vesicular uptake and exocytosis of L-aspartate is independent of sialin', *Faseb j*, 27: 1264-74.

Mortarino, M., A. Negri, G. Tedeschi, T. Simonic, S. Duga, H. G. Gassen, and S. Ronchi. 1996. 'L-aspartate oxidase from Escherichia coli. I. Characterization of coenzyme binding and product inhibition', *Eur J Biochem*, 239: 418-26.

Mosley, C. A., T. M. Acker, K. B. Hansen, P. Mullasseril, K. T. Andersen, P. Le, K. M. Vellano, H. Bräuner-Osborne, D. C. Liotta, and S. F. Traynelis. 2010. 'Quinazolin-4-one derivatives: A novel class of noncompetitive NR2C/D subunit-selective N-methyl-D-aspartate receptor antagonists', *J Med Chem*, 53: 5476-90.

Moussawi, Khaled, Arthur Riegel, Satish Nair, and Peter W. Kalivas. 2011. 'Extracellular glutamate: functional compartments operate in different concentration ranges', *Frontiers in systems neuroscience*, 5: 94-94.

Nadler, J. V. 2011. 'Aspartate release and signalling in the hippocampus', *Neurochem Res*, 36: 668-76.

Nadler, J. V., K. W. Vaca, W. F. White, G. S. Lynch, and C. W. Cotman. 1976. 'Aspartate and glutamate as possible transmitters of excitatory hippocampal afferents', *Nature*, 260: 538-40.

Nadler, J. V., W. F. White, K. W. Vaca, B. W. Perry, and C. W. Cotman. 1978. 'Biochemical correlates of transmission mediated by glutamate and aspartate', *J Neurochem*, 31: 147-55.

Naggie, S., and W. E. Bentley. 1998. 'Appearance of protease activities coincides with p10 and polyhedrin-driven protein production in the baculovirus expression system: effects on yield', *Biotechnol Prog*, 14: 227-32.

Namboodiri, M. A., A. Corigliano-Murphy, G. Jiang, M. Rollag, and I. Provencio. 2000. 'Murine aspartoacylase: cloning, expression and comparison with the human enzyme', *Brain Res Mol Brain Res*, 77: 285-9.

Nasu, S., F. D. Wicks, and R. K. Gholson. 1982. 'L-Aspartate oxidase, a newly discovered enzyme of Escherichia coli, is the B protein of quinolinate synthetase', *J Biol Chem*, 257: 626-32.

Nettleship, J. E., J. Brown, M. R. Groves, and A. Geerlof. 2008. 'Methods for protein characterization by mass spectrometry, thermal shift (ThermoFluor) assay, and multiangle or static light scattering', *Methods Mol Biol*, 426: 299-318.

Pankratov, Y., and U. Lalo. 2015. 'Role for astroglial α1-adrenoreceptors in gliotransmission and control of synaptic plasticity in the neocortex', *Front Cell Neurosci*, 9: 230.

Patneau, D. K., and M. L. Mayer. 1990. 'Structure-activity relationships for amino acid transmitter candidates acting at N-methyl-D-aspartate and quisqualate receptors', *J Neurosci*, 10: 2385-99.

Petroff, O. A. 2002. 'GABA and glutamate in the human brain', *Neuroscientist*, 8: 562-73.

Pierre, A. C. 2004. 'The sol-gel encapsulation of enzymes', *Biocatalysis and Biotransformation*, 22: 145-70.

Pollegioni, L., P. Motta, and G. Molla. 2013. 'L-amino acid oxidase as biocatalyst: a dream too far?', *Appl Microbiol Biotechnol*, 97: 9323-41.

Pollegioni, L., L. Piubelli, S. Sacchi, M. S. Pilone, and G. Molla. 2007. 'Physiological functions of D-amino acid oxidases: from yeast to humans', *Cell Mol Life Sci*, 64: 1373-94.

Reuben Matalon, Kimberlee Michals Matalon. 2015. 'Chapter 62 - Canavan Disease,.' in Juan M. Pascual Editor(s): Roger N. Rosenberg (ed.), *Rosenberg's Molecular and Genetic Basis of Neurological and Psychiatric Disease (Fifth Edition),* .

Rice, M. E. 2000. 'Ascorbate regulation and its neuroprotective role in the brain', *Trends Neurosci*, 23: 209-16.

Rickard, J. J. S., V. Di-Pietro, D. J. Smith, D. J. Davies, A. Belli, and P. G. Oppenheimer. 2020. 'Rapid optofluidic detection of biomarkers for traumatic brain injury via surface-enhanced Raman spectroscopy', *Nat Biomed Eng*, 4: 610-23.

Rocchitta, G., A. Spanu, S. Babudieri, G. Latte, G. Madeddu, G. Galleri, S. Nuvoli, P. Bagella, M. I. Demartis, V. Fiore, R. Manetti, and P. A. Serra. 2016. 'Enzyme Biosensors for Biomedical Applications: Strategies for Safeguarding Analytical Performances in Biological Fluids', *Sensors (Basel)*, 16.

Rodriguez, H. M., M. Vaysberg, A. Mikels, S. McCauley, A. C. Velayo, C. Garcia, and V. Smith. 2010. 'Modulation of lysyl oxidase-like 2 enzymatic activity by an allosteric antibody inhibitor', *J Biol Chem*, 285: 20964-74.

Röhlen, Désirée L., Johanna Pilas, Michael J. Schöning, and Thorsten Selmer. 2017. 'Development of an Amperometric Biosensor Platform for the Combined Determination of l-Malic, Fumaric, and l-Aspartic Acid', *Applied Biochemistry and Biotechnology*, 183: 566-81.

Ruzzo, E. K., J. M. Capo-Chichi, B. Ben-Zeev, D. Chitayat, H. Mao, A. L. Pappas, Y. Hitomi, Y. F. Lu, X. Yao, F. F. Hamdan, K. Pelak, H. Reznik-Wolf, I. Bar-Joseph, D. Oz-Levi, D. Lev, T. Lerman-Sagie, E. Leshinsky-Silver, Y. Anikster, E. Ben-Asher, T. Olender, L. Colleaux, J. C. Décarie, S. Blaser, B. Banwell, R. B. Joshi, X. P. He, L. Patry, R. J. Silver, S. Dobrzeniecka, M. S. Islam, A. Hasnat, M. E. Samuels, D. K. Aryal, R. M. Rodriguiz, Y. H. Jiang, W. C. Wetsel, J. O. McNamara, G. A. Rouleau, D. L. Silver, D. Lancet, E. Pras, G. A. Mitchell, J. L. Michaud, and D. B. Goldstein. 2013. 'Deficiency of asparagine

synthetase causes congenital microcephaly and a progressive form of encephalopathy', *Neuron*, 80: 429-41.

Sampath, Srinivasan, Irena Pankratov, Jenny Gun, and Ovadia Lev. 1996. 'Sol-gel derived ceramic-carbon enzyme electrodes: Glucose oxidase as a test case', *Journal of Sol-Gel Science and Technology*, 7: 123-28.

Sangaraju, D., S. K. Shahidi-Latham, B. L. Burgess, B. Dean, and X. Ding. 2017. 'A multi-matrix HILIC-MS/MS method for the quantitation of endogenous small molecule neurological biomarker N-acetyl aspartic acid (NAA)', *J Pharm Biomed Anal*, 140: 11-19.

Schleinitz, D., A. Seidel, R. Stassart, J. Klammt, P. G. Hirrlinger, U. Winkler, S. Köhler, J. T. Heiker, R. Schönauer, J. Bialek, K. Krohn, K. Hoffmann, P. Kovacs, and J. Hirrlinger. 2018. 'Novel Mutations in the Asparagine Synthetase Gene (ASNS) Associated With Microcephaly', *Front Genet*, 9: 245.

Schmitt, A., E. Asan, B. Püschel, and P. Kugler. 1997. 'Cellular and regional distribution of the glutamate transporter GLAST in the CNS of rats: nonradioactive in situ hybridization and comparative immunocytochemistry', *J Neurosci*, 17: 1-10.

Schneider, C. A., W. S. Rasband, and K. W. Eliceiri. 2012. 'NIH Image to ImageJ: 25 years of image analysis', *Nat Methods*, 9: 671-5.

Schousboe, A., S. Scafidi, L. K. Bak, H. S. Waagepetersen, and M. C. McKenna. 2014. 'Glutamate metabolism in the brain focusing on astrocytes', *Adv Neurobiol*, 11: 13-30.

Šerý, O., N. Sultana, M. A. Kashem, D. V. Pow, and V. J. Balcar. 2015. 'GLAST But Not Least--Distribution, Function, Genetics and Epigenetics of L-Glutamate Transport in Brain--Focus on GLAST/EAAT1', *Neurochem Res*, 40: 2461-72.

Shalev, M., and A. Miriam. 2011. 'Sol-Gel Entrapped Levonorgestrel Antibodies: Activity and Structural Changes as a Function of Different Polymer Formats', *Materials (Basel)*, 4: 469-86.

Shannon, R. J., S. van der Heide, E. L. Carter, I. Jalloh, D. K. Menon, P. J. Hutchinson, and K. L. Carpenter. 2016. 'Extracellular N-Acetylaspartate in Human Traumatic Brain Injury', *J Neurotrauma*, 33: 319-29.

Shimamoto, K., B. Lebrun, Y. Yasuda-Kamatani, M. Sakaitani, Y. Shigeri, N. Yumoto, and T. Nakajima. 1998. 'DL-threo-beta-benzyloxyaspartate, a potent blocker of excitatory amino acid transporters', *Mol Pharmacol*, 53: 195-201.

Singh, A., V. Upadhyay, A. K. Upadhyay, S. M. Singh, and A. K. Panda. 2015. 'Protein recovery from inclusion bodies of Escherichia coli using mild solubilization process', *Microb Cell Fact*, 14: 41.

Slack, J. M., J. Kuzio, and P. Faulkner. 1995. 'Characterization of v-cath, a cathepsin L-like proteinase expressed by the baculovirus Autographa californica multiple nuclear polyhedrosis virus', *J Gen Virol*, 76 (Pt 5): 1091-8.

Stensrud, M. J., C. J. Sogn, and V. Gundersen. 2015. 'Immunogold characteristics of VGLUT3-positive GABAergic nerve terminals suggest corelease of glutamate', *J Comp Neurol*, 523: 2698-713.

Stevens, H., C. Jakobs, A. E. de Jager, R. T. Cunningham, and J. Korf. 1999. 'Neurone-specific enolase and N-acetyl-aspartate as potential peripheral markers of ischaemic stroke', *Eur J Clin Invest*, 29: 6-11.

Storck, T., S. Schulte, K. Hofmann, and W. Stoffel. 1992. 'Structure, expression, and functional analysis of a Na(+)-dependent glutamate/aspartate transporter from rat brain', *Proc Natl Acad Sci U S A*, 89: 10955-9.

Stovell, Matthew G., Jiun-Lin Yan, Alison Sleigh, Marius O. Mada, T. Adrian Carpenter, Peter J. A. Hutchinson, and Keri L. H. Carpenter. 2017. 'Assessing Metabolism and Injury in

Acute Human Traumatic Brain Injury with Magnetic Resonance Spectroscopy: Current and Future Applications', *Frontiers in Neurology*, 8.

Sudhof, T. C. 2004. 'The synaptic vesicle cycle', *Annu Rev Neurosci*, 27: 509-47.

Sun, P., J. E. Tropea, and D. S. Waugh. 2011. 'Enhancing the solubility of recombinant proteins in Escherichia coli by using hexahistidine-tagged maltose-binding protein as a fusion partner', *Methods Mol Biol*, 705: 259-74.

Takahashi, S. 2020. 'D-Aspartate oxidase: distribution, functions, properties, and biotechnological applications', *Appl Microbiol Biotechnol*, 104: 2883-95.

Tedeschi, G., S. Nonnis, B. Strumbo, G. Cruciani, E. Carosati, and A. Negri. 2010. 'On the catalytic role of the active site residue E121 of E. coli L-aspartate oxidase', *Biochimie*, 92: 1335-42.

Tian, F., A. V. Gourine, R. T. Huckstepp, and N. Dale. 2009. 'A microelectrode biosensor for real time monitoring of L-glutamate release', *Anal Chim Acta*, 645: 86-91.

Vasylieva N., Marinesco S. 2013. 'Enzyme Immobilization on Microelectrode Biosensors.' in Dale N. Marinesco S. (ed.), *Microelectrode Biosensors* (Humana Press).

Votyakova, T. V., and I. J. Reynolds. 2004. 'Detection of hydrogen peroxide with Amplex Red: interference by NADH and reduced glutathione auto-oxidation', *Arch Biochem Biophys*, 431: 138-44.

Wall, M. J., A. Atterbury, and N. Dale. 2007. 'Control of basal extracellular adenosine concentration in rat cerebellum', *J Physiol*, 582: 137-51.

Wall, M. J., and N. Dale. 2013. 'Neuronal transporter and astrocytic ATP exocytosis underlie activity-dependent adenosine release in the hippocampus', *J Physiol*, 591: 3853-71.

Wang, L., and J. V. Nadler. 2007. 'Reduced aspartate release from rat hippocampal synaptosomes loaded with Clostridial toxin light chain by electroporation: evidence for an exocytotic mechanism', *Neurosci Lett*, 412: 239-42.

Wang, Z. J., K. Zaitsu, and Y. Ohkura. 1988. 'High-performance liquid chromatographic determination of alpha-keto acids in human serum and urine using 1,2-diamino-4,5-methylenedioxybenzene as a precolumn fluorescence derivatization reagent', *J Chromatogr*, 430: 223-31.

Washio, T., and T. Oikawa. 2018. 'Thermostable and highly specific L-aspartate oxidase from Thermococcus litoralis DSM 5473: cloning, overexpression, and enzymological properties', *Extremophiles*, 22: 59-71.

Werman, R. 1966. 'Criteria for identification of a central nervous system transmitter', *Comp Biochem Physiol*, 18: 745-66.

Wilkinson, R. J., and D. G. Nicholls. 1989. 'Compartmentation of glutamate and aspartate within cerebral cortical synaptosomes: evidence for a non-cytoplasmic origin for the calcium-releasable pool of glutamate', *Neurochem Int*, 15: 191-7.

Wilson, G. S., and R. Gifford. 2005. 'Biosensors for real-time in vivo measurements', *Biosens Bioelectron*, 20: 2388-403.

Wilson, G. S., and M. A. Johnson. 2008. 'In-vivo electrochemistry: what can we learn about living systems?', *Chem Rev*, 108: 2462-81.

Zhou, M., C. L. Peterson, Y. B. Lu, and J. V. Nadler. 1995. 'Release of glutamate and aspartate from CA1 synaptosomes: selective modulation of aspartate release by ionotropic glutamate receptor ligands', *J Neurochem*, 64: 1556-66.

Zhou, Y., and N. C. Danbolt. 2014. 'Glutamate as a neurotransmitter in the healthy brain', *J Neural Transm (Vienna)*, 121: 799-817.